Index 35726 X
ISSN 0867-888X

POLISH
ACADEMY
OF SCIENCES
INSTITUTE
OF FUNDAMENTAL
TECHNOLOGICAL
RESEARCH

NATIONAL
ENGINEERING
SCHOOL
OF METZ

ENGINEERING TRANSACTIONS

ROZPRAWY INŻYNIERSKIE - TRAITE d'INGENIERIE

QUARTERLY
VOLUME 60
ISSUE 3

WARSZAWA - METZ 2012

Faster online
http://et.ippt.pan.pl

Contents of issue 3 vol. LX

187 C. Betts, J. Lin, D. Balint, A. Atkins, *2D FE micromechanics modelling of honeycomb core sandwich panels*

205 J.-J. Arnoux, G. Sutter, G. List, *Characterization of dynamic friction factor for FEM modeling of high speed process*

215 M. Grązka, J. Janiszewski, *Identification of Johnson-Cook equation constants using finite element method*

225 P. Perzyna, *Multiscale constitutive modelling of the influence of anisotropy effects on fracture phenomena in inelastic solids*

Engineering Transactions, Vol. **LX**, No. 3, pp. 185–284, Warszawa - Metz 2012

ENGINEERING TRANSACTIONS

Founded 1952
Appears since 1953

Aims and Scope

ENGINEERING TRANSACTIONS promotes research and practise in engineering science and provides a forum for interdisciplinary publications combining mechanics with material science, electronics (mechanotronics), medical science and biotechnologies (biomechanics), environmental science, photonics, information technologies and other engineering applications. The Journal publishes original papers covering a broad area of research activities including experimental and hybrid techniques as well as analytical and numerical approaches. Engineering Transactions is a quarterly issued journal for researchers in academic and industrial communities.

Address of the Editorial Office:
Engineering Transactions
Institute of Fundamental Technological Research
Pawińskiego 5B, PL 02-106 Warsaw, Poland

Phone: (48-22) 826 12 81 ext. 206, Fax: (48-22) 826 98 15, E-mail: engtrans@ippt.pan.pl

Abstracted/indexed in:

Applied Mechanics Reviews, Current Mathematical Publications, Elsevier, EMBASE, Engineering Village, Inspec, Mathematical Reviews, MathSci, Reaxys, Scopus, Zentralblatt für Mathematik.

http://et.ippt.pan.pl/

Address of the Editorial Office:
Engineering Transactions
Institute of Fundamental Technological Research
Pawińskiego 5B
PL 02-106 Warsaw, Poland
Phone: (48-22) 826 12 81 ext. 206, Fax: (48-22) 826 98 15
E-mail: engtrans@ippt.pan.pl

SUBSCRIPTIONS

Subscription orders for all journals edited by Institute of Fundamental Technological Research (IPPT) may be sent directly to the Publisher:
Institute of Fundamental Technological Research
e-mail: subscribe@ippt.pan.pl

Please transfer the subscription fee to our bank account:
Payee: IPPT PAN
Bank: Pekao S.A. IV O/Warszawa
Account number 05124010531111000004426875.

WARUNKI PRENUMERATY

Prenumeratę na wszystkie czasopisma wydawane przez Instytut Podstawowych Problemów Techniki PAN przyjmuje Dział Wydawnictw IPPT.

Bieżące numery Engineering Transactions można nabyć bezpośrednio w Redakcji:
ul. Pawińskiego 5B, 02-106 Warszawa
Tel.: (48-22) 826 60 22; Fax: (48-22) 826 98 15
e-mail: subscribe@ippt.pan.pl

Arkuszy wydawniczych 7.75; Arkuszy drukarskich 6.25
Papier offset. kl. III 80 g.
Skład w systemie LaTeX K. Jezierska

ENGINEERING TRANSACTIONS • *Engng. Trans.* • **60**, 3, 187–203, 2012
Polish Academy of Sciences • Institute of Fundamental Technological Research (IPPT PAN)
National Engineering School of Metz (ENIM)
SIXTY YEARS OF THE ENGINEERING TRANSACTIONS

2D FE Micromechanics Modelling of Honeycomb Core Sandwich Panels

Charles BETTS, Jianguo LIN, Daniel BALINT, Anthony ATKINS

Head of Mechanics of Materials Division
Department of Mechanical Engineering, Imperial College
Exhibition Road South Kensington London SW7 2AZ
e-mail: Jianguo.Lin@Imperial.ac.uk

A repeating unit cell 2D finite element modelling procedure has been established to model the mechanical behaviour of honeycomb core sandwich panels (e.g. Young's modulus, energy absorbed, etc.). Periodic boundary conditions have been implemented within the model to simulate an infinitely long sandwich panel. An analytical solution using Timoshenko beam theory has been developed to predict the Young's modulus of the honeycomb core, and this has been compared with the FE model results; it is found that there is good agreement between the two values. The FE model can shed light on the mechanics of more complex 3D metal foams.

Key words: micromechanical modelling, sandwich panel, metal foam, honeycomb, finite elements, periodic boundary conditions.

1. Introduction

Metal foams are a relatively new class of materials that show good potential for lightweight structures, energy absorption, and thermal management [1–3]. They are able to combine low density with good bending stiffness and strength [2]. They can also be made with integral skins, which presents the possibility of making composite structures without using adhesive bonding that can be readily formed into curved shapes [4]. They display a densification stage when subjected to a compressive stress, where the stress rises rapidly with strain as the foam cells crush – this has the implication that the integrity of a metal foam core sandwich panel is not necessarily compromised when subjected to impacts. In addition, open-cell foams do not trap moisture (i.e. they are less susceptible to corrosion than honeycomb cores) [5]. Open-cell cores could provide a dual function, and potentially be used for the storage or drainage of fuel [6].

Due to the potential of metal foams, significant efforts have been made to develop analytical as well as finite element modelling techniques for assessing the mechanical properties of foam materials [7–17]. These fall under three categories:

- **Analytical methods**, utilising dimensional analysis that gives the dependence of the foam properties on the relative density but not the cell geometry (e.g. [7]);
- **Finite element methods utilising a repeating unit cell** such as a tetrakaidecahedron. This method can provide the full response of the foam subjected to a stress or strain (e.g. [10]); and
- **Finite element methods utilising the random Voronoi technique**. This approach givers a more accurate representation of the cell geometry of the foams (e.g. [15]).

FE methods are also being developed that utilise a 3D tomographic image (a non-destructive visualisation of a foam at the scale of its cellular microstructure obtained by X-ray tomography) of a real foam as the geometric description of the model (see Fig. 15) [18, 19]. Such techniques could model both open cell as well as closed cell foams and could prove to be useful in predicting the mechanical response of cellular materials.

This paper aims to shed light on the mechanics of complex 3D foams by conducting finite element modelling of 2D regular honeycomb structures. Foams consist of cell walls that form an intricate 3D network which distorts during deformation in ways which are difficult to identify; honeycombs are much simpler. This paper sets out to establish a repeating unit cell 2D finite element modelling procedure to predict the mechanical behaviour of metal foam sandwich panels (e.g. Young's modulus, energy absorbed, etc.). The finite element results are compared to an analytical model developed in Sec. 5 that utilises Timoshenko beam theory to determine the Young's modulus of a honeycomb core.

2. FE model development

2.1. Overview of FE model

Finite element microstructural modelling of regular honeycombs has been conducted in this paper using the software ABAQUS 6.9-1. The model consists of a set area divided into a regular hexagonal tessellation. The honeycomb is enclosed at the top and bottom by solid 0.8 mm thick facesheets to create a sandwich structure. The dimensions of the hexagonal cells were based on those of the open-cell foam ERG Duocel [20]: the strut length was set to 1.5 mm, and the thickness of the struts was set to 0.18 mm [21]. The relative density of the regular hexagon tessellation can be approximated as follows [7]:

$$\frac{\rho^*}{\rho_s} = \frac{2}{\sqrt{3}}\frac{t}{l}\left(1 - \frac{1}{2\sqrt{3}}\frac{t}{l}\right) = 13.4\%, \tag{2.1}$$

where t is the cell wall thickness and l is the strut length (with $t \ll l$).

For practical applications, the thickness of the sandwich panel will be of a specified value in the order of several millimetres. However, the length of the sandwich panel could be up to several metres long; it would be both impractical and computationally inefficient to physically model the full panel length. Therefore, the length of the sandwich panel was progressively increased within the FE model until convergence of the stress-strain plots was achieved so as to identify the smallest length possible that could be modelled while taking into account edge effects. Figure 1 illustrates this principle.

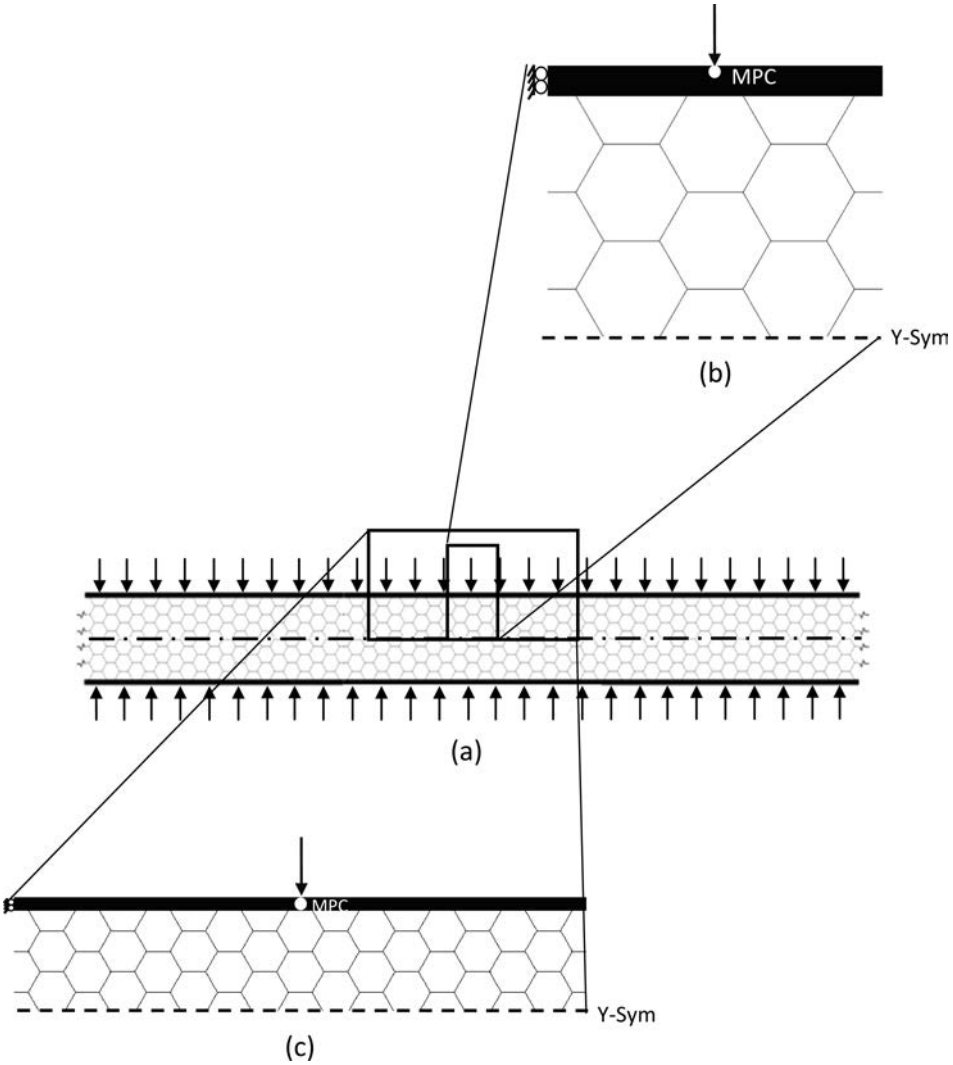

FIG. 1. A sandwich panel structure under uniform loading (a) and its localised micromechanics FE models with different sizes; (b) small size FE model; and (c) larger size FE model.

2.2. Applied boundary conditions and loads

The applied boundary conditions are shown in Fig. 1. A symmetry boundary condition was applied across the horizontal centreline of the sandwich panel. The left face of the upper facesheet was constrained in the horizontal direction.

A uniform compressive load was modelled by applying a multi-point constraint (MPC) along the top face of the upper facesheet, whereby all nodes along that face were tied to the central node. Compressive load vs. displacement plots were obtained by moving this central node in the vertical direction under a controlled, linear displacement.

2.3. Material model

The cell walls of the honeycomb and the facesheets were assigned the material properties of aluminium alloy Al-7075-0: $\rho = 2800$ kg/m^3, $E = 71.7$ GPa, $\sigma_y = 145$ MPa, $\nu = 0.33$. The flow stress was assumed to be given by [20]:

$$\sigma = 400\epsilon^{0.17} \text{ MPa}, \tag{2.2}$$

where σ is the engineering stress, and ϵ the engineering strain.

2.4. Element type, profiles, and time step

The walls of the honeycombs were modelled as beam elements having solid square cross-section. A beam element is a 1D line element in the X-Y plane that has stiffness associated with deformation of the line (the beam's "axis"). These deformations consist of axial stretch/compression and curvature change (bending). The main advantage of beam elements is that they are geometrically simple and have few degrees of freedom.

Specifically, the Timoshenko beam B21 element was used. This allows for transverse shear deformation [23]. For beams made from uniform material, shear flexible beam theory can provide useful results for cross-sectional dimensions up to 1/8 of typical axial distances or the wavelength of the highest natural mode that contributes significantly to the response. Beyond this ratio, the approximations that allow the member's behaviour to be described solely as a function of axial position no longer provide adequate accuracy. ABAQUS assumes that the transverse shear behaviour of Timoshenko beams is linear elastic with a fixed modulus and, thus, independent of the response of the beam section to axial stretch and bending. These elements in ABAQUS are formulated so that they are efficient for thin beams – where Euler-Bernoulli theory is accurate – as well as for thick beams: because of this they are the most effective beam elements in ABAQUS [24].

The B21 element linearly interpolates the displacement field, and hence 15 beam elements were necessary to model each foam strut in order to adequately capture the plastic collapse behaviour of the honeycomb. The upper facesheet was modelled as a shell planar feature comprising of elements of dimensions 0.2×0.2 mm (so, for a model length of 10 mm the upper facesheet comprised of 200 elements). A dynamic, explicit time step was used in order to achieve convergence of the results.

2.5. Connector assignments, constraints, and surface interactions

The foam struts were tied to one another. The joints between the foam struts were constrained in the U1, U2, and U3 translational directions, as well as the UR1, UR2, and UR3 rotational directions. In ABAQUS, this was specified as follows:

- Translational connector type: Join;
- Rotational connector type: Align.

The foam struts at the foam/facesheet interface were tied to the facesheet. Each strut and the facesheet was assigned a tangential frictionless surface interaction property to all part instances in their line of sight.

3. FE results

Figure 2 shows the hexagonal honeycomb stress-strain graph for a relative density of 13.4%, assuming an elastic-plastic material model. The graph displays a trend associated with elastic-plastic honeycombs [7]. There are three distinct regions: a linear-elastic regime, followed by a plateau of roughly constant stress, and finally a regime of steeply rising stress. This behaviour is also typically observed in commercial open-cell foams [2].

The stress-strain behaviour of the honeycombs is described by the different mechanisms of deformation for each region, and can be observed directly from the FE simulations. For the hexagonal honeycomb, the processes are as follows:

1. The cell walls initially bend, resulting in linear-elasticity;
2. Once a critical stress is reached the cells begin to collapse. The cell walls will collapse due to the formation of plastic hinges at the section of maximum moment in the bent members;
3. Finally, the cells collapse to such an extent that opposing cell walls touch one another and further deformation compresses the cell wall material itself. This explains the densification region of the load-displacement graph.

The effect of increasing the length of the sandwich panel can be observed from Fig. 2. As the length is increased from 9 mm to 90 mm, so too is the

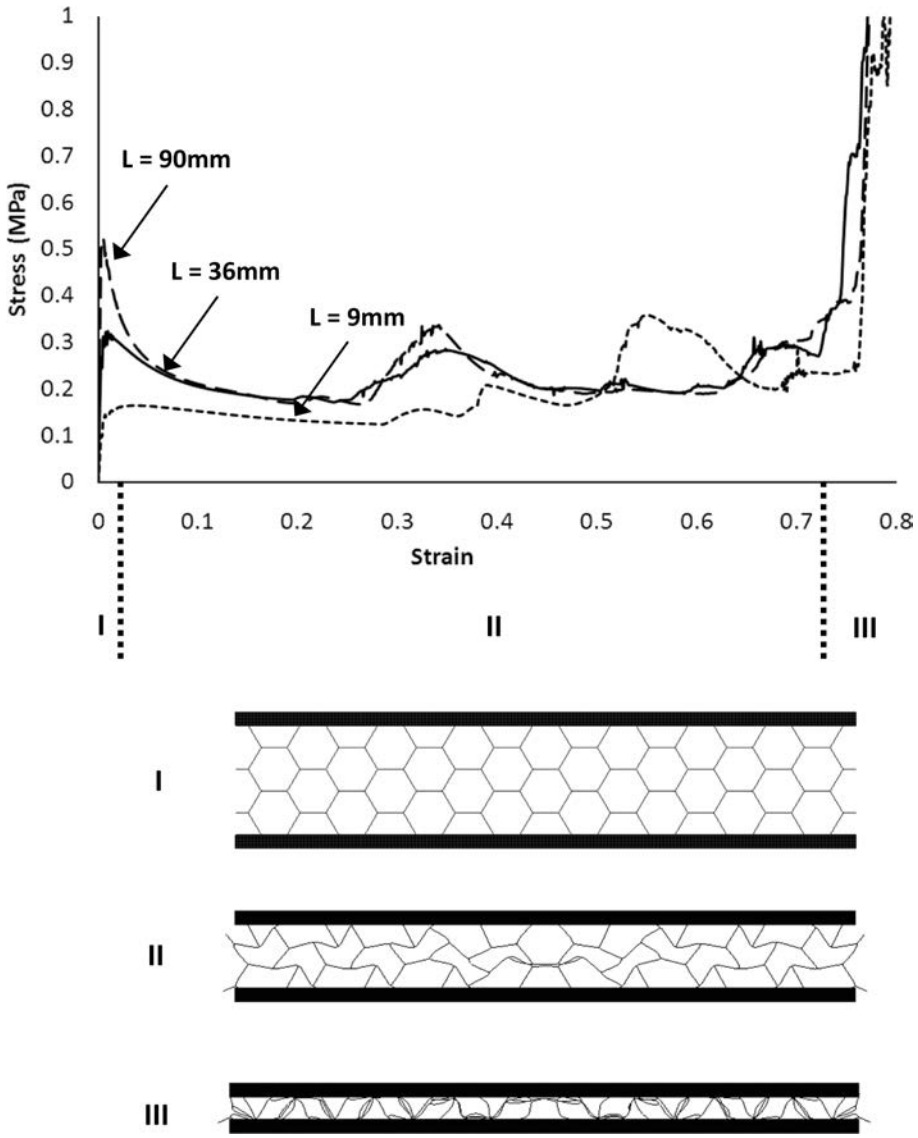

FIG. 2. Nominal stress-strain curves calculated using FE models with different sandwich panel lengths (L). The stress-strain relationships can be divided into three regions as shown: (I) elastic region; (II) plastic collapse followed by plateau; (III) densification.

effective Young's modulus and peak stress. The increase in effective Young's modulus is notable, varying from 36 MPa to 182 MPa. The initial loading peak stress also varies significantly, from 166 kPa to 522 kPa. There is less variation in the plastic properties, and the densification strain is the same for all the models.

As the stress-stain plots do not converge even at a length of 90 mm, it is necessary to investigate implementing periodic boundary conditions at the left and rightmost nodes of the model to describe a sandwich panel of infinite length. This is discussed in Sec. 4.

4. Implementation of Periodic Boundary Conditions

Periodic boundary conditions (PBCs) have been applied to previous FE models of metal foams and honeycombs to simulate an infinite array of cells connected to each other [11, 13, 15]. PBCs effectively eliminate edge effects from the mechanical analysis.

For the 2D case, PBCs assume that for any two corresponding beam nodes on the vertical boundaries of the model, the nodes have the same relative displacement in the vertical and horizontal directions and the same rotational angle in the X-Y plane. This is represented by Eqs. set (4.1).

$$\begin{aligned} U_1^L - U_1^R &= 0, \\ U_2^L - U_2^R &= 0, \\ \emptyset^L - \emptyset^R &= 0, \end{aligned} \tag{4.1}$$

where the superscript L denotes a node on the left vertical boundary, and R is the corresponding node on the right vertical boundary (see Fig. 3). The subscripts 1 and 2 denote the respective degree of freedom (DOF) of the node.

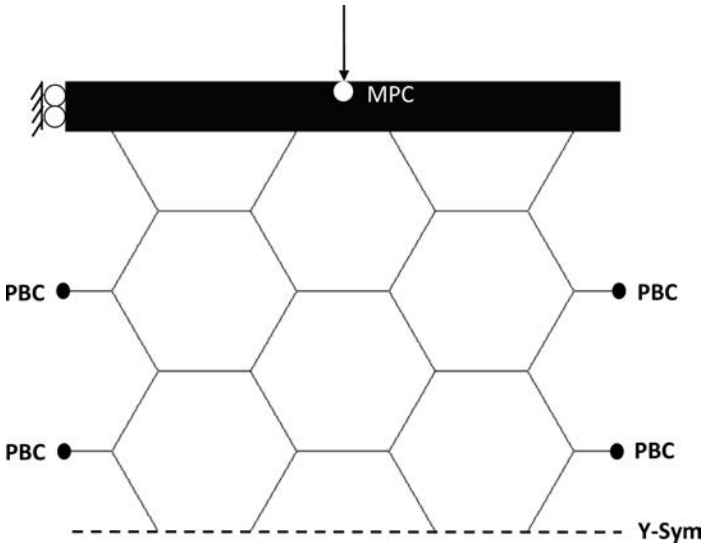

Fig. 3. FE model of hexagonal honeycomb enclosed by metal facesheets, with Periodic Boundary Conditions (PBCs).

The above PBCs were applied to the FE model outlined in Sec. 2, for a facesheet length of 9 mm. PBCs were then applied to the same model for a facesheet length of 45 mm to verify the convergence of the results. Figure 4 shows the stress-strain plots for the two models, and it can be seen that there is a good agreement. The effective Young's modulus varies by 0.2%, whilst the peak stress differs by 0.9% – it is therefore concluded that an infinitely long sandwich panel may be modelled by a facesheet length of 9 mm with PBCs.

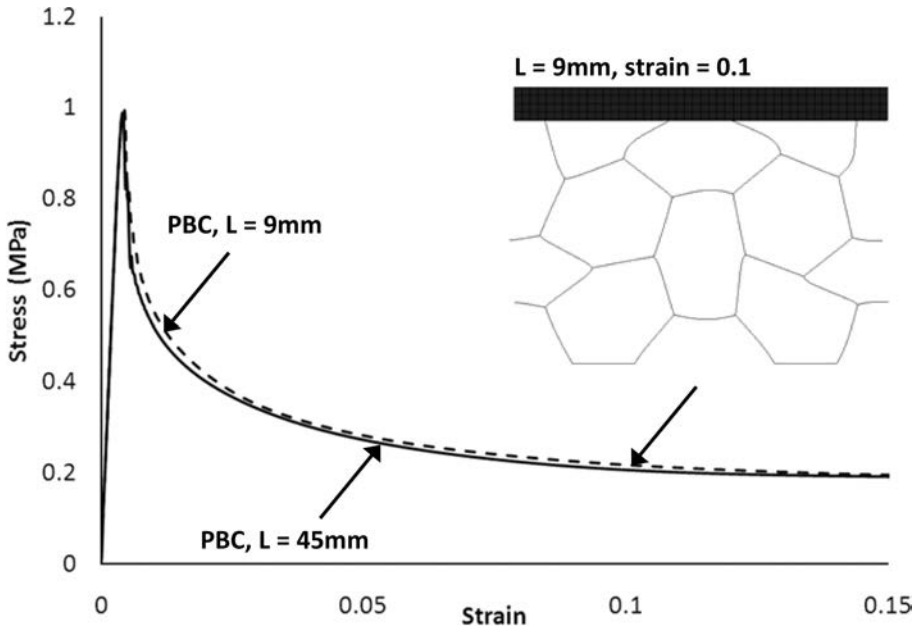

FIG. 4. Comparison of stress-strain relationships calculated using different FE model sizes ($L = 9$ and 45 mm) with PBCs to demonstrate convergence. The deformation for the model length 9 mm at a strain of 0.1 is shown.

4.1. Model convergence

Figure 5 plots the effective Young's modulus and peak stress for the FE models of Fig. 3 – i.e. a facesheet length of 9 mm, 36 mm, and 90 mm without PBCs – and compares these to the value obtained using PBCs as outlined in Sec. 4. It can be ascertained that as the model length increases, it tends towards the solution with PBCs.

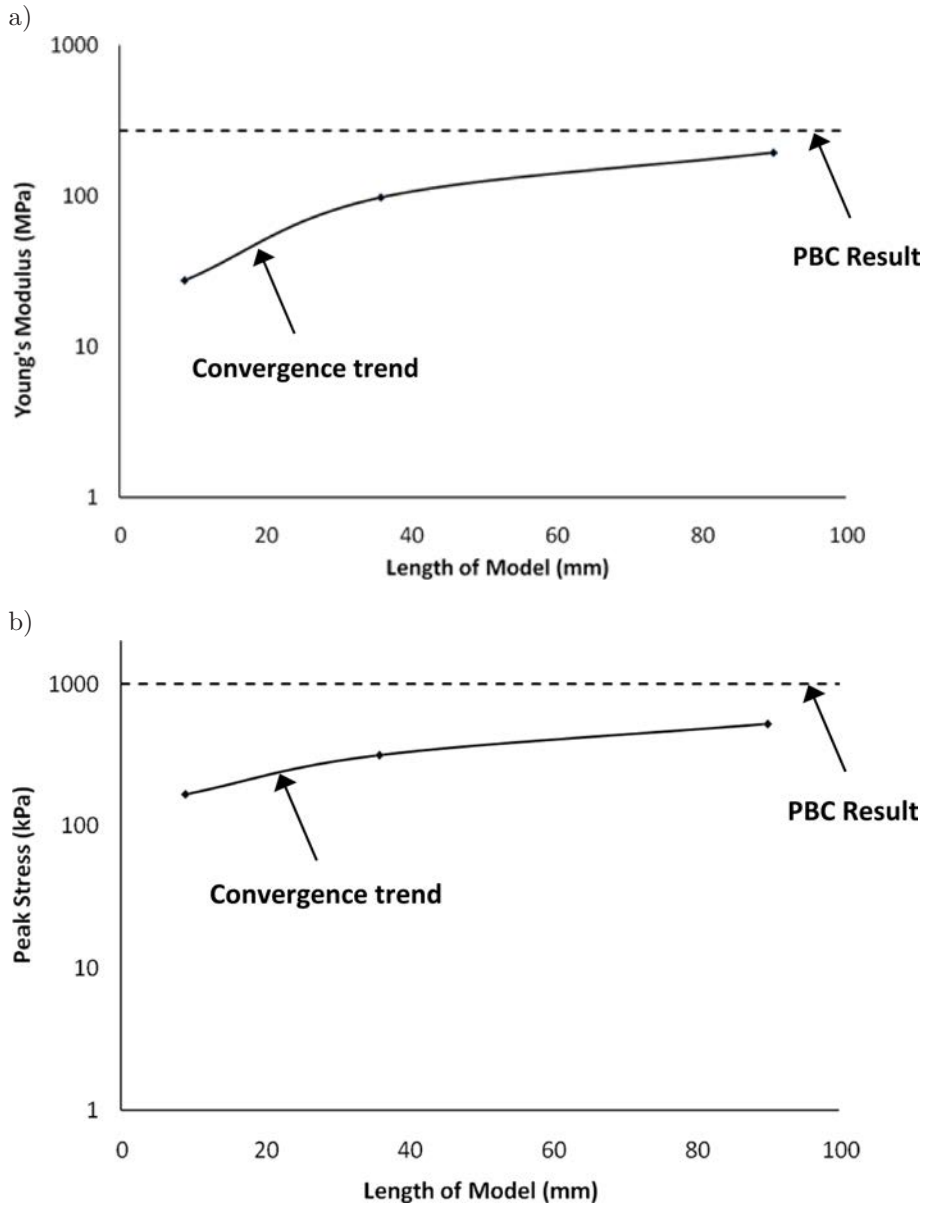

FIG. 5. Convergence of FE models towards PBC solution for: a) Effective Young's modulus and b) peak stress.

5. FE MODEL VALIDATION

ASHBY and GIBSON [7] have previously predicted the Young's modulus of a regular hexagonal honeycomb using Euler-Bernoulli beam theory. In an analogous method to that of [7], Timoshenko beam theory [23] is now used to an-

alytically determine the Young's modulus of a honeycomb in the X_2 direction. Timoshenko beam theory is preferred as it accounts for the effects of transverse shear strain, which are not captured by Euler-Bernoulli beam theory. The latter therefore under-predicts deflections and thus over-predicts beam stiffness. For a homogeneous beam of constant cross-section, Timoshenko beam theory provides the following differential equation to describe the relationship between the beam's deflection and the applied load:

$$E_s I \frac{d^4 w}{dx^4} = q(x) - \frac{E_s I}{kAG} \frac{d^2 q}{dx^2}. \tag{5.1}$$

Consider a honeycomb comprising of regular hexagons of square cross-section and compressed in the X_2 direction, as shown in Fig. 6. By equilibrium, $C = 0$. By separating the load P into components parallel and normal to the beam, the following loading equation for the beam can be written:

$$q(x) = P_n \langle x - 0 \rangle_{-1} - P_n \langle x - l \rangle_{-1} - M \langle x - 0 \rangle_{-2} - M \langle x - l \rangle_{-2}. \tag{5.2}$$

This equation is valid for all values of x from minus infinity to plus infinity, although the beam only exists between $x = 0$ and $x = l$.

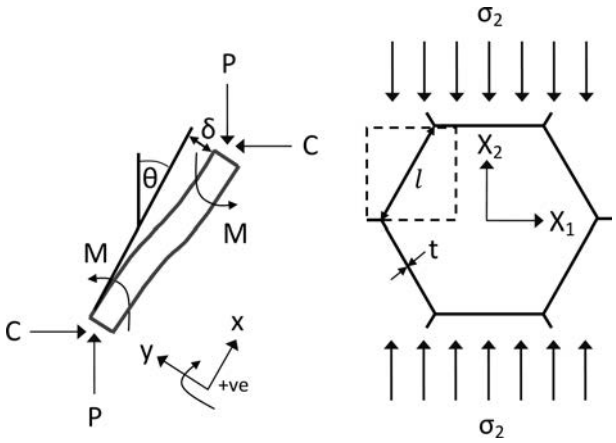

FIG. 6. Free Body Diagram (FBD) of an individual strut subject to uniaxial compression for use in Timoshenko analytical solution.

Inserting the expression for $q(x)$ of Eq. (5.2) into Eq. (5.1) and integrating gives:

$$\begin{aligned} E_s I \frac{d^3 w}{dx^3} &= P_n \langle x - 0 \rangle^0 - P_n \langle x - l \rangle^0 - M \langle x - 0 \rangle_{-1} - M \langle x - l \rangle_{-1} \\ &- \frac{E_s I}{kAG} \left(P_n \langle x - 0 \rangle_{-2} - P_n \langle x - l \rangle_{-2} - M \langle x - 0 \rangle_{-3} - M \langle x - l \rangle_{-3} \right) + C_1. \end{aligned} \tag{5.3}$$

Integrating Eq. (5.3) gives:

$$E_sI\frac{d^2w}{dx^2} = P_n\langle x-0\rangle^1 - P_n\langle x-l\rangle^1 - M\langle x-0\rangle^0 - M\langle x-l\rangle^0 - \frac{E_sI}{kAG}\left(P_n\langle x-0\rangle_{-1} - P_n\langle x-l\rangle_{-1} - M\langle x-0\rangle_{-2} - M\langle x-l\rangle_{-2}\right) + C_1x + C_2. \tag{5.4}$$

The constants C_1 and C_2 can be evaluated by noting that at $x = 0_-$ (i.e. at a point just below $x = 0$):

$$\frac{d^3w(0_-)}{dx^3} = 0 = C_1, \qquad \frac{d^2w(0_-)}{dx^2} = 0 = C_2. \tag{5.5}$$

Integrating Eq. (5.4) twice provides an expression for the slope and deflection of the beam:

$$E_sI\frac{dw}{dx} = \frac{P_n}{2}\langle x-0\rangle^2 - \frac{P_n}{2}\langle x-l\rangle^2 - M\langle x-0\rangle^1 - M\langle x-l\rangle^1 - \frac{E_sI}{kAG}\left(P_n\langle x-0\rangle^0 - P_n\langle x-l\rangle^0 - M\langle x-0\rangle_{-1} - M\langle x-l\rangle_{-1}\right) + C_3,$$

$$E_sI\delta = \frac{P_n}{6}\langle x-0\rangle^3 - \frac{P_n}{6}\langle x-l\rangle^3 - \frac{M}{2}\langle x-0\rangle^2 - \frac{M}{2}\langle x-l\rangle^2 - \frac{E_sI}{kAG}\left(P_n\langle x-0\rangle^1 - P_n\langle x-l\rangle^1 - M\langle x-0\rangle^0 - M\langle x-l\rangle^0\right) + C_3x + C_4. \tag{5.6}$$

The constants C_3 and C_4 can be evaluated by noting that at $x = 0_-$ (i.e. at a point just below $x = 0$):

$$\frac{dw(0_-)}{dx} = 0 = C_3, \qquad w(0_-) = \delta(0_-) = 0 = C_4. \tag{5.7}$$

Hence, from Eq. $(5.6)_2$ at $x = l$ the defection of the beam can be described as follows:

$$E_sI\delta = \frac{P_n}{6}l^3 - \frac{M}{2}l^2 - \frac{E_sI}{kAG}(P_nl - M). \tag{5.8}$$

Now, the moment tending to bend the cell wall is given by:

$$M = \frac{Pl\sin\theta}{2}. \tag{5.9}$$

Inserting Eq. (5.9) in Eq. (5.8), and noting $P_n = P\sin\theta$, gives:

$$E_s I\delta = \frac{Pl^3\sin\theta}{6} - \frac{Pl^3\sin\theta}{4} - \frac{E_s I}{kAG}\left(Pl\sin\theta - \frac{Pl\sin\theta}{2}\right). \tag{5.10}$$

So:

$$|\delta| = \frac{Pl^3\sin\theta}{12E_s I} + \frac{Pl\sin\theta}{2kAG}. \tag{5.11}$$

Now:

$$P = \sigma_2 tl(1+\sin\theta). \tag{5.12}$$

A component $\delta\sin\theta$ of the deflection is parallel to the X_2 axis, giving a strain:

$$\varepsilon_2 = \frac{|\delta|\sin\theta}{l\cos\theta} = \frac{\sigma_2 tl(1+\sin\theta)\sin^2\theta}{\cos\theta}\left(\frac{l^2}{12E_s I} + \frac{1}{2kAG}\right). \tag{5.13}$$

For a beam of square cross-section, $I = t^4/12$ and the Young's modulus is given by (using Eq. (5.13)):

$$E_2^* = \frac{\sigma_2}{\varepsilon_2} = \frac{\cos\theta}{tl(1+\sin\theta)\sin^2\theta\left(\dfrac{l^2}{E_s t^4} + \dfrac{1}{2kAG}\right)}. \tag{5.14}$$

And noting that for a regular hexagon, $\theta = 30°$:

$$E_2^* = \frac{2.3}{\left(\dfrac{l^3}{E_s t^3} + \dfrac{1}{2kG}\right)}. \tag{5.15}$$

For the honeycomb model of Sec. 4, $t = 0.18$ mm, $l = 1.5$ mm, $E_s = 71.7$ GPa, and $G = 27.0$ GPa. The shear coefficient, k, is defined by ABAQUS for a rectangular (or square) cross-section to be equal to 0.85 [24]. So, from Eq. (5.15) $E_2^* = 284$ MPa.

The FE model of Sec. 4, with PBCs, displayed a Young's modulus of 268 MPa, which is in good agreement with the Timoshenko solution (a 6% difference). Figure 7 shows the stress-strain plots for the FE models of facesheet lengths 9 mm, 36 mm, and 90 mm without PBCs, as well as that obtained using PBCs. The Timoshenko analytical solution has been superimposed on the plots.

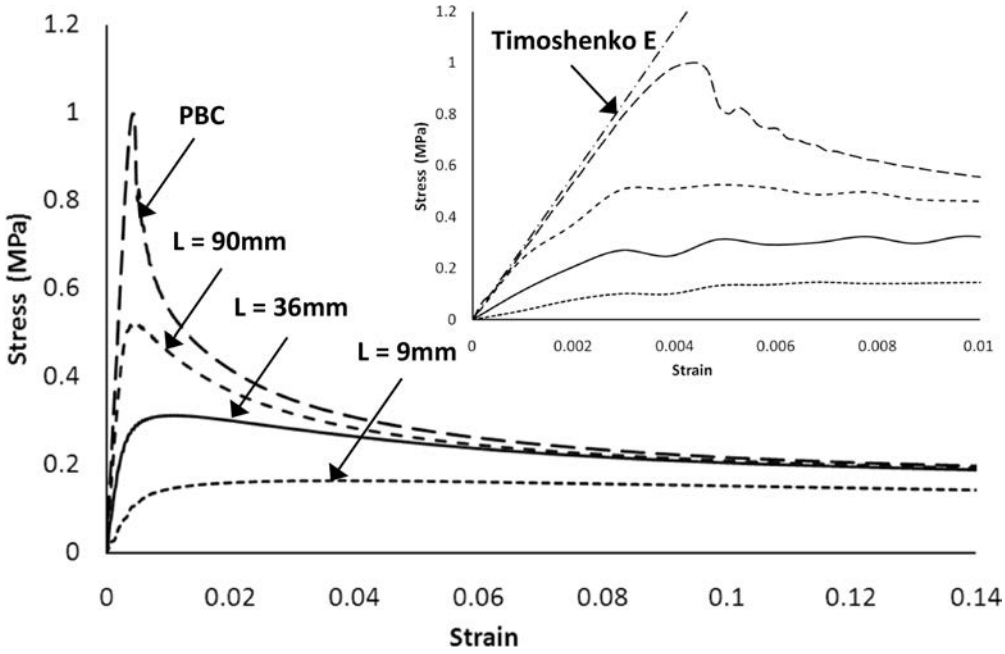

FIG. 7. Comparison of stress-strain plots obtained from different FE model sizes ($L = 9$, 36 and 90 mm) as well as the solution with PBCs. Timoshenko analytical solution is super-imposed to show theoretical Young's modulus in the insert.

5.1. Variance between Euler-Bernoulli and Timoshenko beam theory

For Euler-Bernoulli beam theory, the deflection of a regular hexagonal honeycomb cell wall is given as follows [7]:

$$|\delta| = \frac{Pl^3 \sin\theta}{12E_s I}. \tag{5.16}$$

Comparing this to Eq. (5.11), it is apparent that Euler-Bernoulli beam theory under-predicts deflections. The magnitude of the variation can be expressed by the ratio (for a square cross-section):

$$\frac{\left||\delta|^{\text{Euler}} - |\delta|^{\text{Timoshenko}}\right|}{|\delta|^{\text{Timoshenko}}} = \frac{E_s t^2}{2kGl^2 + E_s t^2}. \tag{5.17}$$

For the FE model of Sec. 4, and varying the beam thickness, this ratio exceeds 10% for values of $t/l > 0.27$. Beyond this value, Euler-Bernoulli beam theory inadequately approximates the deflection of the honeycomb.

Similarly, for Euler-Bernoulli beam theory, the Young's modulus of a regular hexagonal honeycomb cell wall is given as follows [7]:

$$E_2^* = \frac{2.3}{\left(\dfrac{l^3}{E_s t^3}\right)}. \tag{5.18}$$

Comparing this to Eq. (5.15), it is apparent that Euler-Bernoulli beam theory over-predicts the Young's modulus. The magnitude of the variation can be expressed by the ratio (for a square cross-section):

$$\frac{E_2^{*\text{Euler}} - E_2^{*\text{Timoshenko}}}{E_2^{*\text{Timoshenko}}} = \frac{E_s t^3}{2kGl^3}. \tag{5.19}$$

For the FE model of Sec. 4, and varying the beam thickness, this ratio exceeds 10% for values of $t/l > 0.4$ and Euler-Bernoulli beam theory inadequately approximates the Young's modulus of the honeycomb.

6. Relevance to industrial applications

The FE model of Sec. 4 can shed light on the mechanics of more complex 3D metal foams. Indeed, such foams show a similar compressive stress-strain response to the 2D honeycomb structure, with three distinct regions: a linear-elastic regime, followed by a plateau of roughly constant stress, and finally a regime of steeply rising stress [2]. As noted in the Introduction, metal foams can combine low density with good bending stiffness and strength, and are hence attractive as cores of lightweight sandwich structures. Such sandwich structures show promise in the design of aircraft wing boxes, which are at present typically fabricated utilising thin panels that comprise of a skin stiffened by stringers [25]. The resultant panels are light and stiff, but relatively expensive to produce due to high machining costs and the inefficient use of material. Sandwich structures provide a continuous stiffness distribution within the skin panel, which leads to a reduced parts count for assemblies and hence less logistics, parts manufacturing, and assembly work [26]. In addition, open-cell sandwich cores can provide multiple functions and potentially be used for the storage or drainage of fuel within the wings.

It has been ascertained, in Subsec. 5.1, that for values of $t/l > 0.27$, Euler-Bernoulli beam theory inadequately approximates the deflection of a 2D honeycomb structure. X-ray micro-tomography (XMT) scans have been conducted for this paper on individual struts of a commercial open-cell metal foam acquired from BPE International, Germany (a metal matrix composite fabricated from an Al-Zn-Mg-Cu (7xxx series) alloy with TiC particles). From the 3D render

of each scanned strut, and using the imaging software ImageJ, it has been determined that the average strut length and diameter is 1.7 mm and 0.562 mm respectively; i.e. $t/l = 0.33 > 0.27$ (see Fig. 8). Therefore, for this material Timoshenko beam theory is required to accurately predict the deflection of a representative equivalent 2D honeycomb structure.

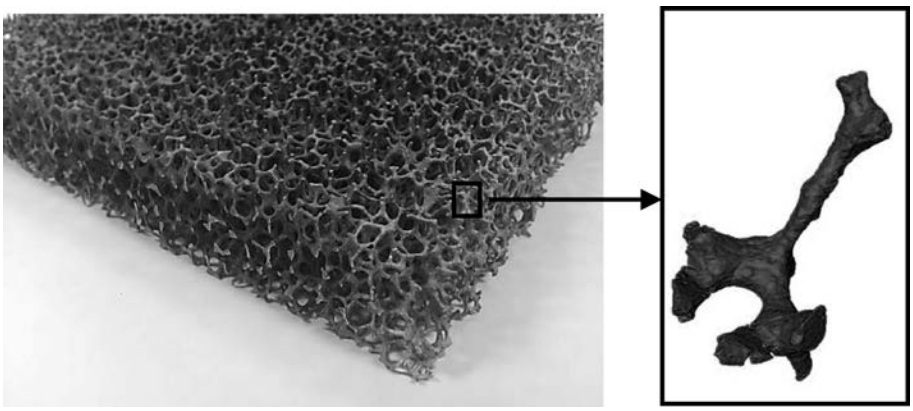

FIG. 8. Morphology of Al-Zn-Mg-Cu foam with TiC particles. The strut dimensions have been determined from XMT scans and imaging software.

Finally, there is scope to conduct FE modelling of other regular tessellated honeycombs (i.e. square and equilateral triangle cell shapes) using the model established in Sec. 4. For a given value of relative density, the energy absorption, initial collapse strength and Young's modulus of sandwich panels constructed from the different cell shapes can be compared, allowing the best choice for lightweight structural applications to be selected.

7. Conclusions

A repeating unit cell 2D finite element modelling procedure has been established in this paper to model the mechanical behaviour of honeycomb core sandwich panels (e.g. Young's modulus, energy absorbed, etc.). Periodic boundary conditions have been implemented within the model to simulate an infinitely long sandwich panel, and to eliminate edge effects from the mechanical analysis. This avoids the need to physically model the actual sandwich panel length, which is advantageous in terms of both the time to construct the model as well as the time to run the model.

The load-displacement plots display three distinct regions: a linear-elastic regime, followed by a plateau of roughly constant stress, and finally a regime of steeply rising stress. This behaviour is also typically observed in commercial open-cell foams.

An analytical solution using Timoshenko beam theory has been developed to predict the Young's modulus of the honeycomb core, and this has been compared with the FE model results; it is found that there is good agreement between the two values. Euler-Bernoulli beam theory is found to be inadequate for predicting the Young's modulus of the modelled honeycomb at values of $t/l > 0.4$, for which Timoshenko beam theory becomes necessary.

The FE model can shed light on the mechanics of more complex 3D metal foams, and could also be used to enable a comparative study of optimal cell shapes for a given application (e.g. energy absorption, lightweight structural applications, etc.).

References

1. Banhart J., *Manufacture, characterisation, and application of cellular materials and metal foams*, Prog. in Mat. Sci., **46**, 559–632, 2001.
2. Ashby M.F., Evans A., Fleck N.A., Gibson L.J., Hutchinson J.W., Wadley H.N.G., *Metal foams: a design guide*, Butterworth-Heinemann, USA 2000.
3. Evans A.G., Hutchinson J.W., Fleck N.A., Ashby M.F., Wadley H.N.G., *The topological design of multifunctional cellular metals*, Prog. in Mat. Sci., **46**, 309–327, 2001.
4. McCormack T.M., Miller R., Kesler O., Gibson L.J., *Failure of sandwich beams with metallic foam cores*, Int. Journal of Solids and Structures, **38**, 4901–4920, 2001.
5. Sypeck D., *Cellular truss core sandwich structures*, Applied Composite Materials, **12**, 229–246, 2005.
6. Wicks N., Hutchinson J.W., *Optimal truss plates*, Int. Journal of Solids and Structures, **38**, 51–65, 2001.
7. Ashby M.F., Gibson L.J., *Cellular solids structure & properties*, Pergamon Press, UK 1998.
8. Onck P.R., Andrews E.W., Gibson L.J., *Size effects in ductile cellular solids: part I modeling*, Int. Journal of Mechanical Sciences, **43**, 681–699, 2001.
9. Chen C., Lu T.J., Fleck N.A., *Effect of imperfections on the yielding of two-dimensional foams*, J. Mech. Phys. Solids, **47**, 2235–2272, 1999.
10. Simone A.E., Gibson L.J., *Effects of solid distribution on the stiffness and srength of metallic foams*, Acta Mater., **46**, 6, 2139–2150, 1998.
11. Hodge A.M., Dunand D.C., *Measurement and modeling of creep in open-cell NiAl foams*, Metallurgical and Materials Transactions, **34A**, 2353–2363, 2003.
12. Shulmeister V., Van der Burg M.W.D., Van der Giessen E., Marissen R., *A numerical study of large deformations of low-density elastomeric open-cell foams*, Mechanics of Materials, **30**, 125–140, 1998.
13. Huang J-S., Gibson L.J., *Creep of open-cell Voronoi foams*, Materials Science and Engineering, **A339**, 220–226, 2003.

14. Silva M.J., Hayes W.C., Gibson L.J., *The effect of non-periodic microstructure on the elastic properties of two-dimensional cellular solids*, Int. J. Mech. Sci., **37**, 1161–1177, 1995.

15. Zhu H.X., Hobdell J.R., Windle A.H., *Effects of cell irregularity on the elastic properties of open-cell foams*, Acta Materialia, **48**, 4893–4900, 2000.

16. Papka S.D., Kyriakides S., *In-plane compressive response and crushing of honeycomb*, J. Mech. Phys. Solids, **42**, 1499–1532, 1994.

17. Gong L., Kyriakides S., Triantafyllidis N., *On the stability of Kelvin cell foams under compressive loads*, J. Mech. Phys. Solids, **53**, 771–794, 2005.

18. Youssef S., Maire E., Gaertner R., *Finite element modelling of the actual structure of cellular materials determined by X-ray tomography*, Acta Materialia, **53**, 719–730, 2005.

19. Maire E., Fazekas A., Salvo L., Dendievel R., Youssef S., Cloetens P., Letang J.M., *X-ray tomography applied to the characterization of cellular materials. Related finite element modeling problems*, Composite Science and Technology, **63**, 2431–2443, 2003.

20. http://www.ergaerospace.com/index.html, (accessed December 2010).

21. Onck P.R., Van Merkerk R., De Hosson T.M., Schmidt I., *Fracture of metal foams: in-situ testing and numerical modeling*, Advanced Engineering Materials, **6**, 429–431, 2004.

22. El-Domiaty A.A., Shabara M.A.N., Al-Ansary M.D., *Determination of stretch-bendability of sheet metals*, Int. J. Adv. Manuf. Technol., **12**, 207–220, 1996.

23. Timoshenko S.P., *Strength of materials: part III, advanced theory and problems*, D. Van Nostrand Co., New Jersey 1956.

24. ABAQUS 6-9.1 User Manual.

25. Worsfold M., *The Effect of Corrosion on the Structural Integrity of Commercial Aircraft Structure*, published in RTO MP-18, 1998.

26. Herrmann A.S., Zahlen P., Zuardy I., *Sandwich Structures Technology in Commercial Aviation*, Sandwich Structures 7: Advancing with Sandwich Structures and Materials, 13–26, 2005.

Received March 18, 2012; revised version August 1, 2012.

ENGINEERING TRANSACTIONS • *Engng. Trans.* • **60**, 3, 205–213, 2012
Polish Academy of Sciences • Institute of Fundamental Technological Research (IPPT PAN)
National Engineering School of Metz (ENIM)
SIXTY YEARS OF THE ENGINEERING TRANSACTIONS

Characterization of Dynamic Friction Factor for FEM Modeling of High Speed Process

Jean-Jacques ARNOUX, Guy SUTTER, Gautier LIST

Laboratoire d'Etude des Microstructures et de Mécanique des Matériaux
UMR CNRS 7239- Ile du Saulcy – 57045 Metz cedex
e-mail: {jean-jacques.arnoux,guy.sutter,gautier.list}@univ-lorraine.fr

The present study aims to establish through a series of friction tests the trends of the dynamic factor according to sliding speed. A ballistic set-up using an air gun launch is used to measure the friction coefficient for the steel/carbide contact between 15 m/s and 80 m/s. Since the experimental characterization of friction is a key factor in the development of high speed process such as high speed machining, the experimental quantification is introduced into a cutting model by finite elements method. Modeling results are compared with cutting forces measured on a similar experimental device, which can reproduce perfect orthogonal cutting conditions.

Key words: dynamic friction, ballistic set-up, high speed process, finite element method.

1. Introduction

The frictional phenomena at the tool-chip interface cause plastic deformations in a region of the chip adjacent to the tool rake face. In this area, called secondary shear zone, the material is subjected to high shear producing an important rise in temperature due to friction and plastic work. Close to the cutting edge, the pressure is very large (∼1 GPa) and the material speed is severely reduced. The friction stress has a value in the order of the flow stress k in the chip. The pressure progressively decreases by moving away the tool tip, and at the end of the contact, the sliding speed tends to the chip velocity V_{chip}. In this zone, the relationship between the normal stress σ_n and the tangential stress τ_n is usually modeled using the friction Coulomb's law:

$$\tau_f = \mu\sigma_n, \tag{1.1}$$

where μ is the friction coefficient. The friction coefficient μ is therefore representative of the sliding contact for pressures of several hundred MPa. In analytical

and numerical models of metal cutting, the knowledge of the value of μ is very important because it controls both the cutting force and the temperature rise at the contact. To choose the suitable value of μ, experimental results such as those found thanks to "split tool" method [1–3], should be used. Unfortunately, these experiments are still infrequent and reserved for conventional machining (low cutting speed). Moreover, experimental results based on the "split-tool" show a high degree of incertitude in the determination of μ.

An alternative way to select the values of μ is to use other experiments that can reproduce the tribological conditions that occurred in machining [4]. A wide variety of experiences are then needed to fully characterize the involved phenomena by reproducing the conditions of local pressure and sliding speeds. These conditions must be achieved with a simple geometry for which the measurement of the contact parameters can be made easily. In this paper, experimental results concerning the values of μ are presented. For characterizing the friction behaviour at the tool-chip interface, a mean normal pressure about 400 MPa and high sliding velocity are imposed during the presented tests. The extreme pressures (> 1 GPa) present near the tip-tool combined with low speed are not considered in the experimental study. An application in the case of FEM modelling of High Speed Machining is discussed.

2. Experimental devices

An original sensor for measuring forces generated during friction is developed to combine high sliding speed and high contact pressure. This load sensor is integrated on a ballistic bench currently being tested at a maximum speed of 120 m/s. The ballistic device, presented in Fig. 1, is made up of two coaxial tubes. The first one is the launch tube and the second is the receiving tube leading to a shock absorber. This equipment was also developed for the study of cutting process under extreme conditions [5] and reproduce perfectly orthogonal cutting conditions without drawback induced by industrial machining. The quasi-instantaneous expansion of a compressed air propels a projectile at high speed into the launch tube. A sufficient length of this tube, combined with

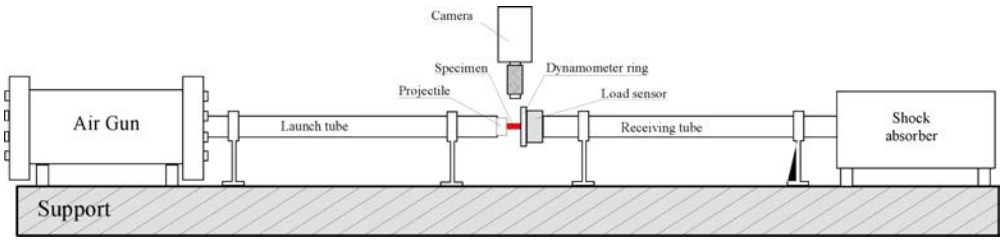

Fig. 1. Ballistic set-up dedicated to the cutting and the friction study.

a mass of the projectile adjusted (different geometries, different materials), provides almost constant speed (less than 4% variation) to the projectile during the process. A set of three sensors record precisely the velocity and acceleration of the projectile.

The load sensor schematically shown in Fig. 2a, attached to the receiving tube, supports a dynamometer ring that imposes a normal force (F_N) adjusted by the dimensions of the different part in contact. This force generates a normal pressure between the cutting tool and the specimen (moving specimen). Setting

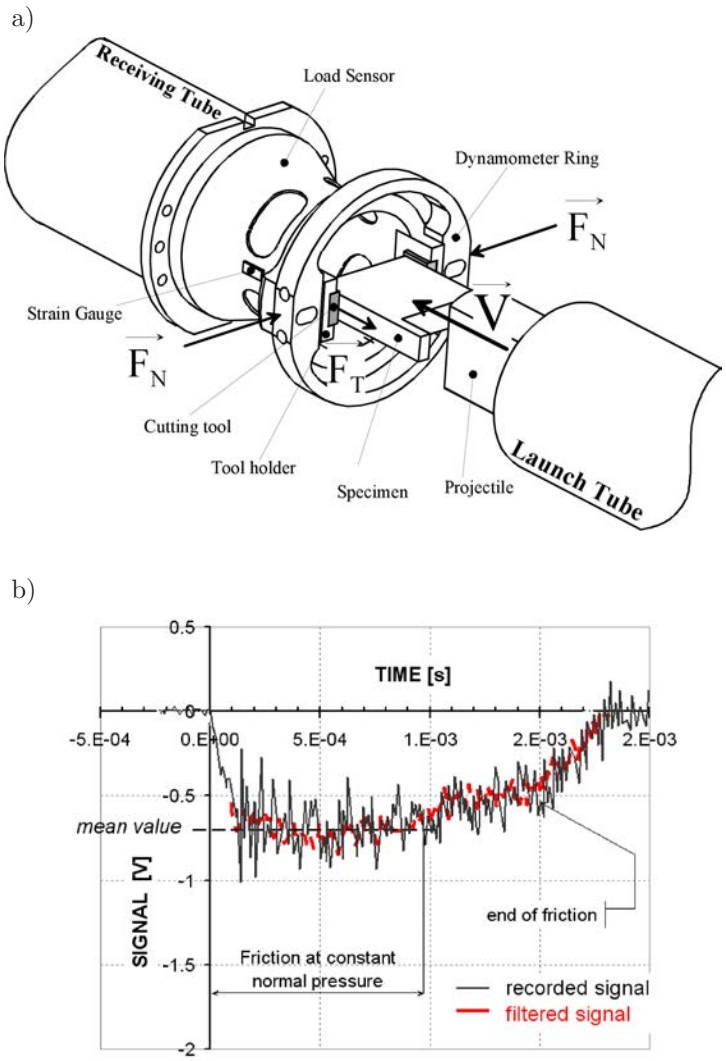

FIG. 2. a) Details of dynamical tribometer designed to able to reproduce the contact between a cutting tool and a workpiece; b) signal recorded by the strain gauge located on the load sensor at 40 m/s.

the translation speed of the specimen is caused by the impact of the projectile. The entire specimen is received in a shock absorber. The post-mortem analysis of rubbed surfaces is then possible. The load sensor was designed to be easily adapted to another propeller as a conventional dynamical hydraulic tensile machine. The hydraulic jack of the tensile machine takes the role of the projectile and ensures the movement of the specimen.

Figure 2b presents a recorded signal used to calculate the tangential force (F_T) and deduce the friction coefficient ($\mu = F_T/F_N$). The filtered signal is deduced from the signal recorded by the stain gauges by applying a LPF (low pass filter) of 10 kHz. The filtered signal significantly improves the visibility of a mean value of the friction force.

Experimental and numerical calibrations are performed to convert the mean signal value into force intensity. The load sensor and its implementation on the dynamic bench have been firstly modeled by FEM in ABAQUS. In a second part, it has been statically and dynamically calibrated, allowing the validation of the FEM model. This dynamic calibration has been achieved thanks to direct impacts of the projectile with different weights and for speeds limited at 10 m/s.

3. Experimental evolution of the friction coefficient

Figure 3 illustrates the evolution of dry friction of a mid-hard steel C22 on an uncoated carbide tool. The steel friction surfaces are obtained by grinding in the same direction as the rubbing movement ($R_a = 0.8$ μm). It is important to note that the tests replicated friction conditions only with a single pass between two new surfaces (not running-in phase). It is observed that friction coefficient decreases with increasing sliding velocity according to previous works [6]. A similar trend has also been observed in [7, 8]. A minimum value of the coefficient seems to be reach and then with further increasing velocity an opposite tendency is observed.

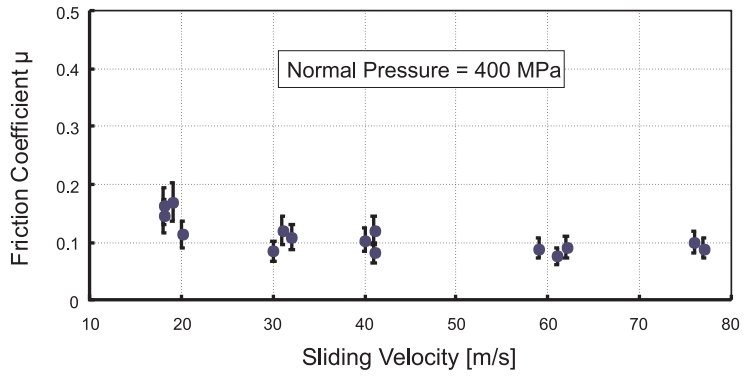

Fig. 3. Dry friction coefficient for the sliding of steel C22 on an uncoated carbide tool.

4. Application to HSM

4.1. Modeling

The metal cutting is modeled by the finite element method thanks to the code ABAQUS/Explicit in version 6.8. The 2D model, with four nodes elements, follows a Lagrangian scheme to study the evolution of chip formation from its initial phase until the steady state. The tool is considered as an elastic rigid body while the workpiece material follows a thermoviscoplastic behavior described by the Johnson-Cook's law [9, 10]:

$$\overline{\sigma} = \left[A + B\left(\overline{\varepsilon}^{p}\right)^{n}\right]\left[1 + C\ln\left(\frac{\dot{\overline{\varepsilon}}^{p}}{\dot{\varepsilon}_{0}^{p}}\right)\right]\left[1 - \left(\frac{T - T_{\text{room}}}{T_{\text{melt}} - T_{\text{room}}}\right)^{m}\right], \tag{4.1}$$

where $\overline{\sigma}$ is the effective flow stress of the material, $\overline{\varepsilon}^{p}$ the effective plastic strain and $\dot{\overline{\varepsilon}}^{p}$ the effective strain rate, $\dot{\varepsilon}_{0}^{p}$ the reference plastic strain-rate of 1/s, T_{room} the room temperature and T_{melt} (1520°C) the melting temperature. A, B, C are the material constants, n the strain hardening exponent and m the thermal softening exponent.

Because of the similarity of compositions between the studied C22 steel and the CRS1018 steel, the other used parameters summarized in Table 1 are approximated by the results presented by [10, 11].

Table 1. Johnson-Cook parameters used for C22 steel.

A [MPa]	B [MPa]	N	C	m	D_1	d_2	d_3
520	269	0.282	0.0476	0.533	0.24	1.1	1.5

A damage criterion is also applied to the workpiece elements allowing the material separation [11, 12]. The failure of an element is effective when the critical the damage parameter D exceeds the value of 1:

$$D = \sum \frac{\Delta\overline{\varepsilon}^{p}}{\overline{\varepsilon}^{f}}. \tag{4.2}$$

$\Delta\overline{\varepsilon}^{p}$ is the increment of plastic deformation during a cycle of integration and $\overline{\varepsilon}_{f}$ the failure strain under the condition of triaxiality:

$$\overline{\varepsilon}_{f} = d_1 + d_2 \exp\left(d_3 \frac{\sigma_m}{\overline{\sigma}}\right), \tag{4.3}$$

where σ_m is the hydrostatic pressure and d_1, d_2 and d_3 are the damage failure material constants reported in Table 1.

To calculate the friction stress, the following relationship is used:

$$\tau_f = \min(\mu p, \tau_{\text{crit}}). \tag{4.4}$$

At very high pressure, $\tau_f = \tau_{\text{crit}}$ where τ_{crit} is a maximum value that τ_f cannot exceed. For lower pressures, the friction Coulomb's law is then effective. The value of τ_{crit} is generally regarded as the shear flow stress k in the material. The choice of the parameters τ_{crit} and μ is critical because τ_{crit} and μp are also criteria to allows a contact element to slide along the tool. Therefore, these parameters control not only the values of the shear stress and the temperature rise but also the morphology of the chip.

4.2. Results and discussion

To study the influence of friction in the numerical model, cutting tests are carried in the same range of velocities. During these tests, the cutting force normal to the rake face is measured and used to emphasize the consequence of the friction parameter. Orthogonal cutting tests are performed on the same ballistic device [5] used for the friction tests. The load sensor is changed to support two symmetric carbide cutting tools. The workpiece is attached on the projectile. An intensified CCD camera is used to record temperature field during the process [13]. To carry out the numerical simulations, different approaches are conducted. In the first one, which is usually adopted, the value of τ_{crit} is constant and equal to the shear yield stress ($\tau_{\text{crit}} = k_0 = \sigma_0/\sqrt{3}$ with $\sigma_0 =$ 289 MPa) and μ is fixed for all speeds. Two values of μ were firstly selected as 0.1 and 0.25. The range for μ was chosen from the experimental results illustrated in Fig. 3. Figure 4 shows the evolution of cutting forces as a function of cutting speed. Compared to the experimental results, the trends are conserved in spite of a certain overestimate for the cutting forces.

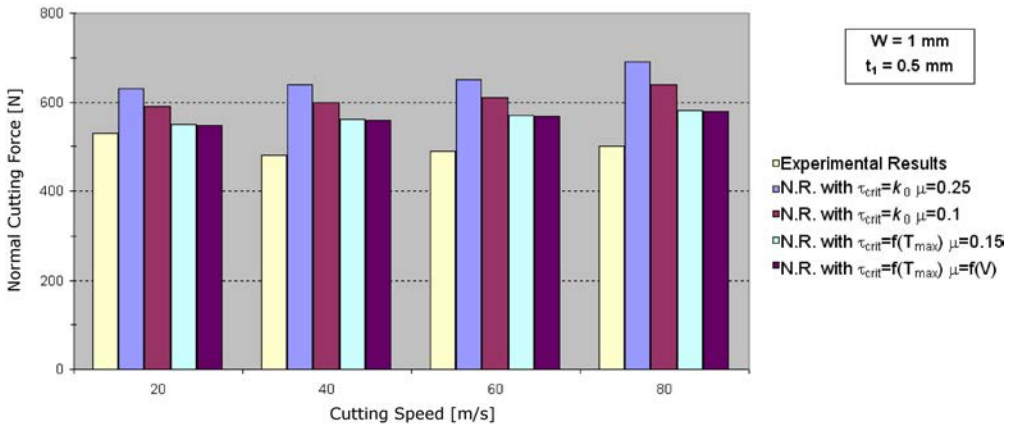

FIG. 4. Experimental and Numerical Results (N.R.) of the normal cutting force as a function of the cutting speed (C22).

A second approach can be performed, with a mean value of μ fixed to 0.15 and the critical stress defined as a function of the maximal contact temperature $T_{\max}$ by Eq. (4.1): $\tau_{\text{crit}} = f(T_{\max})$. $T_{\max}$ is deduced from the experimental temperature field measured in the chip during orthogonal cutting tests as shown in Fig. 5. This second approach is interesting because the numerical results are improved by trending to the experimental measurements. The cutting forces obtained in the simulations decrease due to the drop of τ_{crit} through the effect of thermal softening of the material. The last approach keeps τ_{crit} as a function of the temperature and adjusts the friction coefficient with the experimental values ($\mu = f(V)$), cf. Fig. 3. A weak difference of the results emphasizes that the role of μ is minimized in the friction stress modeling. Indeed, the combination of $\tau_{\text{crit}} = f(T_{\max})$ and $\mu = f(V)$ leads to $\tau_f = \tau_{\text{crit}} \leq \mu p$ over almost the entire contact area.

Figure 5 illustrates a comparison between the experimental and numerical results for the following cutting conditions: the rake angle $\alpha = 0°$, the uncut chip

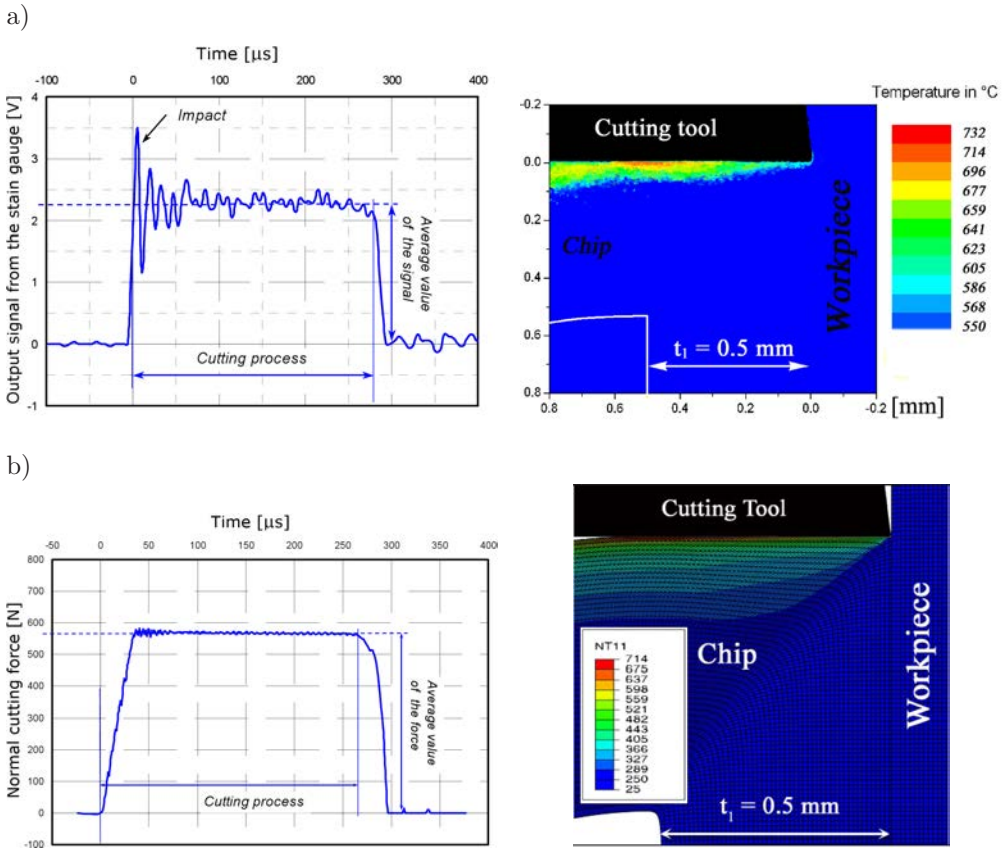

FIG. 5. Cutting forces and temperature maps obtained during orthogonal cutting test – material C22: a) experimental; b) simulation.

thickness $t_1 = 0.5$ mm and the cutting speed $V_C = 42$ m/s. A good correlation is observed not only for the cutting forces but also for the temperature field when the contact parameters are optimized.

5. Conclusion

The combination of three experimental devices allowed defining the friction coefficient for a large range of sliding velocities up to 80 m/s. The obtained values are applied to the high speed cutting process to describe the friction stress at the tool-chip interface. The equipment enables to reach the dry sliding friction condition with pressure of 400 MPa. Complementary orthogonal high cutting tests are also conducted in order to measure cutting forces and temperature fields in the chip. All experimental data are employed to validate the friction modeling in the finite element code ABAQUS. A good correlation is overall obtained. However, the results highlighted limits in the friction model based on Eq. (4.4) because the criterion restrict the effect of the contact temperature and the real friction coefficient μ. Coulomb's friction coefficient could be formulated according to the contact pressure, the temperature and the sliding velocity.

Acknowledgment

The material presented in this paper has been shown at Workshop 2012 on Dynamic Behavior of Materials and Safety of Structures, Poznan, 2–4 May, 2012.

References

1. Childs T.H.C., Mahdi M., *On the stress distribution between the chip and tool during metal turning*, Annals of the CIRP, **38**, 55–58, 1989.
2. Usui E., Shirakashi T., *Mechanics of machining – from descriptive to predictive theory*, ASME Publication PED, **7**, 13–35, 1982.
3. Buryrta D., Sowerby R. and Yellowley I., *Stress distribution on the rake face during orthogonal machining*, Int. J. Mach. Tools Manufacturing, **14**, 721–739, 1994.
4. Brocail J., Watremez M., Dubar L., *Identification of a friction model for modelling of orthogonal cutting*, Int. J. Tools and Manufacture, **50**, 807–814, 2010.
5. Sutter G., *Chip geometries during high speed machining for orthogonal cutting conditions*, J. Mach. Tools Manufacturing, **45**, 719–726, 2005.
6. Sutter G., Philippon S., Molinari A., *An experimental investigation of dry friction for a large range of sliding velocities*, Matériaux et Techniques HS, pp. 33–37, 2004.
7. Lim S.C., Ashby M.F., Brunton J.H., *The effects of sliding conditions on the dry friction of metals*, Metallurgica, **37**, 3, 767–772, 1989.

8. Lim S.C., Ashby M.F., *Wear-Mechanism maps*, Acta Metallurgica, **35**, 1, 1–24, 1987.

9. Johnson G.R., Cook W.H., *A constitutive model and data for metals subjected to large strains, high strain rates and high temperatures*, Proc. 7th Inter. Symp. on Ballistics Proceedings, pp. 541–547, 1983.

10. Sasso M., Newaz G., Amodio D., *Material characterization at high strain rate by Hopkinson bar tests and finite element optimisation*, Mat. Sci. Eng., **A487**, 289–300, 2008.

11. Goto D., Becker R., Orzechowski T., Springer H., Sunwoo A., Syn C., *Investigation of the fracture and fragmentation of explosively driven rings and cylinders*, Int. J. Impact Eng., **35**, 1547–1556, 2008.

12. Johnson G.R., Cook W.H., *Fracture characteristics of three metals subjected to various strains, strain rates, temperatures and pressures*, Eng. Fracture Mech., **1**, 31–48, 1985.

13. Ranc N., Pina V., Sutter G., Philippon S., *Temperature measurement by visible pyrometry: orthogonal cutting application*, J. Heat. Transfer. ASME, **126**, 931–936, 2004.

Received April 14, 2012; revised version August 30, 2012.

ENGINEERING TRANSACTIONS • *Engng. Trans.* • **60**, 3, 215–223, 2012
Polish Academy of Sciences • Institute of Fundamental Technological Research (IPPT PAN)
National Engineering School of Metz (ENIM)
SIXTY YEARS OF THE ENGINEERING TRANSACTIONS

Identification of Johnson-Cook Equation Constants using Finite Element Method

Michał GRĄZKA, Jacek JANISZEWSKI

Military University of Technology, Institute of Armament Technology
Kaliskiego 2, 00-908 Warszawa, Poland
e-mail: {mgrazka; jjaniszewski}@wat.edu.pl

The objective of this work is to develop an identification technique of the Johnson-Cook equation constants for copper Cu-ETP samples. In this paper we describe a method of constant identification using the Taylor impact test and finite element analysis. Nowadays the most popular method of constant identification method is the split Hopkinson pressure bar technique. This method is quite easy but needs very expensive laboratory equipment. To implement this method we have to make a lot of different tests in order to have enough information about dynamic properties. We decided to prepare an identification process algorithm using the Taylor impact test as a basic type of experimental and numerical simulation.

Key words: Johnson-Cook material model, finite element analysis, identification and optimization procedures.

1. Introduction

The Taylor impact test is a one of the oldest of the experimental methods from which we can measure some materials properties. This kind of experiment made its beginning during the Second World War [1]. This method of experiment was used to measure dynamic yield stress. It was important at that time because weapon constructors needed more information about dynamic material properties in order to design better protection barriers.

For many years this kind of experiment was used only for that propose. When the new era of computer techniques started it opened a new door for the Taylor impact test. At that point in time this experiment was not only used to measure dynamic yield stress. Computer techniques and special machines for measurement, high-speed cameras for example, have found a new use for the Taylor impact test. Those new techniques of measurement were used to calculate the propagation of plastic and elastic wave velocities. Information about those parameters is very important if we want to describe the dynamic behavior

of materials. The importance of these parameters grows when computer techniques are used to make simulations of material deformation under dynamic loads. Explicit finite element method was used during the identification process. Researchers using computer simulations can make many different experiments but there is a one big problem. To make these numerical experiments we need information about the constitutive equation which can be used to describe the dynamic behavior of materials in the plastic range.

In this paper we present how the results of laboratory experiments were connected with numerical simulation. In this connection between results of laboratory experiments and numerical simulation is a method which can be used for calculating the constants of the constitutive equation.

2. Taylor impact test

The Taylor impact test is one of a few methods that can be used to calculate dynamic parameters. This experimental method is connected with dynamic deformation of cylindrical samples on a rigid wall (Fig. 1).

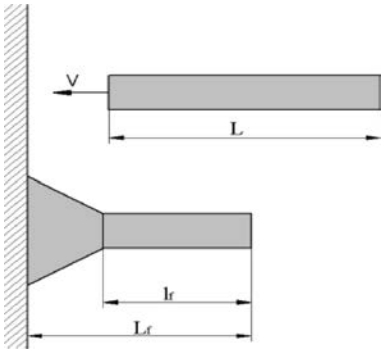

Fig. 1. Illustration of the idea of the Taylor impact test [1].

The result of laboratory experiments consists of a plastically deformed sample. The deformation is at one end of the sample only. Information about the size of this deformation is necessary for calculation of the dynamic yield stress. The calculation can be made using the simple equation [1]:

$$Y = \frac{\frac{1}{2}\rho V^2 \left(1 - \frac{l_f}{L}\right)}{\left(1 - \frac{L_f}{L}\right) \ln\left(\frac{L}{l_f}\right)}. \tag{2.1}$$

To calculate the dynamic yield stress we only need information about the impact velocity V, the length of the undeformed part of sample l_f, and L, L_f – the initial and final length of the sample, respectively.

Information about dynamic yield stress is insufficient if we want to make a computer simulation, but this knowledge is sufficient when we classify the material. During the numerical simulation, we need more than just the dynamic yield stress. All information necessary for analysis with finite element method we have from the constitutive equation.

3. Johnson-Cook model

Johnson-Cook equation is one of the most popular of the material models that can be used for calculation of the relationship during deformation with strain rate order of 10^3 s^{-1}, or higher. Equation (3.1) illustrates a mathematical interpretation of the Johnson-Cook material model [1, 4]. That is:

$$\sigma = [A + B\varepsilon^n] \cdot \left[1 + C \ln\left(\frac{\dot{\varepsilon}}{\dot{\varepsilon}_0}\right)\right] \cdot \left[1 - \left(\frac{T - T_0}{T_m - T_0}\right)^m\right]. \tag{3.1}$$

The model presented by Johnson and Cook in the nineteen-eighties is very simple and is connected by three different parts. The first part describes the relationship between strain and stress; the second part of the equation presents the relationship between strain rate and stress; and the last part of the Johnson-Cook equation connects the stress value with material temperature during plastic deformation (temperature material softening). The Johnson-Cook equation has five constants: *A, B, C, n* and *m* [1, 4]. These five constants are characteristic for the given material. Information about these five constants can be used for calculating material dynamic response during plastic deformation. The Johnson-Cook material model gives information about the strain-stress curve in the plastic range, so it is really useful during computer simulation. This material model has one more thing that made it very popular: we can use it for describing almost any type of material. Moreover, it is a very useful material model because it is easy to use and needs only five constants to describe material stress-strain characteristics.

4. Laboratory equipment

This work is experimental and numerical. In the experimental part of this work, the Taylor impact test was used as a source of measuring the dynamic properties of materials. The most important information used during the numerical procedure was: the impact velocity and sample final shape after deformation on a rigid wall. Laboratory experiments were done on a special experimental setup which was built for the Taylor impact test. Figure 2 presents the helium gas gun setup, as prepared for the Taylor impact test.

a) b)

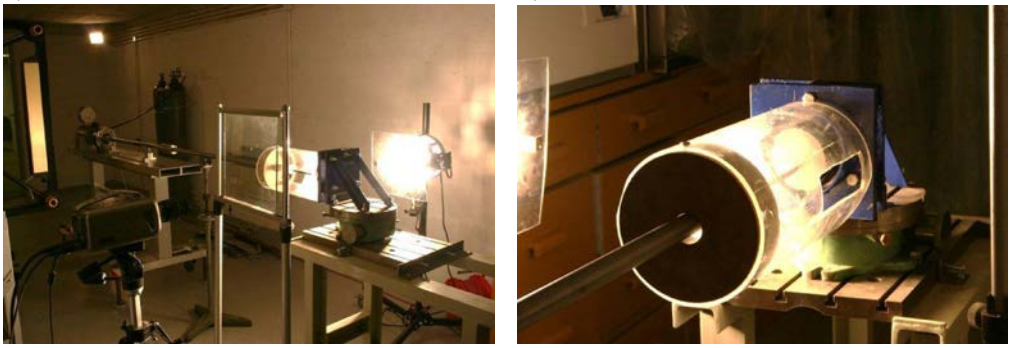

FIG. 2. Picture of the helium gas gun: a) The Taylor impact test setup; and b) a rigid target with protective surface.

After the Taylor impact test, the Copper Cu-ETP samples were deformed on one end. The final shape after deformation was measured using a coordinate measuring machine (a ZEISS measuring machine used) [2]. Figure 3 shows this machine (Fig. 3a) and a sample during the measurement process (Fig. 3b).

a) b)

FIG. 3. a) The Carl Zeiss measuring machine; b) the sample shape measuring process [2].

The coordinate measuring technique was used to measure the shape of the sample after the Taylor impact test. During this process we measured the final length L_f, the length of undeformed sample part l_f and the final diameter $\emptyset_f$ at several points. Information about these parameters was important in the

second part of this work. The next part of this work is related to numerical simulation which was implemented here using the explicit solver of the "Ansys Autodyn" program. The numerical simulation was used to calculate the process of deformation during the Taylor impact test (Fig. 4).

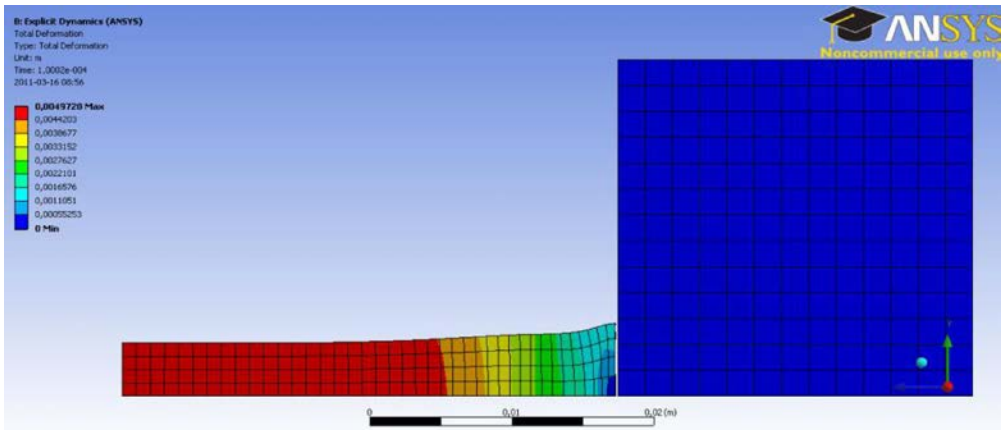

FIG. 4. Results of numerical simulation of the Taylor impact test at a hitting speed $v_o = 130$ m/s (total deformation value).

In Fig. 4 the total deformation of a copper sample is shown after the Taylor impact test. During this numerical analysis the sample hit the rigid wall at a speed of 130 ms^{-1}.

5. Methodology of identification Johnson-Cook equation constants

The aim of this research was to prepare a methodology of investigation of the constants of the Johnson-Cook equation. In this paper we proposed using the Taylor impact test and computer identification as a method of calculating the parameters of the Johnson-Cook equation. Figure 5 illustrates the algorithm of identification and optimization process.

The identification algorithm presented in Fig. 5 was tested on copper cylindrical samples. The samples were 60 mm long and 12.05 mm in diameter. Samples were accelerated to a speed between 100–180 ms^{-1} by a helium gas gun. After the laboratory experiments the samples were deformed at one end. In the next step of the identification process we measured the final sample shape. Information about the final length, maximum diameter and length of the undeformed part of the sample were used at next point of the identification procedure. The Ansys Autodyn computer program was used to make an explicit finite element method calculation. The initial conditions for computer simulation were taken

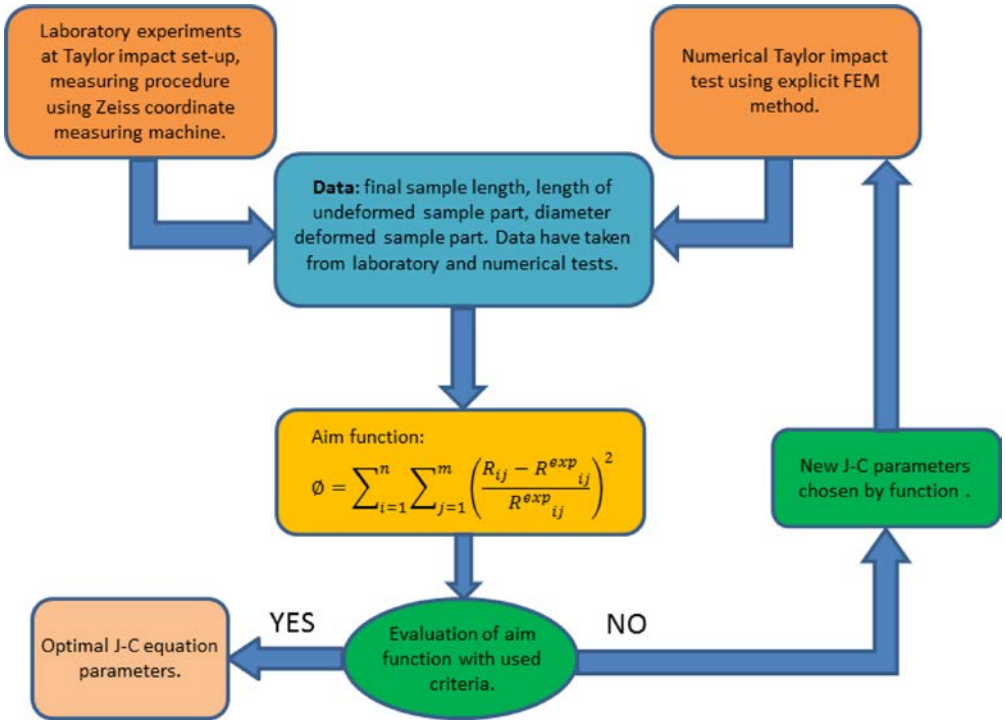

FIG. 5. Schematic of the identification algorithm used for numerical analyses.

from the laboratory experiments. The initial geometry of the sample and the impact velocity are necessary parameters for the numerical simulation, since without these parameters the computer simulation would not make sense. Information about the impact speed was taken from the high-speed camera recording. During the laboratory experiment all tests were recorded using a Phantom V12 high-speed camera and after, the numerical simulation of the Taylor impact test starts. At that point we can not yet make use of the identification and optimization procedure, as we have not declared the aim function which will be used during the identification process. To do this we connect the numerical Taylor test simulation with an optimization program. In optimization program a genetic algorithm was used for the identification procedure. A typical optimization procedure like gradient methods didn't give the correct results to our problem. To solve the problem of the identification Johnson-Cook parameters, we propose the following equation as an aim function:

$$f(R_{ij}) = \sum_{i}^{n} \sum_{j}^{m} \left(\frac{R_{ij} - R_{ij}^{\exp}}{R_{ij}^{\exp}} \right)^2 . \tag{5.1}$$

During identification of parameters of the Johnson-Cook equation, the optimization program looked for a minimum of the aim function. The aim function is a sum of errors between numerical and experiment parameters. Values of R_{ij} represent data from numerical simulation and $R_{ij}^{\exp}$ represents data from the laboratory experiment. For our considerations we propose that the identification procedure be made on the final sample shape after the deformation with different impact speeds. The variable index i represents a geometric parameter, for example, the sample's final length value; and variable index j represents different impact speeds.

6. Results of identification procedure

The result of our work is found values for the Johnson-Cook equation parameters. Calculation was done using the finite element method and an optimization algorithm. Copper Cu-ETP Johnson-Cook parameters were identified during this procedure. Table 1 illustrates values of these parameters.

Table 1. Values of the Johnson-Cook equation parameters calculated during the identification process.

Constant	Value
A	100 MPa
B	263 MPa
n	0.23
C	0.029
m	0.98

Before our experiments began copper samples were annealed at temperature 500°C for one hour. This process was undertaken because in literature [1] we found information about Johnson-Cook parameters for this kind of material. Table 2 presents Johnson-Cook parameters reported from the literature.

Table 2. Johnson-Cook parameters reported from literature [1].

Constant	Value
A	90 MPa
B	292 MPa
n	0.31
C	0.025
m	1.09

In our tests we made ten laboratory experiments with the same type of sample. As can be seen the results of our work (Table 1) are different from those of Table 2; however, we can not say that the values in Table 1 are incorrect because the differences between the parameters in Table 1 and 2 are too small. To make some assessment of those parameter values we prepared a verification method.

In the present work we decided to compare the shape of the sample after the laboratory experiment with the shape of sample calculated in numerical simulation. Figure 6 presents two curves which show the shape of samples after the deformation process.

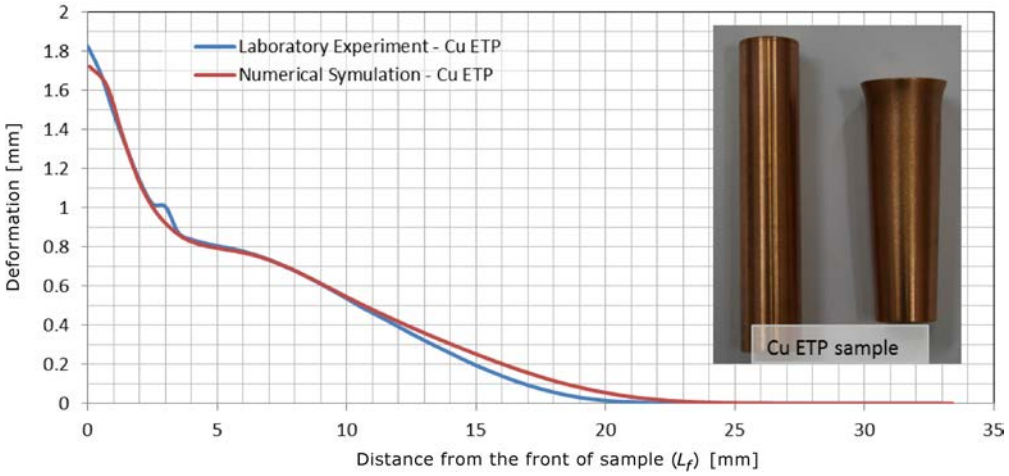

FIG. 6. Sample shape after plastic deformation during the Taylor impact test [5].

The result of comparing these two curves shows small differences. The biggest differences are in the front of the sample and in the place where the plastic wave has stopped. The error in the front of the sample is a result of an incorrect value for the friction coefficient used during the computer simulation. The error in the second place is a result of different Johnson-Cook equation parameters. For better comparison we calculate the value of the area under the curves. This information was used for a global error calculation. The fault was calculated as the quotient of the difference between values under the curves. The fault value is 3.8%.

In conclusion we can say that the proposed method of calculation of the Johnson-Cook equation parameters is practical and can be used as an alternative to the Hopkinson pressure bar test. The main advantage of this method over the Hopkinson pressure bar method is that it does not need a few different types of experiments to identify material model parameters. The proposed method needs only one type of experiment (the Taylor impact test) for the whole identification

procedure. The only problem is that our method needs some kind of verification procedure; a solution to which is being investigated in our laboratory. At this point of our work we can say that the presented method has great potential and can be used as a main identification method like the Hopkinson pressure bar technique.

Acknowledgment

The material presented in this paper has been shown at Workshop 2012 on Dynamic Behavior of Materials and Safety of Structures, Poznan, 2–4 May, 2012.

References

1. Meyers M.A., *Dynamic Behavior of Material*, John Wiley & Sons, New York 1994.
2. Janiszewski J., Grązka M., *Coordinate measuring technique at researching dynamic behavior of materials after the impact Taylor test* [in Polish: *Współrzędnościowa technika pomiarowa w badaniach dynamicznych właściwości materiałów metodą Taylora*], Mechanik nr 1/2011, 56.
3. *Ansys Autodyn User's Manual*, ANSYS, Inc.
4. Zukas J.A., *High Velocity Impact Dynamics*, John Wiley & Sons, New York 1990.
5. Grązka M., *Impact Taylor test during the Johnson-Cook parameters identification* [in Polish: *Zastosowanie testu Taylora do wyznaczania stałych materiałowych modelu konstytutywnego Johnsona-Cooka*], TKI Conference Bełchatów 2011.

Received May 25, 2012; revised version August 21, 2012.

ENGINEERING TRANSACTIONS • *Engng. Trans.* • **60**, 3, 225–284, 2012
Polish Academy of Sciences • Institute of Fundamental Technological Research (IPPT PAN)
National Engineering School of Metz (ENIM)
SIXTY YEARS OF THE ENGINEERING TRANSACTIONS

Multiscale Constitutive Modelling of the Influence of Anisotropy Effects on Fracture Phenomena in Inelastic Solids

Piotr PERZYNA

Institute of Fundamental Technological Research
Polish Academy of Sciences
Pawińskiego 5B, 02-106 Warszawa, Poland
e-mail: pperzyna@ippt.pan.pl

The main objective of the present paper is the consistent development of the thermodynamical theory of elasto-viscoplasticity within the framework of a unique constitutive material structure. The focus of attention on the description of the influence of anisotropy effects on fracture phenomena is proposed.

In the first part a general principle of determinism is formulated and a unique constitutive material structure is developed. The original conception of the intrinsic state of a particle X during motion of a body $\mathcal{B}$ has been assumed. A notion of the method of preparation of the deformation-temperature configuration of a particle X has been proposed as a simple way of the gathering information for the description of the internal dissipation. As the basis of the thermodynamical requirements the dissipation principle in the form of the Clausius-Duhem inequality is assumed. By particular assumption of the method of preparation space for a unique constitutive material structure the internal state variable material structure has been constructed. In the second part the thermodynamical theory of elasto-viscoplasticity within the framework of the internal state variable material structure is formulated. Introduction of a finite set of the internal state variables is based on multiscale considerations in analysis of the physical foundations of inelastic solids and experimental observation results. Particular attention is focused on the determination of the evolution laws for the introduced internal state variables. Fracture criterion based on the evolution of the anisotropic intrinsic microdamage is proposed.

1. Prologue

A main objective of the present paper is the development of the thermodynamical theory of elasto-viscoplasticity as a unique material constitutive structure within the framework of a general covariant deterministic theory. We would like to focus attention on the description of the influence of anisotropy effects

on fracture phenomena as well as on multiscale considerations in the analysis of the physical foundations and experimental motivations.

By a notion of the thermodynamical theory we understand such, which compatible with the principles of thermodynamical processes describes mechanical and thermal phenomena and their interactions.

A theory is called covariant if it is invariant with respect to arbitrary diffeomorphisms (any motion). A theory is deterministic if its internal structure assures a unique evolution of the intrinsic states and it exists a unique mapping between the intrinsic states and values of reactions (cf. NAGEL [61]).

A good physical theory has to describe large range of phenomena based on several simple postulates and should from it result determined predictions, which has to be investigated and according to that what emphasized Karl Popper (cf. POPPER [104]), in principle be suitable to experimental falsification.

Whenever the result of experimental observations agrees with the theoretical predictions, the tested theory becomes certain that is reliable and our confidence to it is growing up, but if new experimental result disclaims theory we have to quit it or to improve it.

The results of experimental observations fulfil in the development of the physical theory a manifold role. The crux of the matter has been presented by Richard Feynman in his Lectures on Physics [37]: "The principle of science, the definition, almost, is the following: The test of all knowledge is experiment. Experiment is the sole judge of scientific "truth". But what is the source of knowledge? Where do the laws that are to be tested come from? Experiment, itself, helps to produce these laws, in the sense that it gives us hints. But also needed is imagination to create from these hints the great generalizations – to guess at the wonderful, simple, but very strange patterns beneath them all, and then to experiment to check again whether we have made the right guess".

Experiment precisely suggests that for proper description of the thermomechanical couplings we have to base our considerations on thermodynamics.

We would like to show advantages, which can be achieved to base the considerations on thermodynamical processes and simultaneously to propose new conception concerning the support the phenomenological thoughts on the results of physics of solids as well as on micro-, meso- and macrosopic, i.e. multiscale experimental investigations. It would be unrealistic to include in the description all the effects observed experimentally. Constitutive modelling is understood as a reasonable choice of effects, which are most important for the explanation of the phenomena described.

Experimental observations concerning investigation of dynamic loading processes have shown that formation of microshear bands influences the evolution of microstructure of material. We can conclude that microshear banding con-

tributes to viscoplastic strain rate effects. On the other hand analysis of recent experimental observations concerning investigations of fracture phenomena under dynamic loading processes suggests that there are two kinds of induced anisotropy: (i) the first caused by the residual type stress produced by the heterogeneous nature of the finite plastic deformation in polycrystalline solids; (ii) the second the fracture induced anisotropy generated by the evolution of the microdamage mechanism. It is noteworthy to stress that both these induced anisotropy effects are coupled.

Section 2 is devoted to the description of kinematics of finite deformation and the stress tensors. The fundamental measures of total deformation are introduced. The description is based on notions of the Riemannien space on manifolds and the tangent space. A multiplicative decomposition of the deformation gradient is adopted. The decomposition of the strain tensor into the elastic and viscoplastic parts is presented. The Lie derivative is used to define all objective rates for the introduced vectors and tensors. The rates of the deformation tensor and the stress tensor are precisely defined.

A general unique constitutive material structure is developed in Sec. 3. The original conception of the intrinsic state of a particle X during motion of a body $\mathcal{B}$ has been assumed. A notion of the method of preparation of the deformation-temperature configuration of a particle X has been proposed as simple way of the gathering information for the description of the internal dissipation. A general principle of determinism for thermodynamical processes has been formulated. The topology for the intrinsic state space and some smoothness assumption for processes and response functions (functionals) are postulated. As the basis of thermodynamic requirements the dissipation principle in the form of the Clausius-Duhem inequality is assumed. The dissipation principle implies two fundamental criteria, namely the criterion of the selection of the response functions (functionals) and the criterion of the accessibility of the intrinsic states. The principle of the increas of entropy has been also deduced. These results have a great importance to the thermodynamical theory of inelastic materials.

In Sec. 4 the internal state variable constitutive structure is presented. Assuming that the method of preparation space for a unique constitutive material structure is a finite dimensional vector space and postulating that the initial value problem for the element of the method of preparation space has unique solutions we construct the material structure with internal state variables. The rate of internal dissipation function for the internal state variable material structure is obtained. From this results we can directly observed that full information given in the method of preparation at the actual intrinsic state essentially determines the rate of internal dissipation for this intrinsic state. This conclusion is of fundamental importance for the physical interpretation of the internal state variables.

Section 5 is focussed on the development of thermo-elasto-viscoplastic constitutive model of a material, which takes into consideration both mentioned earlier induced anisotropy effects as well as observed contribution to strain rate effects generated by microshear banding. The model is developed within the thermodynamic framework of the rate type covariance unique constitutive structure with a finite set of the internal state variables. A set of internal state variables is motivated by experimental observation results, physical foundations and multiscale heuristic considerations, and consists of one scalar and two tensors, namely the equivalent inelastic deformation $\in^p$, the second order microdamage tensor $\boldsymbol{\xi}$, with the physical interpretation that $(\boldsymbol{\xi} : \boldsymbol{\xi})^{1/2} = \xi$ defines the volume fraction porosity and the residual stress tensor (the back stress) $\boldsymbol{\alpha}$.

The equivalent inelastic deformation $\in^p$ describes the dissipation effects generated by viscoplastic flow phenomena, the microdamage tensor $\boldsymbol{\xi}$ takes into account the anisotropic intrinsic microdamage mechanisms on internal dissipation and the back stress tensor $\boldsymbol{\alpha}$ aims at the description of dissipation effects caused by the kinematic hardening. To describe suitably the influence of both induced anisotropy effects and the stress triaxiality observed experimentally the new kinetic equations for the microdamage tensor $\boldsymbol{\xi}$ and for the back stress tensor $\boldsymbol{\alpha}$ are proposed.

The relaxation time is used as a regularization parameter. To describe the contribution to strain rate effects generated by microshear banding we propose to introduce certain scalar function which affects the relaxation time T_m in the viscoplastic flow rule. Fracture criterion based on the evolution of the anisotropic intrinsic microdamege is formulated.

The purpose of the development of this theory is in future applications for the description of important problems in modern manufactoring processes, and particularly for meso-, micro-, and nano-mechanical issues[1)]. This description is needed for the investigation by using the numerical methods how to avoid unexpected plastic strain localization and localized fracture phenomena in new manufacturing technology.

2. Kinematics of finite deformation and fundamental definitions

2.1. Fundamental measures of total deformation

Our notation throughout is as follows: $\mathcal{B}$ and $\mathcal{S}$ are manifolds, points in $\mathcal{B}$ are denoted $\mathbf{X}$ and those in $\mathcal{S}$ by $\mathbf{x}$. The tangent spaces are written $T_{\mathbf{X}}\mathcal{B}$ and

[1)] Good examples of such applications are very recent publications as follows: Glema *et al.* [44], Nowacki *et al.* [66] and Perzyna [93, 94].

$T_{\mathbf{x}}\mathcal{S}$. Coordinate systems are denoted $\{X^A\}$ and $\{x^a\}$ for $\mathcal{B}$ and $\mathcal{S}$, respectively, with corresponding bases $\mathbf{E}_A$ and $\mathbf{e}_a$ and dual bases $\mathbf{E}^A$ and $\mathbf{e}^a$.

Let us take the Riemannian spaces on manifolds $\mathcal{B}$ and $\mathcal{S}$, i.e. $\{\mathcal{B}, \mathbf{G}\}$ and $\{\mathcal{S}, \mathbf{g}\}$, the metric tensors $\mathbf{G}$ and $\mathbf{g}$ are defined as follows $\mathbf{G} : T\mathcal{B} \to T^*\mathcal{B}$ and $\mathbf{g} : T\mathcal{S} \to T^*\mathcal{S}$, where $T\mathcal{B}$ and $T\mathcal{S}$ denote the tangent bundles of $\mathcal{B}$ and $\mathcal{S}$, respectively, and $T^*\mathcal{B}$ and $T^*\mathcal{S}$ their dual tangent bundles.

Let the metric tensor G_{AB} be defined by $G_{AB}(\mathbf{X}) = (\mathbf{E}_A, \mathbf{E}_B)_{\mathbf{X}}$, and similarly define g_{ab} by $g_{ab}(\mathbf{x}) = (\mathbf{e}_a, \mathbf{e}_b)_{\mathbf{x}}$, where $(\ ,\ )_{\mathbf{X}}$ and $(\ ,\ )_{\mathbf{x}}$ denote the standard inner products in $\mathcal{B}$ and $\mathcal{S}$, respectively.

Let

$$\mathbf{x} = \phi(\mathbf{X}, t) \tag{2.1}$$

be regular motion, then $\phi_t : \mathcal{B} \to \mathcal{S}$ is a C^1 actual configuration (at time t) of $\mathcal{B}$ in $\mathcal{S}$. The tangent of ϕ is denoted $\mathbf{F}$ and is called the deformation gradient of ϕ; thus $\mathbf{F} = T\phi$. For $\mathbf{X} \in \mathcal{B}$, we let $\mathbf{F}(\mathbf{X})$ denote the restriction of $\mathbf{F}$ to $T_{\mathbf{X}}\mathcal{B}$.

Thus

$$\mathbf{F}(\mathbf{X}, t) : T_{\mathbf{X}}\mathcal{B} \to T_{\mathbf{x}=\phi(\mathbf{X},t)}\mathcal{S} \tag{2.2}$$

is a linear transformation for each $\mathbf{X} \in \mathcal{B}$ and $t \in I \subset \mathbb{R}$. For each $\mathbf{X} \in \mathcal{B}$ there exists an orthogonal transformation $\mathbf{R}(\mathbf{X}) : T_{\mathbf{X}}\mathcal{B} \to T_{\mathbf{x}}\mathcal{S}$ such that $\mathbf{F} = \mathbf{R} \cdot \mathbf{U} = \mathbf{V} \cdot \mathbf{R}$. Notice that $\mathbf{U}$ and $\mathbf{V}$ operate within each fixed tangent space. We call $\mathbf{U}$ and $\mathbf{V}$ the right and left stretch tensor, respectively. For each $\mathbf{X} \in \mathcal{B}$, $\mathbf{U}(\mathbf{X}) : T_{\mathbf{X}}\mathcal{B} \to T_{\mathbf{X}}\mathcal{B}$ and for each $\mathbf{x} \in \mathcal{S}$, $\mathbf{V}(\mathbf{x}) : T_{\mathbf{x}}\mathcal{S} \to T_{\mathbf{x}}\mathcal{S}$.

The material (or Lagrangian) strain tensor $\mathbf{E} : T_{\mathbf{X}}\mathcal{B} \to T_{\mathbf{X}}\mathcal{B}$ is defined by

$$2\mathbf{E} = \mathbf{C} - \mathbf{I}, \quad (\mathbf{I} \text{ denotes the identity on } T_{\mathbf{X}}\mathcal{B}), \tag{2.3}$$

where

$$\mathbf{C} = \mathbf{F}^T \cdot \mathbf{F} = \mathbf{U}^2 = \mathbf{B}^{-1}. \tag{2.4}$$

The spatial (or Eulerian) strain tensor $\mathbf{e} : T_{\mathbf{x}}\mathcal{S} \to T_{\mathbf{x}}\mathcal{S}$ is defined by

$$2\mathbf{e} = \mathbf{i} - \mathbf{c}, \quad (\mathbf{i} \text{ denotes the identity on } T_{\mathbf{x}}\mathcal{S}), \tag{2.5}$$

where

$$\mathbf{c} = \mathbf{b}^{-1} \qquad \text{and} \qquad \mathbf{b} = \mathbf{F} \cdot \mathbf{F}^T = \mathbf{V}^2. \tag{2.6}$$

The various strain tensors can be redefined in terms of pull-back and push-forward operations. For the material strain tensor $\mathbf{E}$ and the spatial strain tensor $\mathbf{e}$ we have

$$
\begin{aligned}
\mathbf{E}^{\flat} &= \phi^{*}(\mathbf{e}^{\flat}),\\
E_{AB}(\mathbf{X}) &= e_{ab}(\mathbf{x})F^{a}_{A}(\mathbf{X})F^{b}_{B}(\mathbf{X}),\\
\mathbf{e}^{\flat} &= \phi_{*}(\mathbf{E}^{\flat}),\\
e_{ab}(\mathbf{x}) &= E_{AB}(\mathbf{X})(\mathbf{F}(\mathbf{X})^{-1})^{A}_{a}(\mathbf{F}(\mathbf{X})^{-1})^{B}_{b},
\end{aligned}
\tag{2.7}
$$

where the symbol $\flat$ denotes the index lowering operator.

2.2. Finite elasto-viscoplastic deformation

Motivated by the micromechanics of single crystal plasticity we postulate a local multiplicative decomposition of the form

$$
\mathbf{F}(\mathbf{X},t) = \mathbf{F}^{e}(\mathbf{X},t)\cdot\mathbf{F}^{p}(\mathbf{X},t),
\tag{2.8}
$$

where $\mathbf{F}^{e-1}$ is interpreted as the local deformation that releases the stresses from each neighborhood $\mathcal{N}(\mathbf{x}) \subset \phi(\mathcal{B})$ in the current configuration of the body, cf. Fig. 1.

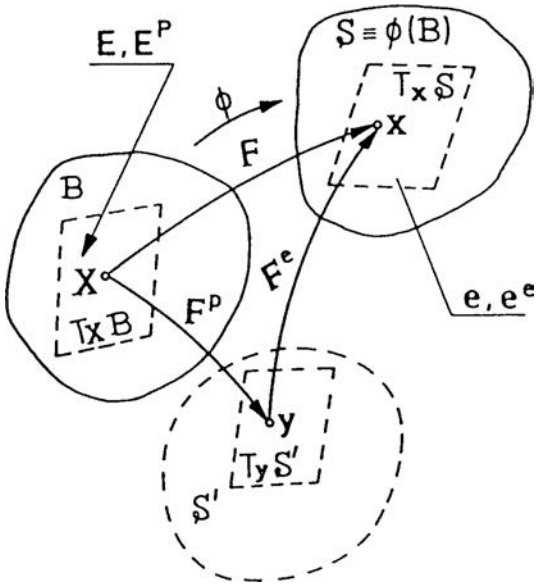

FIG. 1. Schematic representation of the multiplicative decomposition of the deformation gradient.

Let us consider a particle X, which at time $t = 0$ occupied the place $\mathbf{X}$ in the reference (material) configuration $\mathcal{B}$, its current place at time t in the actual

(spatial) configuration $\mathcal{S}$ is $\mathbf{x} = \phi(\mathbf{X}, t)$ and its position in the unloaded actual configuration $\mathcal{S}'$ is denoted by $\mathbf{y}$. Thus we have

$$\begin{aligned} &\mathbf{F}^e : T_{\mathbf{y}}\mathcal{S}' \to T_{\mathbf{x}}\mathcal{S}, \\ &\mathbf{F}^p : T_{\mathbf{X}}\mathcal{B} \to T_{\mathbf{y}}\mathcal{S}', \end{aligned} \tag{2.9}$$

where $T_{\mathbf{y}}\mathcal{S}'$ denotes the tangent space in the unloaded actual configuration $\mathcal{S}'$. It is noteworthy that $\mathbf{F}^e$ and $\mathbf{F}^p$ defined by (2.9) are linear transformations.

We shall tread the tangent space $T_{\mathbf{y}}\mathcal{S}'$ as an auxiliary tool which helps to define the plastic strain tensors[2)].

The plastic strain tensor $\mathbf{E}^p : T_{\mathbf{X}}\mathcal{B} \to T_{\mathbf{X}}\mathcal{B}$ is defined by

$$\mathbf{E}^p = \frac{1}{2}(\mathbf{C}^p - \mathbf{I}), \tag{2.10}$$

where

$$\mathbf{C}^p = \mathbf{F}^{p^T} \cdot \mathbf{F}^p = \mathbf{U}^{p^2} = \mathbf{B}^{p^{-1}} \qquad \text{and} \qquad \mathbf{E}^e \overset{\text{def}}{=} \mathbf{E} - \mathbf{E}^p. \tag{2.11}$$

Similarly the elastic strain tensor $\mathbf{e}^e : T_x\mathcal{S} \to T_x\mathcal{S}$ is defined by

$$\mathbf{e}^e = \frac{1}{2}(\mathbf{i} - \mathbf{c}^e), \tag{2.12}$$

where

$$\mathbf{c}^e = \mathbf{b}^{e^{-1}}, \quad \mathbf{b}^e = \mathbf{F}^e \cdot \mathbf{F}^{e^T} = \mathbf{V}^{e^2} \quad \text{and} \quad \mathbf{e}^p \overset{\text{def}}{=} \mathbf{e} - \mathbf{e}^e. \tag{2.13}$$

It is noteworthy to compare the relation

$$\mathbf{F} = \mathbf{R} \cdot \mathbf{U} = \mathbf{V} \cdot \mathbf{R} \tag{2.14}$$

with

$$\mathbf{F} = \mathbf{F}^e \cdot \mathbf{F}^p = \mathbf{R}^e \cdot \mathbf{U}^e \cdot \mathbf{R}^p \cdot \mathbf{U}^p = \mathbf{V}^e \cdot \mathbf{R}^e \cdot \mathbf{V}^p \cdot \mathbf{R}^p. \tag{2.15}$$

The following commutative diagrams summarize the situation.

[2)] For precise definition of the finite elasto-plastic deformation see PERZYNA [87] and DUSZEK-PERZYNA, PERZYNA [33]. Different approach to define the finite elasto-plastic deformation has been presented by NEMAT-NASSER [62].

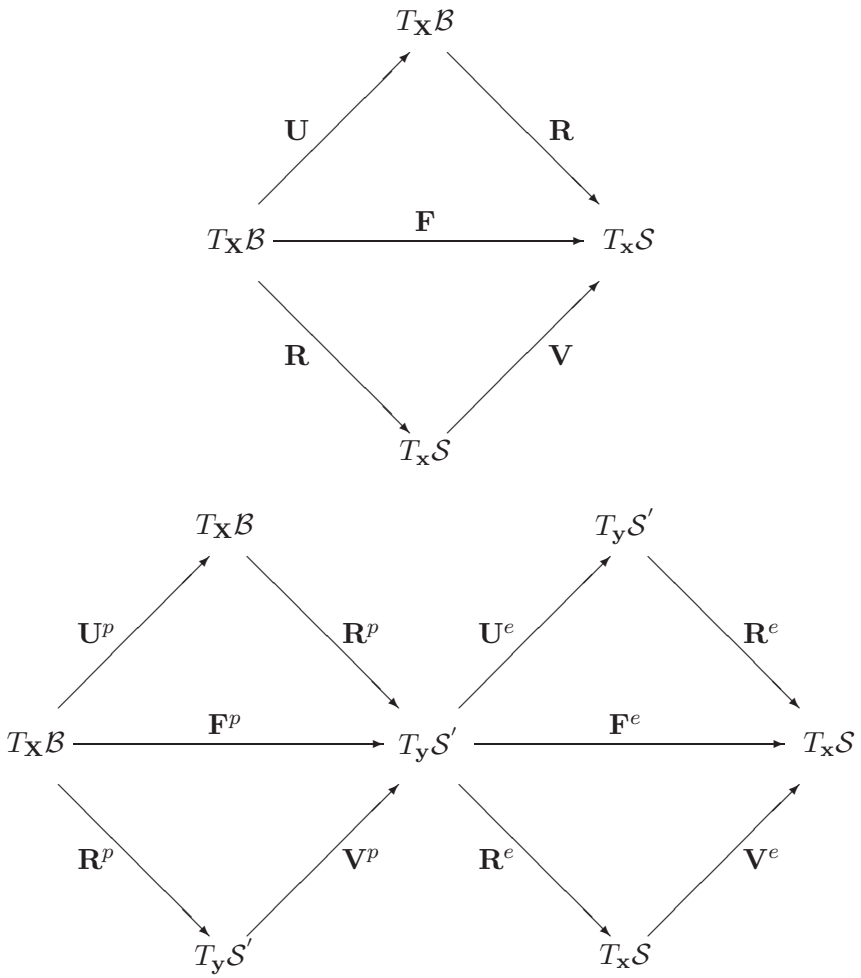

From the second diagram it is clear that the tangent space $T_{\mathbf{y}}\mathcal{S}'$ is playing an auxiliary role indeed.

The plastic tensors $\mathbf{E}^p$and $\mathbf{e}^p$ operate within each fixed tangent space; that is $\mathbf{E}^p : T_{\mathbf{X}}\mathcal{B} \to T_{\mathbf{X}}\mathcal{B}$ and $\mathbf{e}^p : T_{\mathbf{x}}\mathcal{S} \to T_{\mathbf{x}}\mathcal{S}$.

We can show that the following relations are valid

$$\phi_*(\mathbf{E}^{p^\flat}) = \mathbf{e}^{p^\flat}, \qquad \phi^*(\mathbf{e}^{e^\flat}) = \mathbf{E}^{e^\flat}. \tag{2.16}$$

2.3. Rates of the deformation tensor

Let $\phi(\mathbf{X}, t)$ be a C^2 motion of $\mathcal{B}$. Then the spatial velocity is $\boldsymbol{v}_t = \mathbf{V}_t \circ \phi_t^{-1}$, where $\mathbf{V}_t = \dfrac{\partial \phi}{\partial t}$ is the material velocity, i.e. $\boldsymbol{v} : \mathcal{S} \times I \to T\mathcal{S}$, $I \subset I\!R$.

The collection of maps $\phi_{t,s}$ such that for each s and $\mathbf{x}$, $t \to \phi_{t,s}(\mathbf{x})$ is an integral curve of $\boldsymbol{\upsilon}$, and $\phi_{s,s}(\mathbf{x}) = \mathbf{x}$, is called the flow or evolution operator of $\boldsymbol{\upsilon}$, i.e.

$$\{\phi_{t,s} \mid \phi_{t,s} = \phi_t \circ \phi_s^{-1} : \phi_s(\mathcal{B}) \to \phi_t(\mathcal{B})\} \tag{2.17}$$

and

$$\phi_{t,s} \circ \phi_{s,r} = \phi_{t,r}, \qquad \phi_{t,t} = \text{identity} \tag{2.18}$$

for all $r, s, t \in I \subset I\!R$.

If $\mathbf{t}$ is a C^1 (possible time–dependent) tensor field on $\mathcal{S}$, then the Lie derivative of $\mathbf{t}$ with respect to $\boldsymbol{\upsilon}$ is defined by[3)]

$$\mathrm{L}_{\boldsymbol{\upsilon}}\mathbf{t} = \left(\frac{d}{dt}\phi_{t,s}^{*}\mathbf{t}_t\right)|_{t=s}\,. \tag{2.19}$$

If we hold t fixed in $\mathbf{t}_t$, we obtain the autonomous Lie derivative

$$\mathcal{L}_{\boldsymbol{\upsilon}}\mathbf{t} = \left(\frac{d}{dt}\phi_{t,s}^{*}\mathbf{t}_s\right)|_{t=s}\,. \tag{2.20}$$

Thus

$$\mathrm{L}_{\boldsymbol{\upsilon}}\mathbf{t} = \frac{\partial \mathbf{t}}{\partial t} + \mathcal{L}_{\boldsymbol{\upsilon}}\mathbf{t}. \tag{2.21}$$

If $\mathbf{t} \in \mathbf{T}^r{}_s(\mathcal{S})$ (elements of $\mathbf{T}^r{}_s(\mathcal{S})$ are called tensors on $\mathcal{S}$, contravariant of order r and covariant of order s) then $\mathrm{L}_{\boldsymbol{\upsilon}}\mathbf{t} \in \mathbf{T}^r{}_s(\mathcal{S})$.

The spatial velocity gradient $\mathbf{l}$ is defined by

$$\mathbf{l} = D\boldsymbol{\upsilon} : T_{\mathbf{x}}\mathcal{S} \to T_{\mathbf{x}}\mathcal{S}, \quad \text{i.e.} \quad l_b^a = \upsilon^a\,|_b = \frac{\partial \upsilon^a}{\partial x^b} + \gamma_{bc}^a \upsilon^c, \tag{2.22}$$

where γ_{bc}^a denotes the Christoffel symbol for $\mathbf{g}$.

The spatial velocity gradient $\mathbf{l}$ can be expressed as follows

$$\begin{aligned}\mathbf{l} = D\boldsymbol{\upsilon} = \dot{\mathbf{F}} \cdot \mathbf{F}^{-1} = \dot{\mathbf{F}}^e \cdot \mathbf{F}^{e^{-1}} + \mathbf{F}^e \cdot (\dot{\mathbf{F}}^p \cdot \mathbf{F}^{p^{-1}}) \cdot \mathbf{F}^{e^{-1}} \\ = \mathbf{l}^e + \mathbf{l}^p = \mathbf{d} + \boldsymbol{\omega}\mathbf{d}^e + \boldsymbol{\omega}^e + \mathbf{d}^p + \boldsymbol{\omega}^p,\end{aligned} \tag{2.23}$$

where $\mathbf{d}$ denotes the spatial rate of deformation tensor and $\boldsymbol{\omega}$ is called the spin.

[3)] The algebraic and dynamic interpretations of the Lie derivative have been presented by Abraham *et al.* [2], cf. also Marsden, Hughes [58].

Let us define the material (or Lagrangian) rate of deformation tensor $\mathbf{D}$ as follows

$$\mathbf{D}(\mathbf{X},t)=\frac{\partial}{\partial t}\mathbf{E}(\mathbf{X},t). \tag{2.24}$$

We have very important relation

$$\mathbf{d}^{\flat}=\mathrm{L}_{\boldsymbol{\upsilon}}\mathbf{e}^{\flat}=\phi_{*}\frac{\partial}{\partial t}(\phi^{*}\mathbf{e}^{\flat})=\phi_{*}\left(\frac{\partial}{\partial t}\mathbf{E}^{\flat}\right)=\phi_{*}(\mathbf{D}^{\flat}). \tag{2.25}$$

On the other hand

$$\begin{aligned}\mathbf{d}^{\flat}=\mathrm{L}_{\boldsymbol{\upsilon}}\mathbf{e}^{\flat}=\mathrm{L}_{\boldsymbol{\upsilon}}\left[\frac{1}{2}\left(\mathbf{g}-\mathbf{b}^{-1}\right)\right]^{\flat}&=\frac{1}{2}\mathrm{L}_{\boldsymbol{\upsilon}}\mathbf{g}\\&=\frac{1}{2}\left(g_{cb}\upsilon^{c}\,|_{a}+g_{ac}\upsilon^{c}\,|_{b}\right)\mathbf{e}^{a}\otimes\mathbf{e}^{b},\end{aligned} \tag{2.26}$$

i.e. the symmetric part of the velocity gradient $\mathbf{l}$ (the symbol $\otimes$ denotes the tensor product).

The components of the spin $\boldsymbol{\omega}$ are given by

$$\omega_{ab}=\frac{1}{2}\left(g_{ac}\upsilon^{c}\,|_{b}-g_{cb}\upsilon^{c}\,|_{a}\right)=\frac{1}{2}\left(\frac{\partial\upsilon_{a}}{\partial x^{b}}-\frac{\partial\upsilon_{b}}{\partial x^{a}}\right), \tag{2.27}$$

and

$$\mathbf{d}^{e^{\flat}}=\mathrm{L}_{\boldsymbol{\upsilon}}\mathbf{e}^{e^{\flat}},\qquad\mathbf{d}^{p^{\flat}}=\mathrm{L}_{\boldsymbol{\upsilon}}\mathbf{e}^{p^{\flat}}. \tag{2.28}$$

2.4. Rates of the stress tensors

The first Piola-Kirchhoff stress tensor P^{aA} is the two-point tensor obtained by performing a Piola transformation on the second index of the Cauchy stress tensor $\boldsymbol{\sigma}$, i.e.

$$P^{aA}=J(\mathbf{F}^{-1})^{A}_{b}\sigma^{ab}, \tag{2.29}$$

where J denotes the Jacobian of the deformation.

The second Piola-Kirchhoff stress tensor $\mathbf{S}$ is defined as follows

$$S^{AB}=(\mathbf{F}^{-1})^{A}_{a}P^{aB}=J(\mathbf{F}^{-1})^{A}_{a}(\mathbf{F}^{-1})^{B}_{b}\sigma^{ab}=(\mathbf{F}^{-1})^{A}_{a}(\mathbf{F}^{-1})^{B}_{b}\tau^{ab}, \tag{2.30}$$

i.e.

$$\mathbf{S}=\phi^{*}(\boldsymbol{\tau}), \tag{2.31}$$

where $\boldsymbol{\tau}=J\boldsymbol{\sigma}$ is called the Kirchhoff stress tensor.

The rate of the Kirchhoff stress tensor $\boldsymbol{\tau}$ is given by

$$\mathrm{L}_{\boldsymbol{v}}\boldsymbol{\tau} = \phi_* \frac{\partial}{\partial t}(\phi^* \boldsymbol{\tau}) = \phi_* \left(\frac{\partial}{\partial t} \mathbf{S} \right) = \mathbf{F} \cdot \left(\frac{\partial}{\partial t} \mathbf{S} \right) \cdot \mathbf{F}^T \circ \phi_t^{-1}. \tag{2.32}$$

Let us define

$$\begin{aligned} \boldsymbol{\tau}_1 &= \tau^{ab} \mathbf{e}_a \otimes \mathbf{e}_b \in \mathbf{T}^2{}_0(\mathcal{S}), \\ \boldsymbol{\tau}_2 &= \tau_a{}^b \mathbf{e}^a \otimes \mathbf{e}_b \in \mathbf{T}_1{}^1(\mathcal{S}), \\ \boldsymbol{\tau}_3 &= \tau^a{}_b \mathbf{e}_a \otimes \mathbf{e}^b \in \mathbf{T}^1{}_1(\mathcal{S}). \end{aligned} \tag{2.33}$$

Then

$$(\mathrm{L}_{\boldsymbol{v}}\boldsymbol{\tau}_1)^{ab} = \frac{\partial \tau^{ab}}{\partial t} + \frac{\partial \tau^{ab}}{\partial x^c} v^c - \tau^{cb} \frac{\partial v^a}{\partial x^c} - \tau^{ac} \frac{\partial v^b}{\partial x^c}. \tag{2.34}$$

is the rate associated with the name Oldroyd (cf. [68]). The Zaremba-Jaumann rate (cf. Zaremba [118, 119] and Jaumann [46]) is defined as follows

$$\frac{1}{2}\left[(\mathrm{L}_{\boldsymbol{v}}\boldsymbol{\tau}_3)^a{}_c g^{cb} + g^{ac} (\mathrm{L}_{\boldsymbol{v}}\boldsymbol{\tau}_2)_c{}^b \right] = \frac{\partial \tau^{ab}}{\partial t} + \frac{\partial \tau^{ab}}{\partial x^c} v^c + \tau^{ad} \omega_d{}^b - \tau^{db} \omega^a{}_d. \tag{2.35}$$

2.5. Fundamental properties of the Lie derivatives

Let us take again $\mathbf{t} \in \mathbf{T}^r{}_s(\mathcal{S})$ a given time dependent spatial tensor field on $\mathcal{S}$ and let $\boldsymbol{\zeta}$ be a diffeomorphism of $\mathcal{S}$ to another manifold $\boldsymbol{\zeta}(\phi(\mathcal{B}))$, cf. Fig. 2.

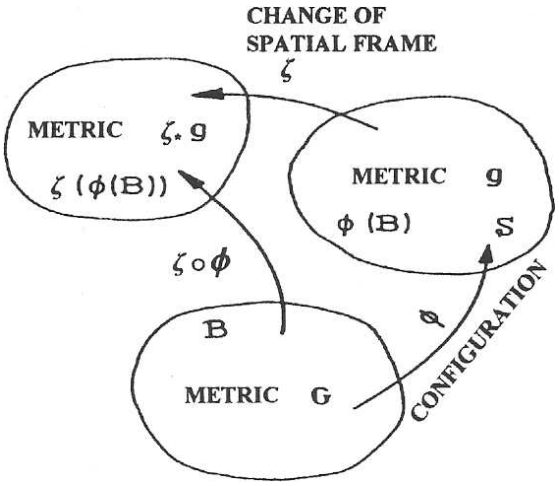

Fig. 2. Schematic representation of the change of spatial frame generated by superposed spatial diffeomorphism.

Any spatial tensor field $\mathbf{t} \in \mathbf{T}^r{}_s(\mathcal{S})$ is said to transform objectively under superposed diffeomorphism $\boldsymbol{\zeta}$ if it transforms according to the rule

$$\mathbf{t}' = \boldsymbol{\zeta}_* \mathbf{t}, \tag{2.36}$$

where $\boldsymbol{\zeta}_*$ is the push-forward operation.

Let $\boldsymbol{v}'$ be the velocity field of $\boldsymbol{\zeta}_t \circ \phi_t$. Then we have (cf. MARSDEN, HUGHES [58])

$$\mathrm{L}_{\boldsymbol{v}'} \mathbf{t}' = \boldsymbol{\zeta}_* (\mathrm{L}_{\boldsymbol{v}} \mathbf{t}). \tag{2.37}$$

This means that objective tensors have objective Lie derivatives. It is noteworthy to recall here that rates which are objective with respect to diffeomorphism are called covariant.

The Oldroyd rate of the Kirchhoff stress tensor (2.34) is objective with respect to diffeomorphisms while the Zaremba-Jaumann rate (2.35) is objective with respect to isometries. The reason of it is caused by the fact that the operations of raising and lowering indices do not commute with Lie differentiation. This corollary has very important consequences for the formulation of the objective constitutive structures.

It f is the time dependent scalar field, then the material derivative

$$\dot{f} = \frac{\partial f}{\partial t} + \frac{\partial f}{\partial x^\alpha} \, v^\alpha. \tag{2.38}$$

3. General principle of determinism. A unique constitutive material structure

3.1. Local thermodynamical process

The main objective of this chapter is the development of a unique constitutive material structure. In other words we would like to describe the physical properties of a material of a body $\mathcal{B}$. Thus, we shall deal with the thermodynamics of continous media.

Let us introduce additional denotations in the actual (spatial) configuration $\phi(\mathcal{B})$ for a body $\mathcal{B}$ for absolute temperature $\vartheta(\mathbf{x}, t)$, the free energy $\psi(\mathbf{x}, t)$, the specific (per unit mass) entropy $\eta(\mathbf{x}, t)$, the mass density $\rho(\mathbf{x}, t)$ and the heat flux vector field $\mathbf{q}(\mathbf{x}, t)$.

Let us define a local thermodynamical process for a body $\mathcal{B}$ by using fields determined in the spatial configuration $\phi_t(\mathcal{B})$ for $t \in [t_o, t_f]$.

Definition 1. A set of the fields

$$\mathcal{P}_{\phi_t(\mathcal{B})} = \{\phi, \vartheta, \rho, \psi, \eta, \boldsymbol{\tau}, \mathbf{q}\}(\mathbf{x}, t) \tag{3.1}$$

given for every $\mathbf{x} \in \phi_t(\mathcal{B})$, for $t \in [t_o, t_f]$ and satisfying the principles:

(i) conservation of mass

$$\dot{\rho} + \rho \operatorname{div} \boldsymbol{v} = 0; \tag{3.2}$$

(ii) balance of momentum

$$\rho \dot{\boldsymbol{v}} = \operatorname{div} \left(\frac{1}{J} \boldsymbol{\tau} \right); \tag{3.3}$$

(iii) balance of angular momentum

$$\boldsymbol{\tau} = \boldsymbol{\tau}^T; \tag{3.4}$$

(iv) balance of energy

$$\rho \left(\dot{\psi} + \vartheta \dot{\eta} + \eta \dot{\vartheta} \right) + \operatorname{div} \mathbf{q} = \frac{\rho}{\rho_{\mathrm{ref}}} \boldsymbol{\tau} : \mathbf{d}; \tag{3.5}$$

(v) entropy production inequality

$$\frac{1}{\rho_{\mathrm{ref}}} \boldsymbol{\tau} : \mathbf{d} - \left(\eta \dot{\vartheta} + \dot{\psi} \right) - \frac{1}{\rho \vartheta} \mathbf{q} \cdot \operatorname{grad} \vartheta \geqq 0; \tag{3.6}$$

will be called a local thermodynamical process.

In a class of processes for a body $\mathcal{B}$ we shall favour the processes which satisfied the principles of thermodynamics.

The pricinple of balance of energy (3.5) expresses the first law of thermodynamics and gives restrictions on the phenomena and the interactions, which we can describe. This principle suggests that our aim of the description will be in mechanical and thermal phenomena.

The different nature represents the entropy production inequality (3.6) called also the reduced dissipation inequality. Marsden and Hughes [58] proved that the reduced dissipation inequality (3.6) is equivalent to the entropy production inequality first introduced by Coleman and Noll [19] in the form of the Clausius-Duhem inequality. In fact the Clausius-Duhem inequality gives a statement of the second law of thermodynamics within the framework of mechanics of continous media. The entropy production inequality poses some restrictions on the constitutive functions of the response of a material of a body $\mathcal{B}$. We can state that the second law of thermodynamics favours in a class of materials the real material. It is noteworthy to cite here Max Planck [103], who the problem of thermodynamical restrictions for physical processes understood in very precise way:

"The principle of balance of energy imposes the restrictions on nature processes, since it states, that energy does never appear or does vanish, but it may be only subject to change.

The second law of thermodynamics increases this restriction, since it says that not all kinds of change are possible, but only some of them and under certain determined conditions."

To relate this thought of Planck to the considered situation we can state that exactly the determination of the restrictions in the description of a material, which satisfy, the realization of the real processes compatible with the principles of thermodynamics is a main problem of the thermodynamical theory of materials.

Definitions 2. A local thermodynamical process $\mathcal{P}_{\phi_t(\mathcal{B})}$ we shall call an admissible process, if it satisfies the constitutive equations for a material in a body $\mathcal{B}$.

We assume as the fundamental principle of physics the objectivity of properties of a material, i.e. we postulate that the constitutive equations describing the material in a body $\mathcal{B}$ have to be invariant with respect to arbitrary diffeomorphism $\boldsymbol{\zeta} : \mathcal{S} \to \mathcal{S}$ (any motion).

Definition 3. Two local thermodynamical processes

$$\{\phi, \vartheta, \rho, \psi, \eta, \boldsymbol{\tau}, \mathbf{q}\} \qquad \text{and} \qquad \{\phi', \vartheta', \rho', \psi', \eta', \boldsymbol{\tau}', \mathbf{q}'\} \tag{3.7}$$

related to each other by arbitrary diffeomorphisms (any motion) we shall call isomorphic processes.

Principle of objectivity of a material (spatial covariance) may be formulated as follows: If the constitutive equations are satisfied for a local thermodynamical process $\{\phi, \vartheta, \rho, \psi, \eta, \boldsymbol{\tau}, \mathbf{q}\}$ then they are also satisfied for the isomorphic process $\{\phi', \vartheta', \rho', \psi', \eta', \boldsymbol{\tau}', \mathbf{q}'\}$.

Definition 4. The four values

$$g = (\mathbf{e}, \mathbf{F}, \vartheta, \operatorname{grad}\vartheta)(\mathbf{x}, t) \tag{3.8}$$

computed for a particle X in actual (spatial) configuration of a body $\mathcal{B}$ at the instant of time $t \in [0, d_p]$ we shall call the local deformation-temperature configuration of X at time t.

A set of all possible spatial configurations of a particle X we denote by $\mathcal{G}$ and shall it call the deformation-temperature configuration space.

Definition 5. The four values

$$s = (\psi, \eta, \boldsymbol{\tau}, \mathbf{q})(\mathbf{x}, t) \tag{3.9}$$

given in a particle X at time $t \in [0, d_Z]$ we shall call the actual local response of a particle X.

A set of all possible responses of a particle X we denote by $\mathcal{S}$ and shall call the response space.

Let us consider processes in the configuration space $\mathcal{G}$ and in the response space $\mathcal{S}$.

A process[4)]

$$P = (\mathbf{e}, \mathbf{F}, \vartheta, \operatorname{grad}\vartheta) : [0, d_P] \to \mathcal{G} \tag{3.10}$$

will determine the change of the deformation-temperature configuration of a particle X in the interval of time $[0, d_P]$. A number d_P will be called the duration of the process P, and $P^i = P(0)$ and $P^f = P(d_P)$ the initial and final values of the process P, respectively.

A process

$$Z \equiv (\psi, \eta, \boldsymbol{\tau}, \mathbf{q}) : [0, d_Z] \to \mathcal{S} \tag{3.11}$$

will determine the change of the response of a particle X in the interval of time $[0, d_Z]$, i.e., the change of the free energy, the entropy, the Kirchhoff stress, and the heat flux.

Let us denote by

$$\Pi \equiv \{P | P : [0, d_P] \to \mathcal{G}\} \tag{3.12}$$

a set of all deformation-temperature configuration processes, and by

$$\mathcal{Z} \equiv \{Z | Z : [0, d_Z] \to \mathcal{S}\} \tag{3.13}$$

a set of all response processes for a particle X.

Definition 6. Every pair $(P, Z) \in \Pi \times \mathcal{Z}$ such that Dom P = Dom Z and for every instant of time $t \in [0, d_P]$ the dissipation principle in the form of Clausius-Duhem inequality (3.6) is satisfied; will be called a local thermodynamical process.

A set of all thermodynamical processes will be denoted by $\mathcal{P}_{\mathrm{X}}$.

3.2. Method of preparation

In a set of local thermodynamical processes $\mathcal{P}_{\mathrm{X}}$ we shall consider a subset which will be compatible with the internal constitutive assumptions describing the intrinsic physical constitution of a body $\mathcal{B}$, i.e. compatible with a material[5)]

[4)] For a thorough discussion of properties of a process and for the definition of a segment of the given process P and the continuation of the process P_1 with P_2, see NOLL [64].

[5)] A material as defined by NOLL [64] is an equivalence class of material structures, the equivalence being material isomorphy, cf. also PERZYNA [78].

of a body $\mathcal{B}$. Such a subset of a local thermodynamical process space will be called admissible for the constitutive assumptions in question. In a set $\mathcal{P}_{\mathrm{X}}$ we shall be interested such local thermodynamical processes which have the characteristic property that deformation-temperature processes $\mathcal{P}$ are in some relation with appropriate response process Z. Thus, in a set $\mathcal{P}_{\mathrm{X}}$ we distinguish some subset R.

Definition 7. A subset R of a set of local thermodynamical processes $\mathcal{P}_{\mathrm{X}}$ of a particle X we shall call the constitutive relation, provided that the conditions are satisfied as follows:

(i) $\mathrm{pr}_{\Pi}(R) = \Pi$,

(ii) if $(P, Z) \in R$ then $(P_{[0,t]}, Z_{[0,t]}) \in R$ for $t \in \mathrm{Dom}P$.

Appearing the relation R in a set of thermodynamical processes $\mathcal{P}_{\mathrm{X}}$ causes that locally in the particle X we introduce the material structure.

Definition 8. A system $(\mathcal{G}, \Pi, R)$ we shall call the body element with the material structure.

The relation R given in a set of thermodynamical processes $\mathcal{P}_{\mathrm{X}}$ does not have to be generally right-hand unique, i.e. in general it does not satisfy the condition

$$\bigwedge_{P\in\Pi} \bigwedge_{Z_1,Z_2\in\mathcal{Z}} [(P, Z_1) \in R \wedge (P, Z_2) \in R] \Rightarrow Z_1 = Z_2. \tag{3.14}$$

If the relation R has this property, i.e. has been the functional relation, then every process $P \in \Pi$ corresponds only one (uniquely determined) response process $Z \in \mathcal{Z}$.

If this case happens, then the material structure of the element $(\mathcal{G}, \Pi, R)$ has to be the elastic material structure.

In the case of inelastic dissipative materials the relation R does not be the functional relation.

From previous consideration follows that if we wish to have the unique relation R in a set of thermodynamical processes $\mathcal{P}_X$, we should to complete our informations about a particle X. Let us focus our attention on the initial configuration $P^i = P(0) = g_0$ of a particle X, from which the deformation-temperature configuration process $P : [0, d_P] \to \mathcal{G}$ has been begun. For an elastic material the knowledge of the configuration g_0 determines uniquely the response of a material at instant of time $t = 0$, i.e. $s_0 = (\psi(0), \eta(0), \boldsymbol{\tau}(0), \mathbf{g}(0))$ at a particle X. In the case of inelastic (dissipative) materials very crucial is also the knowledge in what way the configuration g_0 has been achieved. It is required the additional information about a particle X in instant of time $t = 0$, which is in the configuration g_0.

A main objective the thermodynamics of inelastic continuous media is to predict the response of a particle X of a body $\mathcal{B}$, of which physical properties are know, at the end of a deformation-temperature process. We can give an answer to this question if, and only if, we have full information about particle X before the test, i.e. before a deformation-temperature configuration process. If we have a deformation-temperature configuration process $P \in \Pi$, then the definition of the additional information about the initial configuration g_0 of a particle X, which provides for unique determination of the response process $Z \in \mathcal{Z}_P$ in the response space $\mathcal{S}$, being in the relation R with the process P, we shall call **the method of preparation**[6]. In other words the method of preparation should give the additional information to define uniquely the intrinsic state of a particle X of a body $\mathcal{B}$ during the local thermodynamical process $P_{\phi_t(B)} \in \mathcal{P}_X$.

By the intrinsic state of a particle X we define a pair: the transient configuration of a particle X and corresponded it the method of preparation.

It will be shown that a method of preparation of the deformation-temperature configuration of a particle X is needed to describe the internal dissipation of a material. This is a very important feature of the notion of the method of preparation.

To discuss the general relation between processes $P \in \Pi$ and $Z \in \mathcal{Z}$ which defines a material structure of a body $\mathcal{B}$ let us introduce a space $\mathcal{M}$ connected with the configuration space $\mathcal{G}$ in such a way that elements of the space $\mathcal{M}$, which will be denoted by $m \in \mathcal{M}$, are the method of preparation of the corresponding configuration $g \in \mathcal{G}$. The space $\mathcal{M}$ will be called **the method of preparation space**.

Definition 9. A non-empty set $\mathcal{M}$ will be called the method of preparation space for a particle X if

$$\bigvee_{\Sigma \subset \mathcal{G}\times\mathcal{M}} \bigvee_{\Re:(\Sigma\times\Pi)^*\to\mathcal{Z}} \bigwedge_{g\in\mathcal{G}} \bigwedge_{P\in\Pi_g} \bigwedge_{\mathcal{M}_g\subset\mathcal{M}} \Re(g,\cdot,P) : \mathcal{M}_g \to \mathcal{Z}_P \quad \text{is bijection,} \tag{3.15}$$

where

$$(\Sigma \times \Pi)^* \equiv \left\{ (\sigma, P) \in \Sigma \times \Pi \middle| \bigvee_{\mathcal{M}_{P^i}\subset\mathcal{M}} \sigma \in \{P^i\} \times \mathcal{M}_{P^i} \right\}, \tag{3.16}$$

[6] For a notion of the method of preparation see Bridgman [9] and Giles [39], cf. also Perzyna [72, 73, 75, 76] and Perzyna, Kosiński [96]. The precise definition of the method of preparation space for a pure mechanical process was first given by Perzyna, Kosiński [96]. The generalization to the thermodynamical processes was presented by Perzyna [77]

denotes a set of pairs the intrinsic state and the deformation-temperature configuration processes (σ, P) such, that the process P is initiated at the state σ, i.e. $P^i = g$ if $\sigma = (g, m)$,

$$\Pi_g \equiv \{P \in \Pi | P^i = g\} \tag{3.17}$$

denotes a set of all deformation-temperature configuration processes which are initiated at the configuration $g \in \mathcal{G}$, and $\mathcal{Z}_P$ is a subset of $\mathcal{Z}$ corresponding to the process P.

Definition 10. A set

$$\Sigma \equiv \bigcup_{g \in \mathcal{G}} \{g\} \times \mathcal{M}_g, \qquad \mathcal{M}_g \subset \mathcal{M} \tag{3.18}$$

(constructed by the Definition 9) is called the intrinsic state space[7)] of a particle X of the element body with the material structure $(\mathcal{G}, \Pi, R)$.

The element $\sigma \in \Sigma$ is a pair of the deformation-temperature configuration and the method of preparation, i.e.

$$\sigma \equiv (P(t), M(t)) = (g, m), \qquad g \in \mathcal{G}, \qquad m \in \mathcal{M}_g, \tag{3.19}$$

where by M we denote a process in the method of preparation space $\mathcal{M}$, i.e., $M : [0, d_P] \to \mathcal{M}$.

We define two mappings as follows[8)]

$$\widehat{\mathbf{G}} \equiv \mathrm{pr}_{\mathcal{G}} : \Sigma \to \mathcal{G}, \qquad \widehat{\mathbf{M}} \equiv \mathrm{pr}_{\mathcal{M}} : \Sigma \to \mathcal{M}, \tag{3.20}$$

which determine the projections from the intrinsic space Σ on the configuration space $\mathcal{G}$ and on the method of preparation space $\mathcal{M}$, respectively.

3.3. General principle of determinism. Unique material structure

The notion of a method of preparation is connected with a general principle of determinism in mechanics of continuum medium. The principle of determinism

[7)] The intrinsic state space Σ has been defined by Perzyna, Kosiński [96]. It plays a similar role in the theory of materials as the state space introduced by Noll [64]. The difference between these two notions of state is in the conception of the method of preparation. The elements of the intrinsic state space are pairs. Every pair consists of the local configuration and its method of preparation. There is no notion of the method of preparation in Noll's conception of state. The idea of splitting every element of the intrinsic state space into the local configuration and its method of preparation allows us to characterize precisely the intrinsic state of a particle X and is of great importance for the development of thermodynamics of dissipative material structures.

[8)] The mappings $\widehat{\mathbf{G}}$ and $\widehat{\mathbf{M}}$ were first introduced for a purely mechanical case, the former by Noll [64] and the latter by Perzyna, Kosiński [96].

can be stated as follows: Between an initial deformation-temperature configuration, its method of preparation, a deformation-temperature process beginning at this configuration and a response process of a particle X, there exists a functional relationship. This functional relation will describe a unique material structure in a particle X of a body $\mathcal{B}$.

Let us assume that for the body element with the material structure $(\mathcal{G}, \Pi, R)$ exists the method of preparation space $\mathcal{M}$.

According to Definition 9 there exists a mapping

$$\Re : (\Sigma \times \Pi)^* \to \mathcal{Z}. \tag{3.21}$$

Definition 11. The mapping $\Re$ defined by (3.21) is called the constitutive mapping for the body element with the material structure $(\mathcal{G}, \Pi, R)$.

The constitutive mapping $\Re : (\Sigma \times \Pi)^* \to \mathcal{Z}$ has the property as follows

$$\bigwedge_{\substack{\sigma_1,\sigma_2\in\Sigma \\ \widehat{\mathbf{G}}(\sigma_1)=\widehat{\mathbf{G}}(\sigma_2)}} \bigwedge_{P\in\Pi_g} \{(\sigma_i, P) \in (\Sigma \times \Pi)^*, \; i = 1, 2 \wedge \Re(\sigma_1, P) = \Re(\sigma_2, P)\} \Rightarrow \widehat{\mathbf{M}}(\sigma_1) = \widehat{\mathbf{M}}(\sigma_2). \tag{3.22}$$

Definition 12. The system $(\mathcal{G}, \Pi, \Sigma, \Re)$ is called a unique material structure in a particle X of a body $\mathcal{B}$.

The constitutive mapping $\Re$ with the property (3.22) expresses a general principle of determinism of dissipative continuum body.

A general principle of determinism: A unique response process $Z \in \mathcal{Z}$ corresponds to every deformation-temperature process $P \in \Pi$ beginning at the given intrinsic state $\sigma \in \Sigma$.

This statement of a principle of determinism is very general. It concerns thermodynamic processes and is valid for the arbitrary method of preparation space introduced.

A theory can be called deterministic if the analysis of its internal structure shows that from a theoretical description of the intrinsic state of a particle X of a body $\mathcal{B}$ in an arbitrary initial instant of time results a unique description of the intrinsic state of this particle in the later instant of time and every intrinsic state of particle X corresponds the unique value of the response. In other words, we shall call a theory deterministic if its internal structure assures the unique evolution of the intrinsic states and there exists a unique mapping between the intrinsic states and the values of the responses.

In the definition of the deterministic theory it is included a nature of the irreversibility of the process. The irreversibility results from the turn of the axis of

time. We speak about the initial instant of time and the later instant of time but not about two arbitrary instants of time (cf. GILES [39] and LANDSBERG [53]).

We shall show that the constitutive mapping $\Re$ generates the evolution function $\widehat{\mathbf{e}}$ and the material function $\widehat{\mathbf{S}}$, which the first assures the evolution of the intrinsic states, and the second guarantees a unique mapping between the intrinsic states and the values of responses.

3.4. Evolution of intrinsic states

Let us assume that a unique material structure $(\mathcal{G}, \Pi, \Sigma, \Re)$ is given. If we have the initial intrinsic state and the deformation-temperature process beginning at this intrinsic state we are interested then in the intrinsic state at the end of the process. The problem will be solved if a mapping between the intrinsic state at the end of the deformation-temperature process and the initial intrinsic state is given.

Definition 13. It is said that a mapping

$$\widehat{\mathbf{e}} : (\Sigma \times \Pi)^* \to \Sigma \tag{3.23}$$

is the evolution function, if for every pair $(\sigma, P) \in (\Sigma \times \Pi)^*$ the equation

$$\Re(\widehat{\mathbf{e}}(\sigma, P), P^f_{(0)}) = [\Re(\sigma, P)]^f \tag{3.24}$$

is satisfied, where $[\Re(\sigma, P)]^f$ denotes the final value of the response process $Z = \Re(\sigma, P)$ and $P^f_{(0)}$ is the deformation-temperature process of duration zero.

3.5. The mapping from the intrinsic state space into the response space

In the practical applications it will be convenient to have a mapping from the intrinsic state space Σ into the response space $\mathcal{S}$. So, it is useful to define a new mapping

$$\widehat{\mathbf{S}} : \Sigma \to \mathcal{S} \tag{3.25}$$

by the expression

$$\widehat{\mathbf{S}}(\sigma) \equiv \Re(\sigma, \widehat{\mathbf{G}}(\sigma)_{(0)}). \tag{3.26}$$

Taking into account the last expression we can write the definition of the evolution function in the form as follows

$$\bigwedge_{t \in \mathrm{Dom} P} \widehat{\mathbf{S}}(\widehat{\mathbf{e}}(\sigma_0, P_{[0,t]}) = [\Re(\sigma_0, P_{[0,t]})]^f. \tag{3.27}$$

The principle of determinism can be expressed by the relation[9)]

$$Z(t) = s = \widehat{S}(\widehat{\mathbf{e}}(\sigma_0, P)) = \widehat{\mathbf{S}}(\sigma) \tag{3.28}$$

for every $(\sigma_0, P) \in (\Sigma \times \Pi)^*$, cf. Fig. 3.

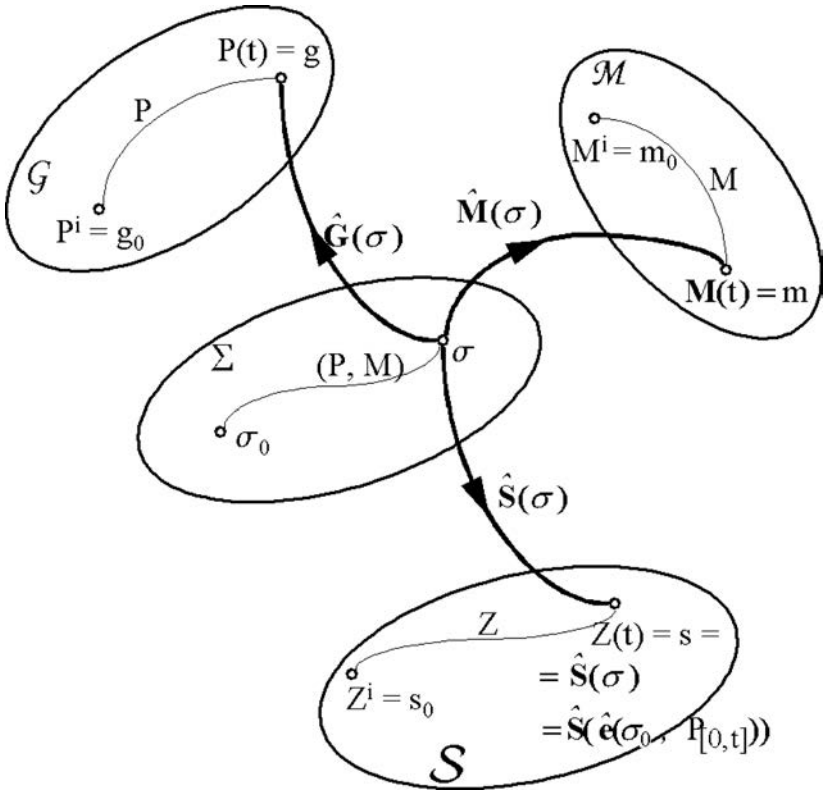

FIG. 3. Geometrical interpretation of mappings for a unique constitutive material structure.

The principle of determinism can be stated as follows: A unique value of the response $s \in \mathcal{S}$ (i.e. unique values of the free energy $\psi(t)$, the entropy $\eta(t)$, the Kirchhoff stress tensor $\boldsymbol{\tau}$ and the heat flux vector $\mathbf{q}(t)$) corresponds to every intrinsic state $\sigma \in \Sigma$.

The mapping $\widehat{\mathbf{S}}$ is called the response function (functional) or the constitutive function (functional).

Definition 14. The system $(\mathcal{G}, \Pi, \Sigma, \widehat{\mathbf{S}}, \widehat{\mathbf{e}})$ is also a unique material structure in a particle X of a body $\mathcal{B}$.

[9)] It is noteworthy that both mappings $\widehat{\mathbf{e}}$ and $\widehat{\mathbf{S}}$ are similar to those introduced by NOLL [64] in a purely mechanical consideration but in the present theory, as in PERZYNA, KOSIŃSKI [96] and PERZYNA [77], the mappings $\widehat{\mathbf{e}}$ and $\widehat{\mathbf{S}}$ are generated by the constitutive mapping $\Re$.

The constitutive function $\widehat{\mathbf{S}}$ and the evolution function $\widehat{\mathbf{e}}$ will play a fundamental role in various descriptions of material constitutive structure. These descriptions will depend on different determination of the method of preparation space $\mathcal{M}$.

Recalling that a mapping $\widehat{\mathbf{S}}$ determines the response of a material we can write

$$\widehat{\mathbf{S}} \equiv \{\widehat{\Psi}, \widehat{\mathrm{H}}, \widehat{\mathbf{T}}, \widehat{\mathbf{Q}}\}, \tag{3.29}$$

where $\widehat{\Psi}$ denotes the constitutive function of the free energy, $\widehat{\mathrm{H}}$ the constitutive function of the entropy, $\widehat{\mathbf{T}}$ the constitutive function of the Kirchhoff stress tensor and $\widehat{\mathbf{Q}}$ the constitutive function of the heat flux vector.

3.6. Consequences of the dissipation principle

Taking account of Definition 2 we can state.

Definition 15. A local thermodynamical process $\mathcal{P}_{\phi_t(B)} \subset \mathcal{P}_X$ compatible with a unique material structure $(\mathcal{G}, \Pi, \Sigma, \widehat{\mathbf{S}}, \widehat{\mathbf{e}})$ will be called an admissible process.

A set of all admissible local thermodynamical processes we shall denote by $\mathcal{P}_X^*$.

The principle of dissipation. For every admissible local thermodynamical process the rate of entropy production in actual instant of time $t \in [0, d_P]$ has nonnegative valued, i.e. the Clausius-Duhem inequality has to be satisfied, cf. Coleman, Noll [19] and Truesdell [114]. The fundamental problem of the thermodynamics of materials is as follows: Within a set of admissible local thermodynamical processes $\mathcal{P}_X^*$ and within a class of the constitutive functions $\widehat{\mathbf{S}} = \{\widehat{\Psi}, \widehat{\mathrm{H}}, \widehat{\mathbf{T}}, \widehat{\mathbf{Q}}\}$ to determine those, which satisfy the dissipative principle. Thus, it can be said that the main problem of the thermodynamics of materials is the determination of an admissible local thermodynamical process.

It is noteworthy that the answer to the main problem of the thermodynamics of materials depends on the topology assumed for the method of preparation space.

It will be proved that the dissipation principle will imply two fundamental criteria in the theory of materials.

(i) The criterion of the selection of the response functions (functionals) $\widehat{\mathbf{S}} = \{\widehat{\Psi}, \widehat{\mathrm{H}}, \widehat{\mathbf{T}}, \widehat{\mathbf{Q}}\}$[10)].

[10)] It seems that Eckart [34] was the first who understood properly the consequences of the Clausius-Duhem inequality for constitutive assumptions. Further development of his idea was done by Coleman, Noll [19], Coleman [16], Coleman, Gurtin [17], Coleman, Mizel [18], Coleman, Owen [20, 21] and Trusdell, Noll [115].

(ii) The criterion of the accessibility of an intrinsic state $\sigma \in \Sigma$ from the given initial intrinsic state $\sigma_0 \in \Sigma$[11)].

3.7. Topological and smoothness assumptions

To investigate restrictions placed on a local thermodynamical process by the dissipation principle we assume:

1. The deformation-temperature configuration space $\mathcal{G}$ and the method of preparation space $\mathcal{M}$ are complete metrizable topological spaces (Banach spaces)[12)].
2. Processes $P \in \Pi$ considered in the configuration space $\mathcal{G}$ are continuous and continuously differentiable with respect to time t, i.e. for every $t \in [0, d_P]$ exists the Lie derivative $\mathrm{L}_{\boldsymbol{v}} P(\tau)|_{\tau=t} = \mathrm{L}_{\boldsymbol{v}} P(t)$, which determines the rate of change of the process P at t.
3. Processes M determined in the method of preparation space $\mathcal{M}$ are continuous and continuously differentiable with respect to time t, i.e. for every $t \in [0, d_P]$ exists the Lie derivative $\mathrm{L}_{\boldsymbol{v}} M(\tau)|_{\tau=t} = \mathrm{L}_{\boldsymbol{v}} M(t)$, which determines the rate of change of the process M at t.
4. The rate $\mathrm{L}_{\boldsymbol{v}} M(t)$ is independent of the rate $\mathrm{L}_{\boldsymbol{v}} P(t)$ for every instant of time $t \in [0, d_P]$[13)].
5. The real value free energy response function $\widehat{\Psi}$ defined on $\Sigma \subset \mathcal{G} \times \mathcal{M}$ is continuously differentiable on Σ, i.e. the gradient $\partial_{P(\tau)} \widehat{\Psi}|_{\tau=t}$ with fixed $M(t)$ and the gradient $\partial_{M(\tau)} \widehat{\Psi}|_{t=\tau}$ with fixed $P(t)$ exist and are continuous functions on Σ. This property is called a chain rule property.

[11)] The exploration of similar criterion to this has been taken, in another connection, by Coleman, Owen [21].

[12)] For the exact meaning of the mathematical terms introduced please consult Kelly [48] and Engelking [35].

[13)] Since the rate $\mathrm{L}_{\boldsymbol{v}} M(t)$ is independent of the rate $\mathrm{L}_{\boldsymbol{v}} P(t)$, then we may postulate

$$(*) \qquad \mathrm{L}_{\boldsymbol{v}} M(t) = \widehat{\mathcal{M}}(P(t), M(t)), \qquad t \in [0, d_P].$$

Under this assumption the rate of change of the process $M(t)$ in the method of preparation space $\mathcal{M}$ is completely determined by the actual intrinsic state $\sigma \in \Sigma$.
Two interesting cases can be considered:

(i) $M(0) = m_o \in \mathcal{M}$,
(ii) $M(-\infty) = m_{-\infty} \in \mathcal{M}$.

The differential equation (*) is called the evolution equation in the method of preparation space $\mathcal{M}$, and together with appropriate initial value (i) or (ii) for the given deformation-temperature configuration process $P : [0, d_P] \to \mathcal{G}$ completely determines the evolution of the intrinsic state, i.e. the evolution function $\widehat{\mathbf{e}} : (\Sigma \times \Pi)^* \to \Sigma$.
The differential equation (*) with the initial value (i) leads to the unique material structure with internal state variables, and the initial value problem (*) and (ii) is isomorphic with the unique material structure with memory, cf. Kosiński, Wojno [50] and Leitman, Mizel [56].

Since $\mathcal{G}$ and $\mathcal{M}$ have been normed spaces (Banach spaces), then it has been more convenient to consider a subset $\mathcal{D}$ of the intrinsic state space Σ, being the complete normed space (Banach space). We shall assume that the constitutive functions (functionals) $\widehat{\mathbf{S}} \equiv \{\widehat{\Psi}, \widehat{\mathrm{H}}, \widehat{\mathbf{T}}, \widehat{\mathbf{Q}}\}$ are defined on a set $\mathcal{D}$.

To speak precisely, a property of chain rule for the constitutive function (functional) of the free energy $\widehat{\Psi}$ is assumed in the topology of $\mathcal{D}$.

3.8. Constitutive restriction

Thanks to previous assumptions, from the satisfaction of the dissipative principle in the form of the Clausius-Duhem inequality (3.6), we receive the results as follows[14)]

$$\begin{gathered}\partial_{\mathrm{grad}\vartheta(t)}\widehat{\Psi}(\cdot) = 0, \qquad \boldsymbol{\tau}(t) = \rho_{\mathrm{Ref}}\partial_{\mathbf{e}(t)}\widehat{\Psi}(\cdot), \qquad \eta(t) = -\partial_{\vartheta(t)}\widehat{\Psi}(\cdot), \\ -\partial_{M(t)}\widehat{\Psi}(\cdot)\square \mathrm{L}_{\boldsymbol{v}}M(t) - \frac{1}{\rho\vartheta(t)}\widehat{\mathbf{Q}}(\cdot)\cdot\mathrm{grad}\vartheta(t) \geq 0,\end{gathered} \tag{3.30}$$

valid at every instant of time $t \in [0, d_P]$. The expression $\partial_{M(t)}\widehat{\Psi}(\cdot)\square \mathrm{L}_{\boldsymbol{v}}M(t)$ denotes the product of two geometrical objects with full contraction. Let us introduce the following denotations

$$\begin{aligned}\widehat{d}(\sigma) &= -\partial_{M(t)}\widehat{\Psi}(\cdot)\square \mathrm{L}_{\boldsymbol{v}}M(t) - \frac{1}{\rho\vartheta(t)}\widehat{\mathbf{Q}}(\cdot)\cdot\mathrm{grad}\vartheta(t), \\ \widehat{i}(\sigma) &= -\frac{1}{\vartheta(t)}\partial_{M(t)}\widehat{\Psi}(\cdot)\square \mathrm{L}_{\boldsymbol{v}}M(t).\end{aligned} \tag{3.31}$$

The mapping $\widehat{d} : \Sigma \to \mathbf{R}^+$ (where $\mathbf{R}^+$ denotes the set of non-negative real numbers) is called the general dissipation function, and $\widehat{d}(\sigma)$ denotes the value of the general dissipation function at the intrinsic state $\sigma \in \Sigma$.

The mapping $\widehat{i} : \Sigma \to \mathbf{R}^+$ is called the internal dissipation function, and $\widehat{i}(\sigma)$ is its value at the intrinsic state $\sigma \in \Sigma$.

The inequality $(3.30)_4$ is called the general dissipation inequality and using the denotations (3.31), it can be written in the form

$$\widehat{d}(\sigma) = \vartheta(t)\widehat{i}(\sigma) - \frac{1}{\rho\vartheta(t)}\widehat{\mathbf{Q}}(\sigma)\cdot\mathrm{grad}\vartheta(t) \geqq 0. \tag{3.32}$$

The results (3.30) express the criterion of the selection of the response functions (functionals) $\widehat{\mathbf{S}} \equiv \{\widehat{\Psi}, \widehat{\mathrm{H}}, \widehat{\mathbf{T}}, \widehat{\mathbf{Q}}\}$, which can be stated as follows:

[14)] To prove this statement we can use a similar procedure to that of Coleman, Gurtin [17] and Valanis [116].

Choosing the free energy constitutive function $\widehat{\Psi}(\cdot)$ which is independent of the actual temperature gradient $\mathrm{grad}\vartheta(t)$ and the heat flux response function $\widehat{\mathbf{Q}}(\cdot)$ such that the general dissipation inequality (3.32) is satisfied at every instant of time $t \in [0, d_P]$, or for every intrinsic state σ determined by the relation $\sigma = \widehat{\mathbf{e}}(\sigma_0, P_{[0,t]})$, where σ_0 denotes the initial intrinsic state and $P_{[0,t]}$ the segment of the given deformation-temperature process P, the response Kirchhoff stress function $\widehat{\mathbf{T}}$ and the response entropy function $\widehat{\mathrm{H}}$ are uniquely determined by the relations $(3.30)_2$ and $(3.30)_3$. It is noteworthy that for the adiabatic thermodynamical process, when $\mathbf{q}(t) \equiv 0$ or $\mathrm{grad}\vartheta(t) \equiv 0$ for $t \in [0, d_P]$ the general dissipation inequality (3.32) takes the particular form

$$\widehat{i}(\sigma) = -\frac{1}{\vartheta(t)} \partial_{M(t)} \widehat{\Psi}(\cdot) \square \mathrm{L}_{\boldsymbol{\upsilon}} M(t) \geqq 0, \qquad t \in [0, d_P] \tag{3.33}$$

which is called the internal dissipation inequality.

3.9. Accessibility criterion

Let us assume that the initial intrinsic state $\sigma_0 \in \Sigma$ is known, and let us choose an arbitrary intrinsic state $\sigma^* \in \Sigma$. The question arises whether the intrinsic state σ^* is accessible from the initial intrinsic state σ_0, or in other words, what is the condition of accessibility of σ^* from σ_0.

If the intrinsic state σ^* is accessible from the initial intrinsic state σ_0. then the deformation-temperature process P has to exist which generates the process in the method of preparation space $M : [0, d_P] \to \mathcal{M}$ such that

$$\begin{aligned} \sigma_0 &= (P(0), M(0)) = (g_0, m_0), \\ \sigma^* &= (P(d_P), M(d_P)) = (g^*, m^*) \end{aligned} \tag{3.34}$$

and for every instant of time $t \in [0, d_P]$ the dissipation principle is satisfied. The response of a material corresponding to the intrinsic state σ^* is determined by the constitutive relation

$$Z(d_P) = \widehat{\mathbf{S}}(\widehat{\mathbf{e}}(\sigma_0, P)) = \widehat{\mathbf{S}}(\sigma^*). \tag{3.35}$$

The dissipation principle requires that for a given process P such a process $M : [0, d_P] \to \mathcal{M}$ be chosen that the general dissipation inequality

$$\widehat{d}(\sigma) \geqq 0, \qquad \sigma = (P(t), M(t)) = (g, m) \tag{3.36}$$

for every instant of time $t \in [0, d_P]$ has to be satisfied.

Accessibility criterion of the intrinsic states. An arbitrary intrinsic state $\sigma^* \in \Sigma$ is accessible from the initial intrinsic state $\sigma_0 \in \Sigma$ if there exists a pair of processes $(P, M) : [0, d_P] \to \mathcal{G} \times \mathcal{M}$ such that the following conditions are satisfied:

$$\text{(3.37)} \quad \text{(i)} \quad (P(0), M(0)) = (g_0, m_0) = \sigma_0, \quad (P(d_P), M(d_P)) = (g^*, m^*) = \sigma^*,$$

$$\text{(3.38)} \quad \text{(ii)} \quad \widehat{d}(\sigma) = \widehat{d}(\widehat{\mathbf{e}}(\sigma_0, P_{[0,t]})) \geqq 0 \quad \text{for every instant of time} \quad t \in [0, d_P].$$

It is noteworthy that the accessibility criterion places some restrictions on the evolution function $\widehat{\mathbf{e}} : (\Sigma \times \Pi)^* \to \Sigma$.

3.10. Principle of the increase of entropy

Let us consider the intrinsic state space Σ. In this space we choose the initial intrinsic state σ_0 and an arbitrary intrinsic state σ. Let us assume that there exists a pair of processes $(P, M) : [0, d_P] \to \mathcal{G} \times \mathcal{M}$ such that

$$\text{(3.39)} \quad \begin{aligned} (P(0), M(0)) &= (g_0, m_0) = \sigma_0, \\ (P(t), M(t)) &= (g, m) = \sigma. \end{aligned}$$

The pair of the processes (P, M) is represented in the intrinsic state space Σ by the curve $\mathcal{L}$.

We define the curvilinear integral along the curve $\mathcal{L}$, which due to natural time parametrization can be written in the form

$$\text{(3.40)} \quad J(\sigma_0, \sigma) = \int_0^t \widehat{d}(P(\tau), M(\tau))d\tau = \int_0^t \widehat{d}(\widehat{\mathbf{e}}(\sigma_0, P_{[0,\tau]}))d\tau, \qquad t \in [0, d_P].$$

In a similar way we can define the integral

$$\text{(3.41)} \quad I(\sigma_0, \sigma) = \int_0^t \widehat{i}(P(\tau), M(\tau))d\tau = \int_0^t \widehat{i}(\widehat{\mathbf{e}}(\sigma_0, P_{[0,\tau]}))d\tau, \qquad t \in [0, d_P].$$

The integrals $J(\sigma_0, \sigma)$ and $I(\sigma_0, \sigma)$ are called the general dissipation integral and the internal dissipation integral, respectively.

Let us consider in the intrinsic state space Σ two intrinsic states σ_a and σ_b, which lie on the curve $\mathcal{L}$. The intrinsic state σ_a corresponds to the instant of time $t_a \in [0, d_P]$ and the intrinsic state σ_b to the instant of time $t_b \in [0, d_P]$, and of course $t_b > t_a$.

The dissipation principle requires that

$$J(\sigma_0, \sigma_b) - J(\sigma_0, \sigma_a) \geqq 0. \tag{3.42}$$

Principle of the increase of entropy: For all σ_a, $\sigma_b \in \Sigma$, σ_b is accessible from σ_a if, and only if, the general dissipation integral of σ_b is not less than that of σ_a.

It is important to note that the internal dissipation integral (3.41) is a measure of the irreversibility of a local thermodynamical process for the case when $\mathbf{q}(t) \equiv 0$ or $\nabla\vartheta(t) \equiv 0$ for $t \in [0, d_P]$ (i.e. for an adiabatic process), and may be interpreted as the empirical entropy[15)] or as the irreversibility function[16)].

If we assume this interpretation and the condition $\mathbf{q}(t) \equiv 0$ for $t \in [0, d_P]$ we can state the principle of increase of entropy in the form as follows (cf. RASTALL [105]): For all σ_a, $\sigma_b \in \Sigma$, σ_b is adiabatically accessible from σ_a if, and only if, the empirical entropy of σ_b is not less than that of σ_a.

The principle of the increase of entropy was first formulated by PLANCK [101, 102].

It is worth pointing out on some features of the thermodynamics of materials presented. We started from the dissipation principle in the form of the Clausius-Duhem inequality and we deduced two fundamental criteria for the thermodynamics of materials, namely the criterion of the selection of the response functions (functionals) occurring in the mathematical statement of the general principle of determinism and the accessibility criterion in the intrinsic state space Σ.

The accessibility criterion is connected withe the Caratheodory formulation of the second law of thermodynamics, cf. CARATHEODORY [14][17)].

As a consequence of the dissipation principle we also deduced the principle of the increase of entropy. Appropriate interpretation of the general dissipation integral (or the internal dissipation integral) led to the very old statement of the second law of thermodynamics first presented by PLANCK [101, 102][18)].

It is noteworthy to stress that all considerations concerned a general unique material structure before a particular realization of the method of preparation had been assumed.

[15)] The clear meaning of the empirical entropy can be found in the papers by BUCHDAHL [10, 11], cf. also BUCHDAHL, GREVE [12], COOPER [22], RASTALL [105] and BOYLING [7, 8].

[16)] The concept of the irreversibility function was introduced by GILES [39].

[17)] Caratheodory's formulation of classical thermodynamics has been developed further by BORN [6], BUCHDAHL [10, 11], FALK, JUNG [36], BERNSTEIN [4], BUCHDAHL, GREVE [12], LANDSBERG [52, 53, 54], COOPER [22], RASTALL [105] and BOYLING [7, 8].

[18)] Extension of Planck's idea has been done by BUCHDAHL [10], RASTALL [105] and BOYLING [7, 8].

4. Internal state variable material structure

4.1. Fundamental assumptions

Proposition 1. The method of preparation space for the element body with a unique material structure $(\mathcal{G},\ \Pi,\ \Sigma,\ \Re)$ is a finite dimensional vector space $\mathcal{W}$, i.e.

$$\mathcal{M} = \mathcal{W}, \tag{4.1}$$

and the intrinsic state space Σ is the set

$$\Sigma \equiv \{(g,m) \mid g \in \mathcal{G}, \qquad m \in \mathcal{W}_g, \qquad \overline{\overline{\mathcal{W}}}_g = \overline{\overline{\mathcal{Z}}}_P, \tag{4.2}$$

where $P \in \Pi_g$.

Elements of the method of preparation space $m \in \mathcal{W}$ are vectors. Components of the vector $m \in \mathcal{W}$ are called the internal state variables.

Proposition 2. Let us assume that such a mapping exists

$$\widehat{\mathcal{M}} : \Sigma \to \mathcal{W}, \tag{4.3}$$

that for every $P \in \Pi$ and $m_0 \in \mathcal{W}_{P^i}$ the initial value problem

$$\mathrm{L}_{\boldsymbol{v}} M(t) = \widehat{\mathcal{M}}(P(t), M(t)), \qquad M(0) = m_0 \tag{4.4}$$

has the unique solution $M : [0, d_P] \to \mathcal{W}$.

The constitutive mapping $\Re : (\Sigma \times \Pi)^* \to \mathcal{Z}$ has to satisfied the condition

$$\Re(\widehat{G}(\sigma), \cdot, P) : \mathcal{W}_{pi} \to \mathcal{Z}_P \quad \text{must be bijection} \tag{4.5}$$

for arbitrary $(\sigma, P) \in (\Sigma \times \Pi)^*$.

The evolution function $\widehat{\mathbf{e}} : (\Sigma \times \Pi^*) \to \Sigma$ is generated by the constitutive mapping $\Re$ and has the form

$$\widehat{\mathbf{e}}(\sigma, P) = (P^f, \mathcal{F}_{d_P}(P, \widehat{\mathbf{M}}(\sigma))), \tag{4.6}$$

where $\mathcal{F}$ denotes the solution functional of the initial value problem (4.4), i.e.

$$M(t) = \mathcal{F}_t(P, \widehat{\mathbf{M}}(\sigma)). \tag{4.7}$$

Equation $(4.4)_1$ is called the evolution equation for the internal state variable vector m, and $\widehat{\mathcal{M}}$ is called the method of preparation evolution function.

The principle of determinism for the material structure with internal state variables can be written as follows

$$Z(t) = s = \widehat{\mathbf{S}}(\sigma), \qquad \sigma = (P(t), M(t)) = (g, m), \tag{4.8}$$

or by using the evolution function in the form

$$Z(t) = \widehat{\mathbf{S}}(\widehat{\mathbf{e}}(\sigma_0, P_{[0,t]})), \qquad \sigma_0 = (g_0, m_0). \tag{4.9}$$

This principle of determinism can be expressed as follows: Transient value of the deformation-temperature configuration and transient value of the internal state variable vector determine the unique transient value of the reaction at a particle X in a body $\mathcal{B}$.

4.2. Investigation of the thermodynamical restrictions

The function $\widehat{\mathbf{S}}$ represents the constitutive functions $\widehat{\Psi}$, $\widehat{\mathrm{H}}$, $\widehat{\mathbf{T}}$, $\widehat{\mathbf{Q}}$. The domain of the constitutive functions is a subset of the intrinsic state $\Sigma = \mathcal{G} \times \mathcal{W}$. Since the method of preparation space $\mathcal{W}$ is a finite dimensional vector space and the deformation-temperature configuration space is also a finite dimensional space, hence the intrinsic state space Σ is the complete normed space (Banach space). Assuming the conditions 2–5 o of Section 3 we have the results $(3.30)_{1-3}$ valid for the material structure with the internal state variables, and the general dissipation inequality $(3.30)_4$ takes the form

$$\widehat{d}(\sigma) = -\partial_{M(t)}\widehat{\Psi}(\cdot) \cdot \mathrm{L}_{\boldsymbol{v}} M(t) - \frac{1}{\rho\vartheta(t)}\widehat{\mathbf{Q}}(\cdot) \cdot \mathrm{grad}\vartheta(t) \geqq 0. \tag{4.10}$$

The internal dissipation function $\widehat{i} : \Sigma \to \mathrm{R}^+$ for this material structure is determined by

$$\widehat{i}(\sigma) = -\frac{1}{\vartheta(t)}\partial_{M(t)}\widehat{\Psi}(\cdot) \cdot \mathrm{L}_{\boldsymbol{v}} M(t). \tag{4.11}$$

Taking advantage of the evolution equation $(4.4)_1$ we have

$$\widehat{i}(\sigma) = -\frac{1}{\vartheta(t)}\partial_{M(t)}\widehat{\Psi}(\cdot) \cdot \widehat{\mathcal{M}}((P(t), M(t)). \tag{4.12}$$

Now we can return to the discussion of the notion of the method of preparation as such information which is required for the description of the internal dissipation of an inelastic material. The expression (4.12) which defines the value of the internal dissipation function at the intrinsic state σ shows that full information given in the method of preparation, i.e. $M(t) = m$ and the evolution function $\widehat{\mathcal{M}}$, essentially determines the rate of internal dissipation for this intrinsic state σ. This conclusion is of fundamental importance for the physical interpretation of the internal state variables. Indeed, the internal dissipation in this conception is a key for this interpretation.

Definition 15. The body element with a unique material structure ($\mathcal{G}$, Π, Σ, $\widehat{\mathbf{S}}$, $\widehat{\mathbf{e}}$) satisfying the **Proposition 1 and 2** is called the material structure with internal state variables.

The using of the conception of the internal state variables for the mechanics of continuous media was proposed by COLEMAN, GURTIN [17]. In the theory of elasto-viscoplasticity this idea has been applied for the first time by PERZYNA, WOJNO [98], cf. also PERZYNA [72, 73, 75, 76, 77, 81] and PERZYNA, WOJNO [99].

5. Thermodynamical theory of elasto-viscoplasticity

5.1. Physical foundations and experimental motivations

5.1.1. Physical origin of elastic-viscoplastic response of a material of solids The high-rate deformation of face-centered cubic (f.c.c.) metals, such as copper, aluminum, lead and nickel has been recently extensively studied (cf. review paper by FOLLANSBEE [38]). It has been shown that the apparent strain rate sensitivity of f.c.c. metals has two origins: that associated with the finite velocity of dislocations, and that connected with the evolution of the dislocation substructure. The first of these two components – the instantaneous rate sensitivity – is related to the wait-times associated with thermally activated dislocation motion. The second component has more to do with the relative importance of dislocation generation and annihilation at different strain rates, and shall be referred to as the strain rate history effect.

The rate and temperature dependence of the flow stress of metal crystals can be explained by different physical mechanisms of dislocation motion. The microscopic processes combine in various ways to give several groups of deformation mechanisms, each of which can be limited to the particular range of temperature and strain rate changes, cf. PERZYNA [91].

It will be profitable for further considerations to discuss the interaction of the thermally activated and phonon dumping mechanisms.

5.1.2. Interaction of the thermally activated and phonon damping mechanisms If a dislocation is moving through the rows of barriers, then its velocity can be determined by the expression (cf. Fig. 4)

$$\mathrm{v} = AL^{-1}/(t_S + t_B), \tag{5.1}$$

where AL^{-1} is the average distance of dislocation movement after each thermal activation, t_S is the time a dislocation spent at the obstacle, and t_B is the time of travelling between the barriers.

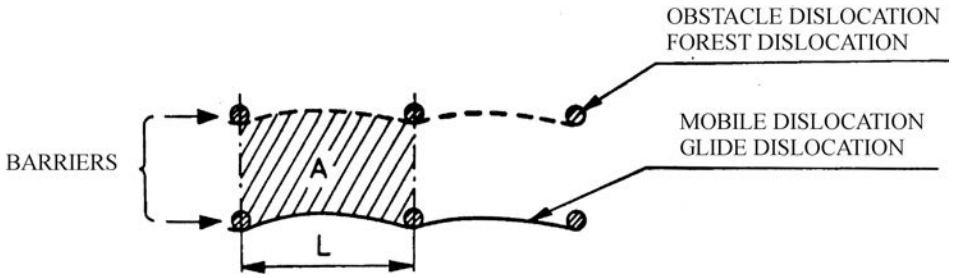

FIG. 4. Intersection of forest dislocations.

The shearing rate in single slip is given by the relationship (cf. SEEGER [108, 109, 110], KUMAR, KUMBLE [51], TEODOSIU, SIDOROFF [113] and PERZYNA [79, 85, 90, 91])

$$\dot{\in}^p = \frac{1}{T_{mT}} \langle \exp\{U[(\tau - \tau_\mu)Lb]/k\vartheta\} + BAL^{-1}\nu/(\tau - \tau_B)b\rangle^{-1}, \tag{5.2}$$

where U is the activation energy (Gibbs free energy), b denotes the Burgers vector, k is the Boltzman constant, ϑ actual absolute temperature, B denotes the dislocation drag coefficient, ν is the frequency of vibration of the dislocation, τ_μ denotes the athermal stress and τ_B is attributed to the stress needed to overcome the forest dislocation barriers to the dislocation motion and is called the back stress.

The two relaxation times

$$\frac{1}{T_{mT}} \frac{b\tau_B}{BAL^{-1}\nu} = \frac{\alpha b^2 \tau_B}{B} = \frac{1}{T_{mD}}, \tag{5.3}$$

and two effective resolved shear stresses

$$\tau_T^* = \tau - \tau_\mu \qquad \text{and} \qquad \tau_D^* = \tau - \tau_B \tag{5.4}$$

are separately defined for the thermally activated and phonon damping mechanisms, respectively.

If the time t_B taken by the dislocation to travel between the barriers in a viscous phonon medium is negligible when compared with the time t_S spent at the obstacle, then

$$\mathrm{v} = \frac{AL^{-1}}{t_S} \tag{5.5}$$

and we can focus our attention on the analysis of the thermally activated process.

When the ratio t_B/t_S increases then the dislocation velocity (5.1) can be approximated by the expression

$$\mathrm{v} = \frac{AL^{-1}}{t_B} \tag{5.6}$$

for the phonon damping mechanism.

It is noteworthy to stress that the relaxation time varies when the mechanism of the dislocation motion changes from the thermally activated to the phonon damping.

Experimental justifications of the thermally activated and phonon damping mechanisms as well as the discussion of their range rate and temperature changes for particular materials have been given in many papers. Particular importance for our purposes have results obtained by CAMPBELL, FERGUSON [13]. In their paper an account is given of experiments in which the shear flow stress of mild steel was measured at temperature from 195 to 713 K and strain rate from 10^{-3} to $4 \cdot 10^4$ s^{-1}. The flow stress at lower yield is plotted in Fig. 5 as shear stress against the logarithm of shear strain rate, for the various temperatures used throughout the investigation.

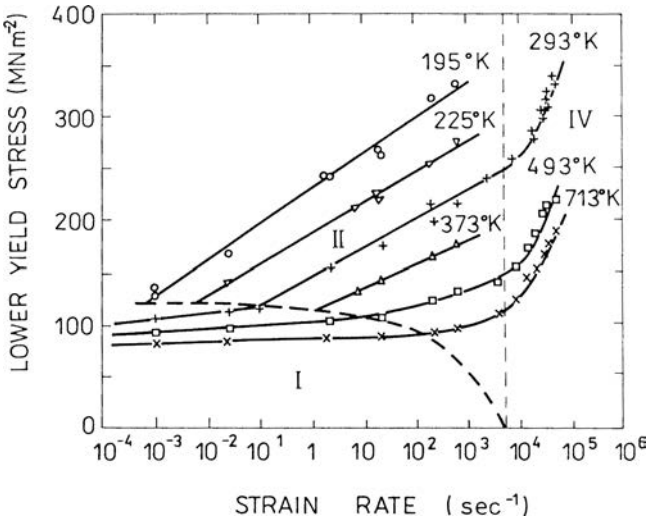

FIG. 5. Variation of lower yield stress with strain rate, at constant temperature. After CAMPBELL, FERGUSON [13].

For the purpose of the discussion which follows, it is convenient to divide the curves into three regions, each corresponding to a certain range of strain rate which is a function of the temperature. Following ROSENFIELD, HAHN [106] these will be referred to as region I, II and IV. These regions are indicated in Fig. 5, cf. also Fig. 6.

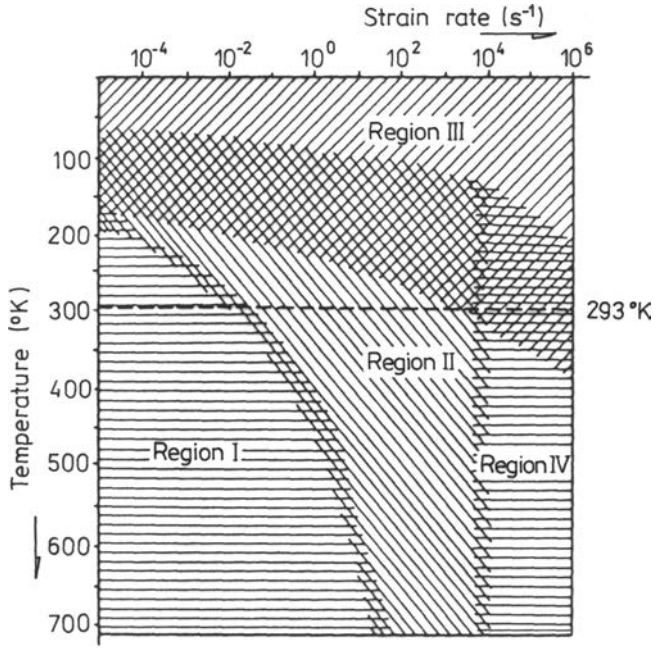

FIG. 6. Regions of the temperature strain rate spectrum of low carbon steel that reflect different mechanisms of yielding. After ROSENFIELD, HAHN [106] and CAMPBELL, FERGUSON [13].

In region I the flow stress shows a small temperature and strain rate sensitivity, the latter decreasing with increasing temperature. Prestraining increases the flow stress but has little effect on the rate sensitivity of the flow stress, $(\partial\tau/\partial \ln \dot{\epsilon}^p)_\vartheta$, at room temperature, cf. Fig. 7. The dominant factor in region I seems to be the long-range internal stress fields due to dislocations, precipitate particles, grain boundaries etc.

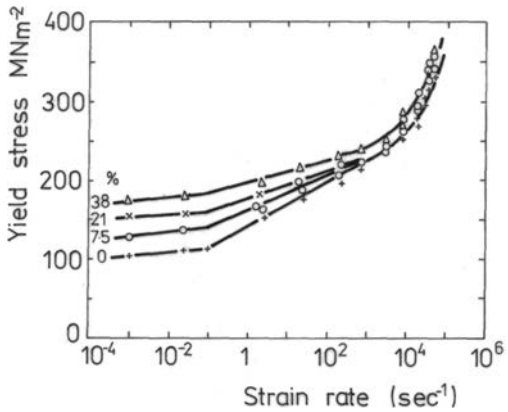

FIG. 7. Effect of pre-straining on variations of yield stress with strain rate. After CAMPBELL, FERGUSON [13].

In region II the flow stress shows greater rate and temperature sensitivities. From a survey of their own and previous work, ROSENFIELD, HAHN [106] concluded that in this region the rate sensitivity $(\partial\tau/\partial \ln \dot{\in}^p)_\vartheta$ is independent of temperature and strain rate. However, the data of CAMPBELL, FERGUSON [13] show a consistent increase in $(\partial\tau/\partial \ln \dot{\in}^p)_\vartheta$ as temperature is reduced.

It has been suggested by CAMPBELL, FERGUSON [13] that the flow behaviour throughout region II can be explained by the thermal activation of dislocation motion.

Since the relaxation time T_{mT} is related to the dislocation structure it may be governed by the deformation history, rather than a function of the state variables $\in^p$, τ and ϑ.

The experimental data obtained by CAMPBELL, FERGUSON [13] for mild steel in region II are properly interpreted by the linear approximation of the thermally activated theory.

Region IV is characterized by a rapid increase in semi- logarithmic rate sensitivity $(\partial\tau/\partial \ln \dot{\in}^p)_\vartheta$ with increasing strain rate, this parameter being approximately independent of temperature in the range 293 to 713 K.

In Fig. 8 the experimental data of CAMPBELL, FERGUSON [13] for region IV are replotted using a linear strain-rate scale, and it is seen that, within the accuracy of measurement, they can be represented by straight lines at all three temperatures and all three values of pre-strain. While the slopes of these lines show only a small dependence on temperature, their intercepts on the stress axis vary greatly with temperature.

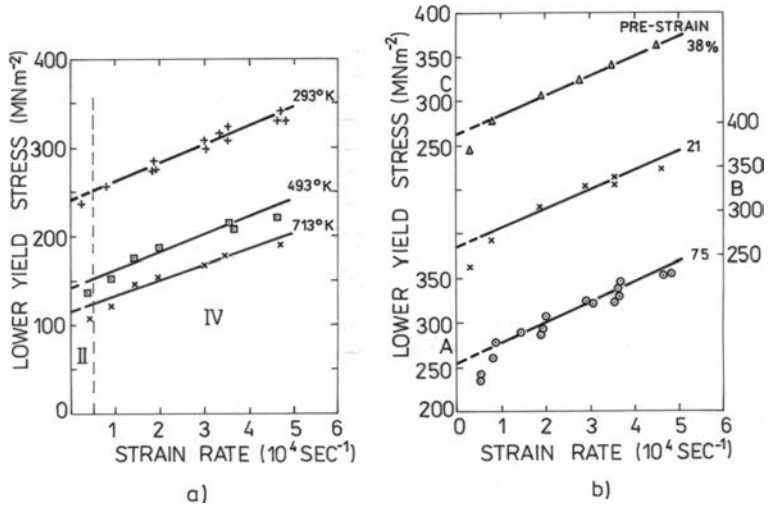

FIG. 8. Variation of lower yield stress with strain rate (region IV). (a) Zero pre-strain; temperature 293, 493, 713 K. (b) Pre-strain 7.5, 21, 38%; temperature 293 K. After CAMPBELL, FERGUSON [13].

5.1.3. Microshear banding effects Basing on the analysis of dynamical experimental observations for single crystals and polycrystalline metals (cf. PERZYNA [92]) we can conclude that microshear banding influences very much a substructure of a material under consideration. As a result of this it contributes mainly to viscoplastic strain rate effects.

For the elastic-viscoplastic model of polycrystalline solids the relaxation time T_m governs the viscoplastic flow in the entire range of strain rate changes and for classical models it is generally assumed as constant value. However, in real case it has to be a function of the rate of equivalent inelastic deformation $\dot{\epsilon}^P$ and the active microshear bands fraction f_{ms} (cf. NOWAK *et al.* [67], PERZYNA [92]).

For the description of plastic deformation of polycrystalline metals accounting for the effects of microshear bands please consult paper by PĘCHERSKI [100].

5.1.4. Induced anisotropy effects For our considerations of anisotropic effects, the metallurgical aspects of fracture and spalling have great importance. Effects of parameters such as grain size and substructure, crack/void initiation sites, micromechanical aspects of growth, and coalescence can influence fracture and spalling mechanisms.

There are essentially two modes of dynamic fracture: ductile and brittle. Ductile fracture is characterized by voids which, in spalling, tend to be spherical up to a certain size. Brittle fracture shows cracks with sharp tips at which fracture proceeds with relatively little plastic deformation. FCC metals exhibit a higher ductility at high strain rates and tend to spall in a ductile manner. BCC and HCP metals tend to spall by a brittle mode.

It is generally accepted that the intrinsic microdamage process consists of nucleation, growth and coalescence of microcracks (microvoids). Microfracture nucleation is classified into homogeneous and heterogeneous. Homogeneous nucleation takes place when thermal energy fluctuations is assisted (cf. MEYERS, AIMONE [60]). Heterogeneous nucleation is realized as the result of fracture of inclusions or second-phase particles, separation of interfaces, fracture of the matrix and fracture at grain boundaries, cf. Figs. 9, 10 and 11.

To show the complexity of the anisotropy phenomena in microdamage process we shell discuss several available experimental results.

The most popular dynamical experiment[19)] in the investigation of the fracture phenomenon in metals is a plate-impact configuration system. This experimental system consists of two plates, a projectile plane plate impacts against

[19)] For a thorough discussion of the experimental and theoretical works in the field of dynamic fracture and spalling of metals please consult the review papers by MEYERS, AIMONE [60] and CURRAN *et al.*[25], cf. also MEYERS [59].

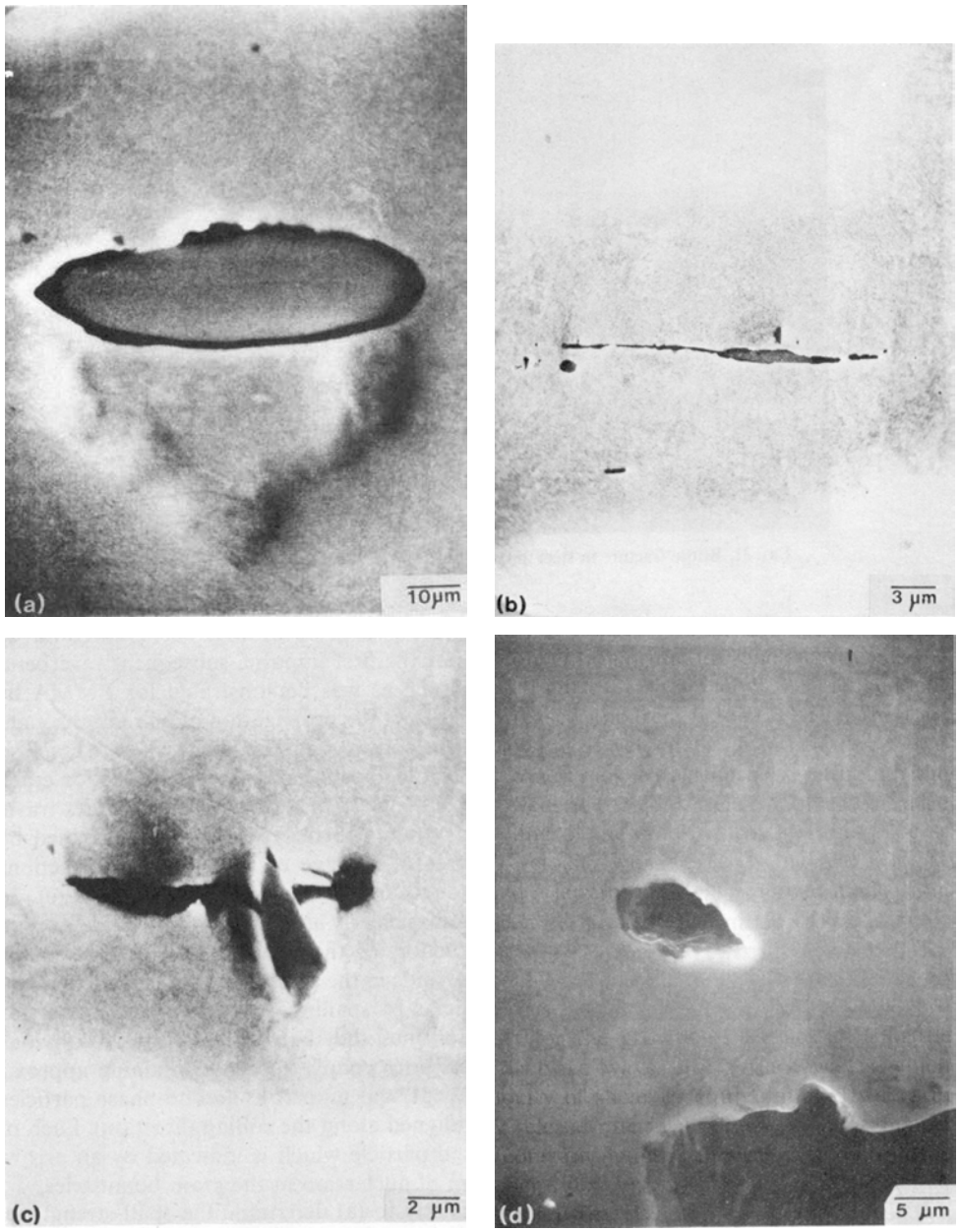

FIG. 9. Four different sources of spall initiation in steel. (a) Debonding at MnS – matrix interface; (b) crack starting at MnS and propagating into matrix; (c) crack starting at silicate interface and propagating into matrix; (d) void apparently homogeneously generated (After SHOCKEY *et al.* [111]).

a target plane. This is a good example of a dynamic deformation process. If impact velocity is sufficiently high the propagation of a plastic wave through

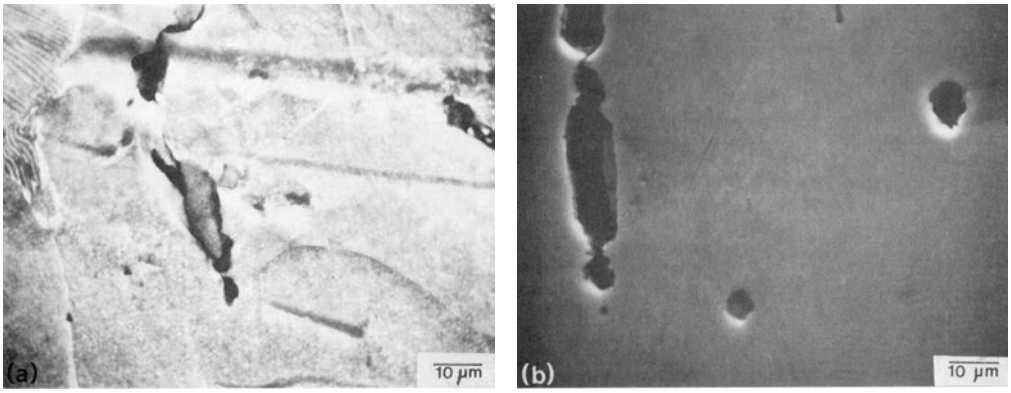

FIG. 10. Two incidences of fracture initiation at MnS – matrix interface in steel. In (b) fracture propagates in a ductile manner, by void nucleation and growth (After SHOCKEY *et al.* [111]).

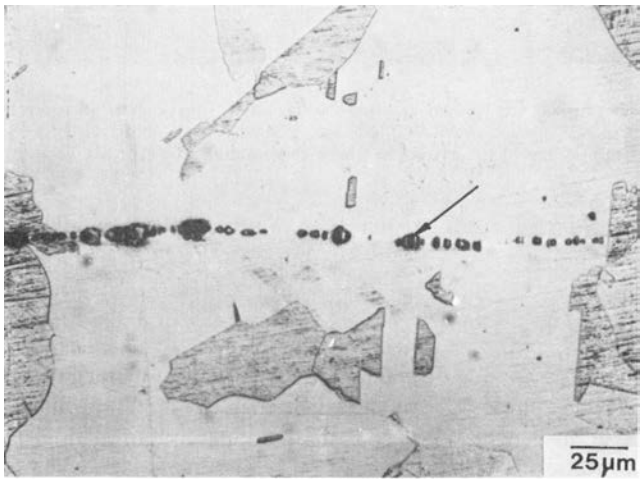

FIG. 11. Formation of a string of voids by nucleation at second-phase particles in nickel. Some second-phase particles that are fractured can be seen (After SHOCKEY *et al.* [111]).

the target is generated. The reflection and interaction of waves result a net tensile pulse in the target plate. If this stress pulse has sufficient amplitude and sufficient time duration, it will cause separation of the material and spalling process.

The reason for choosing this particular kind of dynamical experiment is that postshot photomicrographic observations of the residual porosity are available, and the stress amplitude and pulse duration can be performed sufficiently great to produce substantial porosity and the spall of the target plate.

The experimental data presented by SEAMAN *et al.* [107] illustrate damage phenomena and provide a common basis for considering damage criteria. They

have used a plate-impact configuration system. Following the compression waves resulting from the impact, rarefaction waves have intersected near the middle of the target plate to cause damage in the form of nearly spherical voids. The heaviest damage is localized in a narrow zone, which is called the spall plane. Both the number and the size of voids decrease with distance from this zone. This type of damage is termed ductile fracture because of high ductility (ability to flow) required of the plate material, Fig. 12.

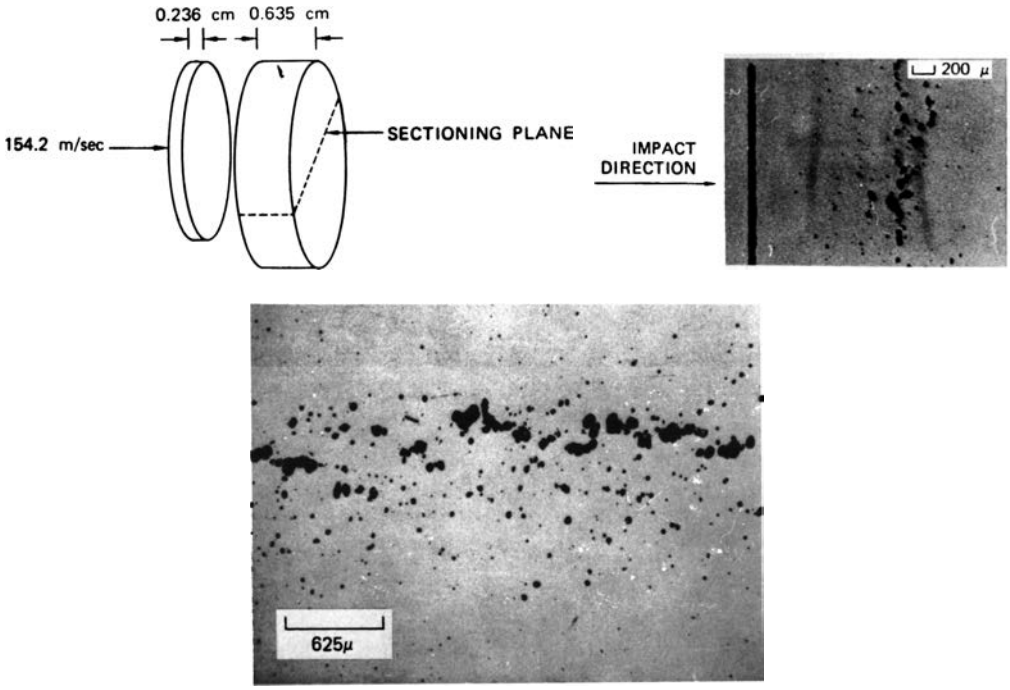

FIG. 12. A cross section of an aluminium target plate that has undergone a planar impact by another aluminium plate (After SEAMAN *et al.* [107]).

The final damage of the target plate (aluminium 1145) for a constant shot geometry but for different impact velocities has been performed by BARBEE *et al.* [3]. The results suggest dependence of spalling process on the pulse amplitude, Fig. 13.

A sample of full separation is shown in Fig. 14, an aluminium target impacted by a plate has been damaged to the extent that full separation occurred near the center of the target, cf. SEAMAN *et al.* [107]. The authors suggested that this full separation appears as a macrocrack propagating through heavily damaged material. The macrocrack occurs as a result of coalescence of microvoids which is also visible in Fig. 14.

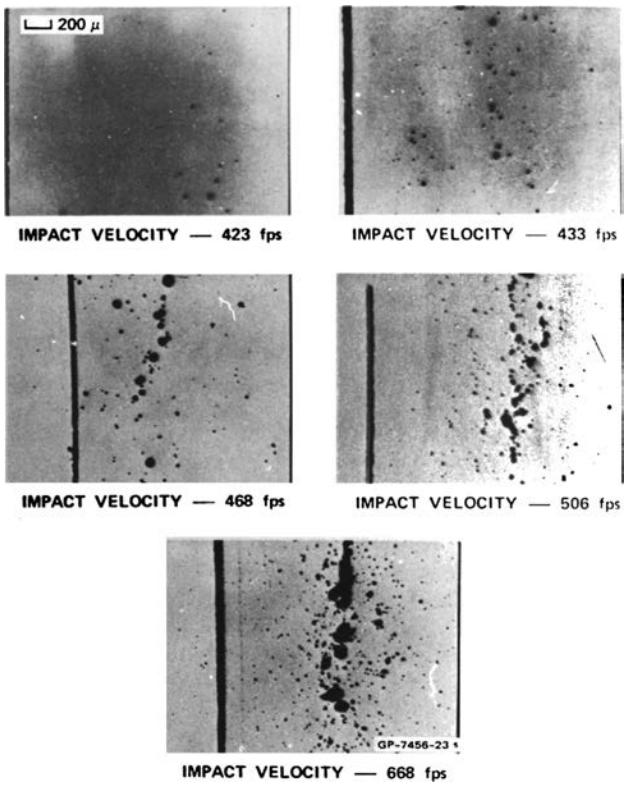

FIG. 13. The final damage of the aluminum 1145 target plate for a constant shot geometry but for different impact velocities (After BARBEE *et al.* [3]).

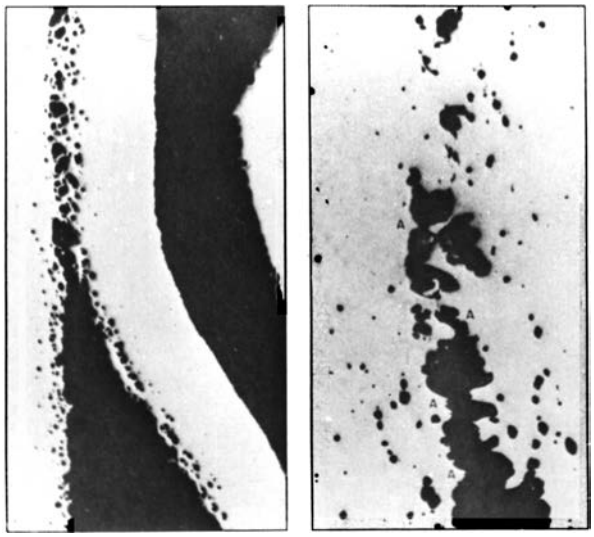

FIG. 14. A sample of full separation of an aluminum target. Impact test performed by SEAMAN *et al.* [107].

Spalling by ductile void formation in nickel is characterized by ellipsoidal cracks with large axes perpendicular to the direction of the applied tensile stress, cf. Fig. 15. A more advanced microdamage process has been shown in Fig. 16, where crack nucleation growth, and coalescence mechanisms in nickel have been observed.

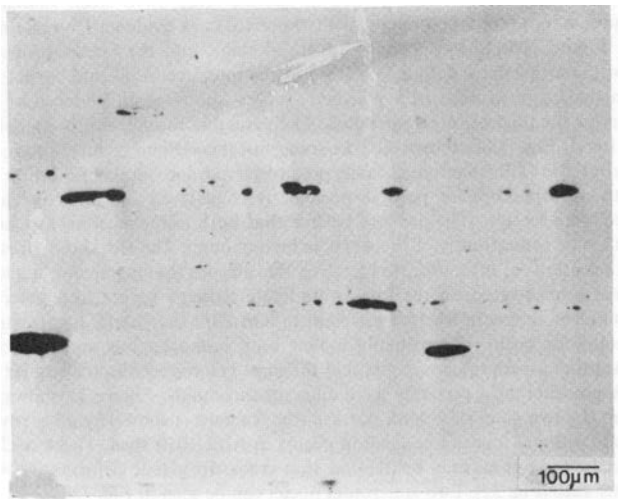

FIG. 15. Spalling by ductile void formation in nickel (After SHOCKEY *et al.* [111]).

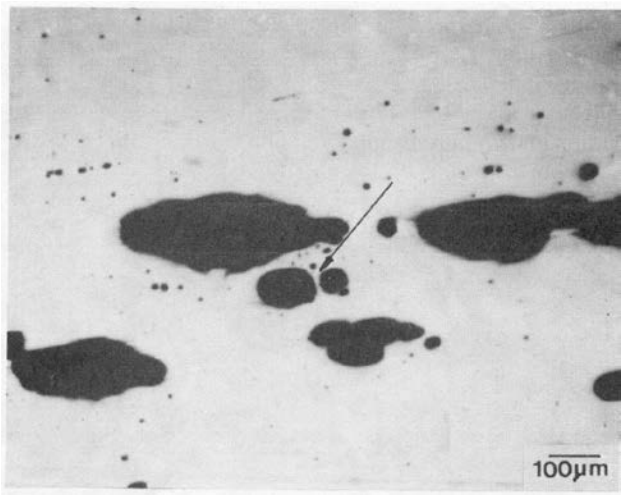

FIG. 16. Void nucleation, growth, and coalescence observed in nickel (After SHOCKEY *et al.* [111]).

Spalling by brittle fracture in low-carbon steel is shown in Fig. 17 (cf. CURRAN *et al.* [24]).

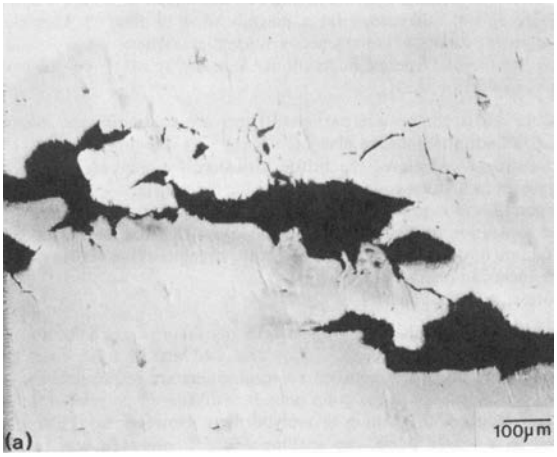

FIG. 17. Spalling by brittle fracture in low-carbon steel (After SHOCKEY *et al.* [111]).

An example of brittle fracture for Armco iron is presented in Fig. 18 (cf. CURRAN *et al.* [24]). It shows the polished cross section through plate impact specimen with very well visible cleavage (penny shape) microcracks. The damage, which appears as randomly oriented planar microcracks, depends on the impact velocity as well as on the duration of the tensile wave. The second property is directly observed from the results presented in Fig. 19 (cf. CURRAN *et al.* [23]). Use of a tapered flyer results in longer tensile impulses at the thicker end. As it is shown in Fig. 19 these longer pulses lead to greater damage in the Armco iron target (the inset gives to approximate durations of the tensile pulses). The damage observed in this experiment is termed brittle, although the microcrack growth is much slower than elastic crack velocities, indicating considerable plastic flow at micro crack tips.

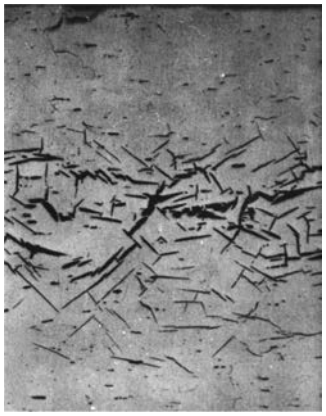

FIG. 18. Internal cleavage (penny shape) microcracks caused by shock loading in the polished cross section of an Armco iron specimen (After CURRAN *et al.* [24]).

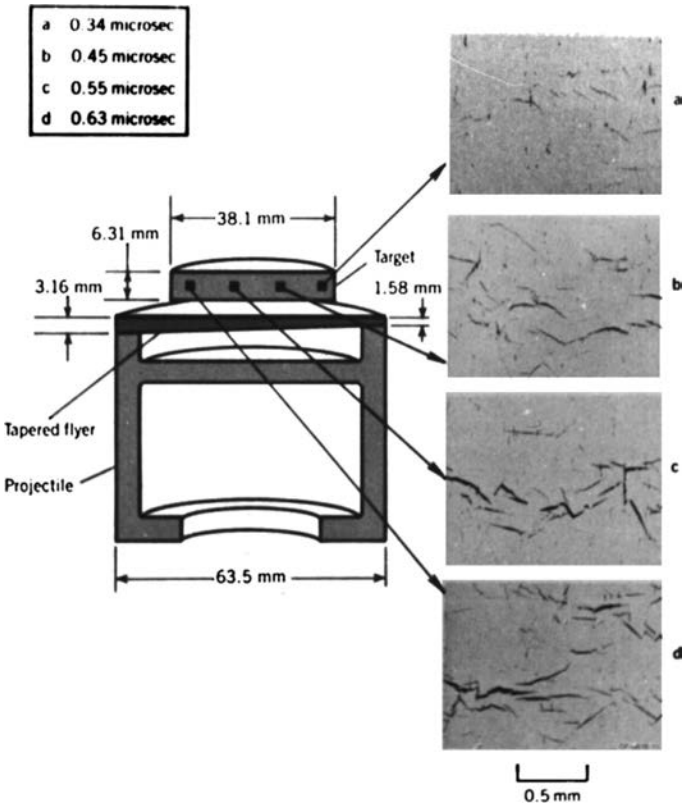

FIG. 19. Tapered flyer impact experimental results for the Armco iron target (After CURRAN *et al.* [23]).

Adiabatic shear band localization during dynamic process can be another good example of anisotropic effects. Shear band form in one direction, which is determined by the state of stress and the properties of the material of a body, as well as by the boundary conditions.

GREBE, PAK and MEYERS [45] were conducted ballistic impact experiments on 12.5 mm thick commercial purity titanium and T-6pct Al-4pct V alloy plates using steel projectiles with 10.5 mm diameter. The impact velocities in their experiments varied between 578 m/s and 846 m/s. The microstructural damage mechanisms associated with shear band formation, shock wave and dynamic fracture were investigated by optical and scanning and transmission electron microscopy. The shear band were found along the two sides of the cross-section passing through the axis of the projectile. The measured shear band width in T6A14V varied between 1 and 10 μm. Observations of the onset of fracture along the shear band were also conducted. Spherical and ellipsoidal microcracks in T6A14V were found along the bands, Fig. 20. The mechanism of final fail-

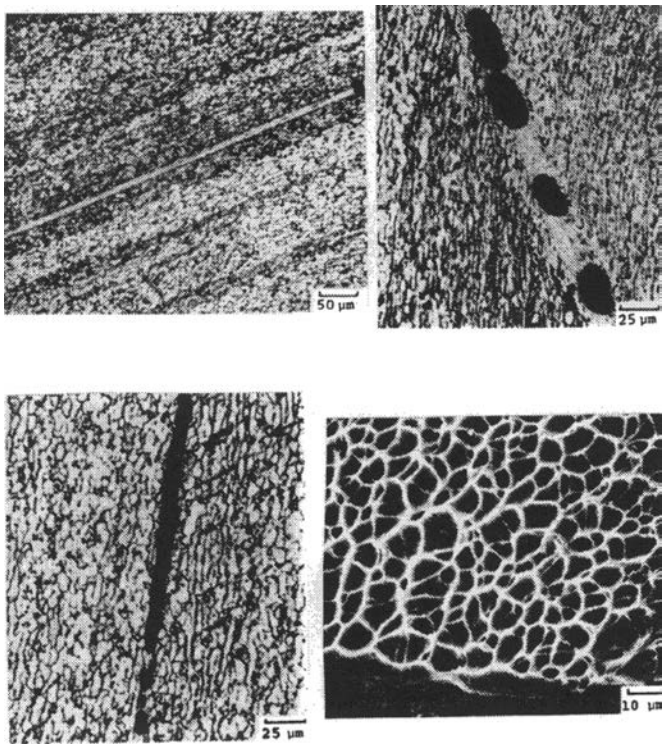

FIG. 20. Shear band in Ti6Al4V target impacted at 846 m/s (After GREBE *et al.* [45]): a) single shear band, b) microcracks in the shear band region, c) elongated macrocracks along the shear band, d) characteristic dimples observed in spall region.

ure in T6A14V is a simple propagation of a macrocrack along the damaged material within the shear band region. In the explanation of the phenomenon of fracture along shear band very important role has the microdamage process which consists of the nucleation, growth and coalescence of microvoids.

The investigations reported by GREBE *et al.* [45] indicated that in dynamic processes the shear band regions behave differently than adjacent zones, cf. Fig. 20. Within the shear band region the deformation process is characterized by very large strains (shear strains over 100%) and very high strain rates (10^3–10^5 s^{-1}). The strain rate sensitivity of a material becomes very important feature of the shear band region and the micro-damage process is intensified.

5.1.5. Heuristic multiscale considerations Let us consider a body $\mathcal{B}$, on a part $\partial\mathcal{B}_1$ of $\partial\mathcal{B}$ is prescribed sudden deposition of intense pulses of energy, and another part $\partial\mathcal{B}_2$ is free. This macroscopic situation is shown in Fig. 23 (macroscale). In a body $\mathcal{B}$ let us consider a subbody $\mathcal{A}$ with the particle A described by $(\mathbf{x}, t)$. Figure 23 (mesoscale) (cf. Fig. 21) shows a typical polished sur-

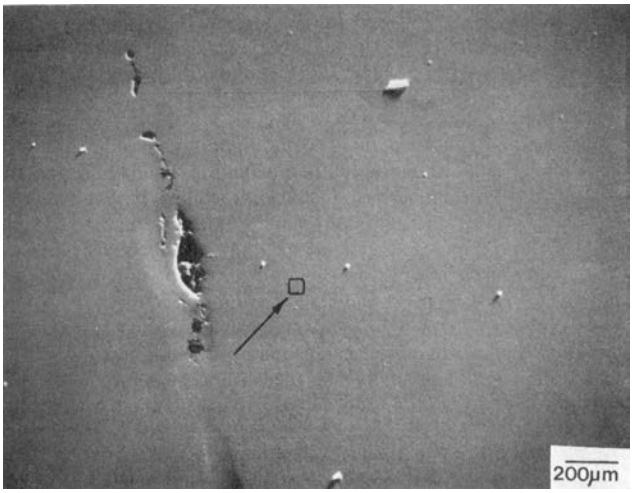

FIG. 21. Appearance of surroundings of spall in nickel (SEM of polished section); square indicates portion that was magnified (After SHOCKEY *et al.* [111]).

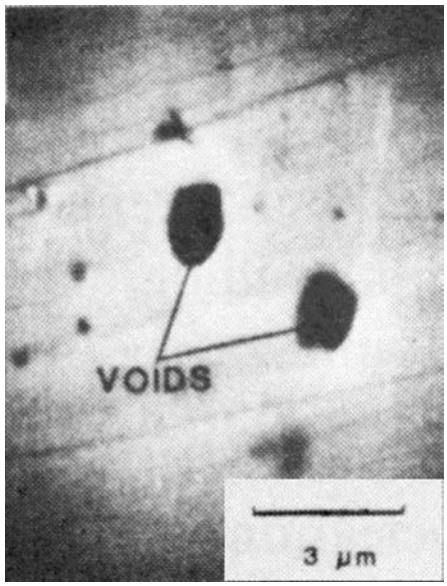

FIG. 22. Magnified view of area shown in Fig. 21; individual photomicrograph taken at 10 000× magnification. Two ductile microvoids forming homogeneously in matrix (After SHOCKEY *et al.* [111]).

face of spall nickel, taken from the neighbourhood of a particle A, at a magnification 75x. In an attempt to pay attention to smaller microcracks (microvoids), the region marked with a square was observed by scanning-electron microscopy individual photomicrograph is taken at 10 000x. Figure 23 (microscale) (cf. Fig. 22)

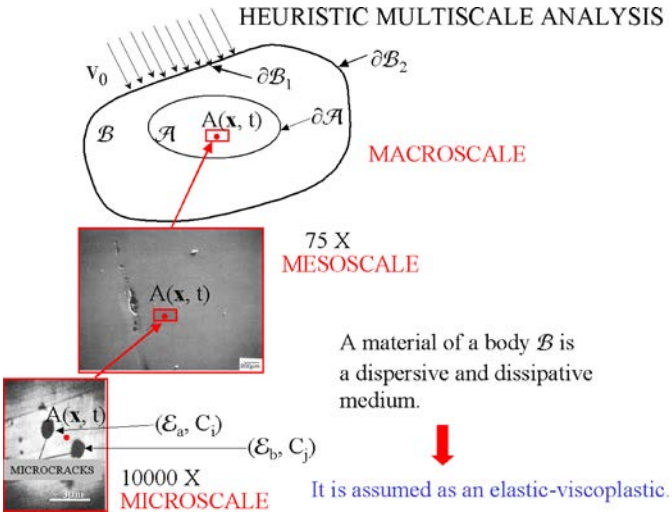

FIG. 23. Heuristic multiscale considerations.

shows two nucleated microcracks in the vicinity of the particle $\mathrm{A}(\mathbf{x}, t)$. To analyse more precisely the situation in the microscale let us take the properties of nickel into account. We assume that a material of a body $\mathcal{B}$ is a dispersive and dissipative medium. In a dispersive medium any initial disturbance is broken up into a system of wavegroups. Then the energy is propagated to the particular nucleated microcrack with the group velocity. Thus, each of these two microcracks will receive different portion of energy: ε_a and ε_b, distributed by the group velocities C_i and C_j, respectively. This important fact observed leads to the fundamental conclusion that the evolution of microdamage has anisotropic nature.

As the result of this multiscale analysis we have very crucial suggestions concerning the constitutive description:

(i) Since a material of a body $\mathcal{B}$ (for various metals like nickel, copper, aluminium, lead and mild steel) is a dispersive and dissipative medium, then it can be modelled as an elastic-viscoplastic.

(ii) Since the dispersive effects for propagation of wave phenomena play so important role, then we have very heterogeneous deformation processes which lead to the residual type stresses and generate the strain induced anisotropy.

(iii) The anisotropy of intrinsic microdamage processes observed experimentally and discussed on the basis of multiscale consideration is very fundamental for the proper description of fracture phenomena.

Finally, we have good foundations to suggest a finite set of the internal state variables. We propose to assume as the internal state variables: the equivalent viscoplastic deformation $\in^p$, which will describe inelastic flow phenomena, the

microdamage second order tensor $\boldsymbol{\xi}$, to take account for the anisotropic microdamage mechanisms, and the back stress (residual stress) $\boldsymbol{\alpha}$, which will model the kinematic hardening intrinsic mechanism as an approximate description of the strain induced anisotropy.

5.2. Constitutive postulates and fundamental assumptions

Our main objective is the development of an elasto-viscoplastic material model within the thermodynamical covariant unique constitutive structure with a finite set of the internal state variables.

Let us assume that we have the material structure with a finite set of the internal state variables $(\mathcal{G}, \Pi, \Sigma, \widehat{\mathbf{S}}, \widehat{\mathbf{e}})$ and additionally let us introduce for our practical purposes the fundamental postulates as follows:

(i) The internal state variable vector has the form

$$m = \boldsymbol{\mu} = (\in^p, \boldsymbol{\xi}, \boldsymbol{\alpha}), \tag{5.7}$$

thus it consists of one scalar value and two second order tensors, namely the equivalent viscoplastic deformation, i.e.

$$\in^p = \int_0^t \left(\frac{2}{3}\mathbf{d}^p; \mathbf{d}^p\right)^{1/2} dt, \tag{5.8}$$

which aims to describe dissipation generated by elastic-viscoplastic flow phenomena; $\boldsymbol{\xi}$ denotes the microdamage second order tensor, with the physical interpretation that $(\boldsymbol{\xi} : \boldsymbol{\xi})^{1/2} = \xi$ defines the volume fraction porosity and takes account for dissipation produced by microdamage mechanisms; and $\boldsymbol{\alpha}$ is the residual stress (the back stress) and aims at the description of dissipation occured during the kinematic hardening mechanism.

(ii) It is assumed that the free energy function is given by

$$\psi = \widehat{\psi}(\mathbf{e}, \mathbf{F}, \vartheta, \boldsymbol{\mu}). \tag{5.9}$$

(iii) The viscoplastic potential function is defined as

$$f = f(\widetilde{J}_1, \widetilde{J}_2, \vartheta, \boldsymbol{\mu}), \tag{5.10}$$

where $\widetilde{J}_1$, $\widetilde{J}_2$ denote the first two invariants of the stress tensor $\widetilde{\boldsymbol{\tau}} = \boldsymbol{\tau} - \boldsymbol{\alpha}$.

(iv) It is proposed the evolution equations for a set of the internal state variables

$$\mathbf{d}^p = \Lambda \mathbf{P}, \qquad \mathrm{L}_{\boldsymbol{v}}\boldsymbol{\xi} = \boldsymbol{\Xi}, \qquad \mathrm{L}_{\boldsymbol{v}}\boldsymbol{\alpha} = \mathbf{A} \tag{5.11}$$

and for the plastic spin

$$\boldsymbol{\omega}^p = \Lambda \boldsymbol{\Omega}, \tag{5.12}$$

where for an elasto-viscoplastic model of a material we assume (cf. PERZYNA [70, 71, 72, 73, 87, 88, 91])

$$\Lambda = \frac{1}{T_m} \left\langle \Phi \left(\frac{f}{\kappa} - 1 \right) \right\rangle, \tag{5.13}$$

T_m denotes the relaxation time for mechanical disturbances, the isotropic work-hardening-softening function is

$$\kappa = \widehat{\kappa}(\in^p, \vartheta, \boldsymbol{\xi}), \tag{5.14}$$

Φ is the empirical overstress function, the bracket $\langle \cdot \rangle$ defines the ramp function,

$$\mathbf{P} = \left. \frac{\partial f}{\partial \boldsymbol{\tau}} \right|_{\boldsymbol{\xi}=\text{const}} \left(\left\| \frac{\partial f}{\partial \boldsymbol{\tau}} \right\| \right)^{-1}, \tag{5.15}$$

$\boldsymbol{\Xi}$, $\mathbf{A}$ and $\boldsymbol{\Omega}$ denote the evolution functions which have to be determined.

5.3. Microshear banding effects

To describe the microshear banding effects let us assume that the relaxation time T_m depends on the active microshear bands fraction f_{ms} and on the rate of equivalent viscoplastic deformation $\dot{\in}^P$ (cf. PĘCHERSKI [100], NOWAK *et al.* [67], Perzyna [92]), i.e.

$$T_m = T_m \left(f_{ms}, \dot{\in}^P \right). \tag{5.16}$$

Additionally we introduce the simplification as follows

$$T_m = T_m^0 \phi_1 \left(f_{ms} \right) \phi_2 \left(\dot{\in}^P \right). \tag{5.17}$$

For example, for mild steel (cf. Perzyna [92]) we can postulate

$$\phi_1 \left(f_{ms} \right) = \left[1 - f_{ms} \left(\in^P \right) \right] = \left[1 - f_{ms}^0 \frac{1}{1 + \exp\left(a - b \in^P \right)} \right], \tag{5.18}$$

and

$$\phi_2 \left(\dot{\in}^P \right) = \left(\frac{\dot{\in}^P}{\dot{\in}_s^P} - 1 \right)^{1/p}, \tag{5.19}$$

where f_{ms}^0, a, b and p are material parameters.

Finally we have

$$T_m = T_m^0 \left[1 - f_{ms}^0 \frac{1}{1 + \exp\left(a - b \in^P \right)} \right] \left(\frac{\dot{\in}^P}{\dot{\in}_s^P} - 1 \right)^{1/p}. \tag{5.20}$$

5.4. Constitutive assumption for the plastic spin

Let us postulate that $\boldsymbol{\Omega}$ has the form[20] (cf. DAFALIAS [26] and LORET [57])

$$\boldsymbol{\Omega} = \eta^*(\boldsymbol{\alpha}\cdot\mathbf{P} - \mathbf{P}\cdot\boldsymbol{\alpha}), \tag{5.21}$$

where η^* denotes the scalar valued function of the invariants of the tensors $\boldsymbol{\alpha}$, $\boldsymbol{\xi}$ and $\mathbf{P}$, and may depend on temperature ϑ.

5.5. Anisotropic intrinsic microdamage mechanisms

To take into consideration the observed time dependent effects it is advantageous to use the proposition of the description of the intrinsic microdamage process presented by PERZYNA [83, 84], DUSZEK-PERZYNA, PERZYNA [32], and DORNOWSKI, PERZYNA [28].

Let us assume that the intrinsic microdamage process consists of the nucleation and growth mechanisms[21].

Based on the heuristic suggestions and taking into account the influence of the stress triaxiality and anisotropic effects on the nucleation and growth mechanisms we assume the evolution equation for the microdamage tensor $\boldsymbol{\xi}$ as follows

$$\mathrm{L}_{\boldsymbol{v}}\boldsymbol{\xi} = \frac{\partial h^*}{\partial \boldsymbol{\tau}}\frac{1}{T_m}\left\langle \Phi\left[\frac{\widetilde{I}_n}{\tau_n(\boldsymbol{\xi},\boldsymbol{\alpha},\vartheta,\in^p)} - 1\right]\right\rangle + \frac{\partial g^*}{\partial \boldsymbol{\tau}}\frac{1}{T_m}\left\langle \Phi\left[\frac{\widetilde{I}_g}{\tau_{eq}(\boldsymbol{\xi},\boldsymbol{\alpha},\vartheta,\in^p)} - 1\right]\right\rangle. \tag{5.22}$$

The tensorial function $\dfrac{\partial h^*}{\partial \boldsymbol{\tau}}$ describes the mutual microcrack interaction for nucleation mechanism, while the tensional function $\dfrac{\partial g^*}{\partial \boldsymbol{\tau}}$ represents the mutual microcrack interaction for growth process, τ_n and τ_{eq} denote the threshold stresses for microcrack nucleation and growth, respectively.

$$\widetilde{I}_n = a_1\widetilde{J}_1 + a_2\sqrt{\widetilde{J}_2'} + a_3\left(\widetilde{J}_3'\right)^{1/3} \tag{5.23}$$

[20] For a thorough discussion of a concept of the plastic spin and its constitutive description in phenomenological theories for macroscopic large plastic deformations please consult the critical review paper by VAN DER GIESSEN [117].

[21] Recent experimental observation results (cf. SHOCKEY *et al.* [112]) have shown that coalescence mechanism can be treated as nucleation and growth process on a smaller scale.

defines the stress intensity invariant for nucleation, a_i $(i = 1, 2, 3)$ are the material constants, $\widetilde{J}_2'$ and $\widetilde{J}_3'$ are the second and third invariants of the stress deviator $\widetilde{\boldsymbol{\tau}}' = (\boldsymbol{\tau} - \boldsymbol{\alpha})'$,

$$\widetilde{I}_g = b_1 \widetilde{J}_1 + b_2 \sqrt{\widetilde{J}_2'} + b_3 \left(\widetilde{J}_3' \right)^{1/3}, \tag{5.24}$$

defines the stress intensity invariant for growth and b_i $(i = 1, 2, 3)$ are the material constants. This determines the evolution function $\boldsymbol{\Xi}$.

In the evolution equation (5.22) the functions

$$h = \widehat{h} \left(\boldsymbol{\tau}, \vartheta, \in^P, \boldsymbol{\xi}, \boldsymbol{\alpha} \right), \tag{5.25}$$

$$g = \widehat{g} \left(\boldsymbol{\tau}, \vartheta, \in^P, \boldsymbol{\xi}, \boldsymbol{\alpha} \right) \tag{5.26}$$

play the fundamental role, and have to be determined based on available experimental observation data. We also introduced the denotations as follows

$$\frac{\partial h^*}{\partial \boldsymbol{\tau}} = \frac{\partial \widehat{h}}{\partial \boldsymbol{\tau}} \left(\left\| \frac{\partial \widehat{h}}{\partial \boldsymbol{\tau}} \right\| \right)^{-1}, \qquad \frac{\partial g^*}{\partial \boldsymbol{\tau}} = \frac{\partial \widehat{g}}{\partial \boldsymbol{\tau}} \left(\left\| \frac{\partial \widehat{g}}{\partial \boldsymbol{\tau}} \right\| \right)^{-1}. \tag{5.27}$$

The threshold stress τ_n and τ_{eq} for microcrack nucleation and growth, respectively, can be assumed as the material functions in the form

$$\tau_n = \tau_n \left(\boldsymbol{\xi}, \boldsymbol{\alpha}, \vartheta, \in^P \right), \qquad \tau_{eq} = \tau_{eq} \left(\boldsymbol{\xi}, \boldsymbol{\alpha}, \vartheta, \in^P \right). \tag{5.28}$$

5.6. Kinematic hardening

To determine the evolution function $\mathbf{A}$ we shall follow some results obtained by Duszek, Perzyna [30]. The kinematic hardening evolution law takes the form

$$\mathrm{L}_{\boldsymbol{\upsilon}} \boldsymbol{\alpha} = \frac{1}{T_m} \left\langle \Phi \left(\frac{f}{\kappa} - 1 \right) \right\rangle \left[r_1 \mathbf{P} + r_2 \frac{\mathbf{P} : \mathbf{Q}}{\widetilde{\boldsymbol{\tau}} : \mathbf{Q} + r_3 \boldsymbol{\xi} : \mathbf{Q}} (\widetilde{\boldsymbol{\tau}} + r_3 \boldsymbol{\xi}) \right], \tag{5.29}$$

where r_1, r_2 and r_3 are the material coefficients and

$$\mathbf{Q} = \left[\frac{\partial f}{\partial \boldsymbol{\tau}} + \left(\frac{\partial f}{\partial \boldsymbol{\xi}} - \frac{\partial \kappa}{\partial \boldsymbol{\xi}} \right) : \frac{\partial \boldsymbol{\xi}}{\partial \boldsymbol{\tau}} \right] \left\| \frac{\partial f}{\partial \boldsymbol{\tau}} + \left(\frac{\partial f}{\partial \boldsymbol{\xi}} - \frac{\partial \kappa}{\partial \boldsymbol{\xi}} \right) : \frac{\partial \boldsymbol{\xi}}{\partial \boldsymbol{\tau}} \right\|^{-1}. \tag{5.30}$$

The kinetic law (5.29) represents the linear combination of the Prager and Ziegler kinematic hardening rules and additionally depends linearly on the microdamage tensor $\boldsymbol{\xi}$.

5.7. Thermodynamic restrictions and rate type constitutive relations

Suppose the axiom of the entropy production holds. Then the constitutive assumption (5.9) and the evolution equations (5.11) and (5.12) lead to the results as follows

$$\boldsymbol{\tau} = \rho_{Ref}\frac{\partial\widehat{\psi}}{\partial\mathbf{e}}, \qquad \eta = -\frac{\partial\widehat{\psi}}{\partial\vartheta}, \qquad -\frac{\partial\widehat{\psi}}{\partial\boldsymbol{\mu}}\cdot \mathrm{L}_{\boldsymbol{v}}\boldsymbol{\mu} - \frac{1}{\rho\vartheta}\mathbf{q}\cdot \mathrm{grad}\vartheta \geq 0. \tag{5.31}$$

The rate of internal dissipation is determined by

$$\begin{aligned}\widehat{\vartheta i} &= -\frac{\partial\widehat{\psi}}{\partial\boldsymbol{\mu}}\cdot \mathrm{L}_{\boldsymbol{v}}\boldsymbol{\mu} \\ &= -\left[\frac{\partial\widehat{\psi}}{\partial\in^{P}}\sqrt{\frac{2}{3}} + \frac{\partial\widehat{\psi}}{\partial\boldsymbol{\alpha}} : \left(r_1\mathbf{P} + r_2\frac{\mathbf{P}:\mathbf{Q}}{\widetilde{\boldsymbol{\tau}}:\mathbf{Q} + r_3\boldsymbol{\xi}:\mathbf{Q}}\left(\widetilde{\boldsymbol{\tau}} + r_3\boldsymbol{\xi}\right)\right)\right]\Lambda - \frac{\partial\widehat{\psi}}{\partial\boldsymbol{\xi}} : \boldsymbol{\Xi}.\end{aligned} \tag{5.32}$$

Operating on the stress relation $(5.31)_1$ with the Lie derivative and keeping the internal state vector constant, we obtain

$$\mathrm{L}_{\boldsymbol{v}}\boldsymbol{\tau} = \mathcal{L}^{e} : \mathbf{d} - \mathcal{L}^{th}\dot{\vartheta} - \left[\left(\mathcal{L}^{e} + \mathbf{g}\boldsymbol{\tau} + \boldsymbol{\tau}\mathbf{g} + \mathcal{W}\right) : \mathbf{P}\right]\frac{1}{T_m}\left\langle \Phi\left(\frac{f}{\kappa} - 1\right)\right\rangle, \tag{5.33}$$

where

$$\begin{gathered}\mathcal{L}^{e} = \rho_{Ref}\frac{\partial^2\widehat{\psi}}{\partial\mathbf{e}^2}, \qquad \mathcal{L}^{th} = -\rho_{Ref}\frac{\partial^2\widehat{\psi}}{\partial\mathbf{e}\partial\vartheta}, \\ \mathcal{W} = \eta^{*}[(\mathbf{g}\boldsymbol{\tau} - \boldsymbol{\tau}\mathbf{g}) : (\boldsymbol{\alpha}\mathbf{g} - \mathbf{g}\boldsymbol{\alpha})].\end{gathered} \tag{5.34}$$

Substituting $\dot{\psi}$ into the energy balance equation (3.5) and taking into account the results $(5.31)_3$ and (5.32) gives

$$\rho\vartheta\dot{\eta} = -\mathrm{div}\mathbf{q} + \rho\widehat{\vartheta i}. \tag{5.35}$$

Operating on the entropy relation $(5.31)_2$ with the Lie derivative and substituting the result into (5.35) we obtain

$$\rho c_p\dot{\vartheta} = -\mathrm{div}\mathbf{q} + \vartheta\frac{\rho}{\rho_{Ref}}\frac{\partial\boldsymbol{\tau}}{\partial\vartheta} : \mathbf{d} + \rho\chi^{*}\boldsymbol{\tau} : \mathbf{d}^{p} + \rho\chi^{**}\mathbf{K} : \mathrm{L}_{\boldsymbol{v}}\boldsymbol{\xi}, \tag{5.36}$$

where the specific heat

$$c_p = -\vartheta\frac{\partial^2\widehat{\psi}}{\partial\vartheta^2}, \tag{5.37}$$

and the irreversibility coefficients χ^* and χ^{**} are determined by

$$\chi^* = -\left[\left(\frac{\partial\widehat{\psi}}{\partial\in^P} - \vartheta\frac{\partial^2\widehat{\psi}}{\partial\vartheta\partial\in^P}\right)\sqrt{\frac{2}{3}} + \left(\frac{\partial\widehat{\psi}}{\partial\boldsymbol{\alpha}} - \vartheta\frac{\partial^2\widehat{\psi}}{\partial\vartheta\partial\boldsymbol{\alpha}}\right) : \left(r_1\mathbf{P} + r_2\frac{\mathbf{P}:\mathbf{Q}}{\widehat{\boldsymbol{\tau}}:\mathbf{Q} + r_3\boldsymbol{\xi}:\mathbf{Q}}(\widehat{\boldsymbol{\tau}} + r_3\boldsymbol{\xi})\right)\right]\frac{1}{\boldsymbol{\tau}:\mathbf{P}},$$

$$\chi^{**}\mathbf{K} = -\left(\frac{\partial\widehat{\psi}}{\partial\boldsymbol{\xi}} - \vartheta\frac{\partial^2\widehat{\psi}}{\partial\vartheta\partial\boldsymbol{\xi}}\right). \tag{5.38}$$

5.8. Fracture criterion based on the evolution of microdamage

We base the fracture criterion on the evolution of the microdamage tensor $\boldsymbol{\xi}$.

Let us assume that for $(\boldsymbol{\xi}:\boldsymbol{\xi})^{1/2} = \xi^F$ catastrophe takes place (cf. PERZYNA [82]), that is

$$\kappa = \widehat{\kappa}(\in^p, \vartheta, \boldsymbol{\xi})|_{(\boldsymbol{\xi}:\boldsymbol{\xi})^{1/2}=\xi^F} = 0. \tag{5.39}$$

It means that for $(\boldsymbol{\xi}:\boldsymbol{\xi})^{1/2} = \xi^F$ the material loses its carrying capacity. The condition (5.39) describes the main feature observed experimentally that the load tends to zero at the fracture point.

It is noteworthy that the isotropic hardening-softening material function $\widehat{\kappa}$ proposed in Eq. (5.14) should satisfy the fracture criterion (5.39).

5.9. Length-scale sensitivity of the constitutive model

The constitutive equations for a thermo-elastic-viscoplastic model introduce implicitly a length-scale parameter into the dynamic initial-boundary value problem, i.e.

$$l = \beta c T_m \qquad \text{or} \qquad l = \beta c T_m^0 \phi_1(f_{ms})\phi_2(\dot{\in}^P), \tag{5.40}$$

and as example for mild steel we have

$$l = \beta c T_m^0 \left[1 - f_{ms}^0 \frac{1}{1+\exp(a - b\in^P)}\right]\left(\frac{\dot{\in}^P}{\dot{\in}_s^P} - 1\right)^{1/p}, \tag{5.41}$$

where T_m is the relaxation time for mechanical disturbances, and is directly related to the viscosity of the material, c denotes the velocity of the propagation of the elastic waves in the problem under consideration, and the proportionality factor β depends on the particular initial-boundary value problem and may also be conditioned on the microscopic properties of the material.

The relaxation time T_m can be viewed either as a microstructural parameter to be determined from experimental observations or as a mathematical regularization parameter.

It is noteworthy to stress that the length-scale sensitivity of the constitutive structure is of great importance for proper description of meso- and micromechanical problems.

6. Epilogue

Our description of the thermo-elasto-viscoplastic constitutive structure is invariant with respect to any diffeomorphism. It means that the constitutive structure is invariant to any superposed motion[22)]. Such constitutive structure is called covariant, cf. Marsden, Hughes [58].

The covariance property of the constitutive structure has been achieved due to the assumption that the rates of the deformation tensors and the stress tensors (as well as all vectors and tensors) are defined based on the Lie derivative. Of course, the covariance description has very important consequence for proper mathematical investigations of some phenomena which can be discussed in the solution of the evolution problems. It will be also very crucial for proper description of meso-, micro-, and nano-mechanical problems and particularly in their numerical solutions.

The experimental works have brought deep understanding of the evolution of the dislocation substructure and the intrinsic microdamage mechanism during dynamic loading processes and clearly have shown that microshear banding influence a substructure of a polycrystalline material and fracture mechanism of metals does very much depend on the strain rate and wave shape effects.

The crucial idea in the theory of elasto-viscoplasticity developed is the very efficient interpretation of a finite set of the internal state variables as the equivalent plastic deformation, the microdamage tensor and the residual stress (the back stress). To describe suitably the time and temperature dependent effects observed experimentally and the accumulation of the plastic deformation and anisotropic damage during dynamic loading processes the thermomechanical coupling has been taken into account and the kinetics of microdamage and kinematic hardening law have been modified and generalized.

It is very well known fact that the stress wave propagation in an elasto-viscoplastic medium has the dispersive nature.

[22)] We can say that the thermodynamical theory of elasto-viscoplasticity satisfies very crucial property of symmetry, because is invariant with respect to diffeomorphism transformation, it means, that it is symmetric with respect to arbitrary motion, cf. Noether [63], Lederman, Hill [55] and Penrose [69].

The dispersion effect is very important for the development of the regularization procedure for the rate independent plastic flow evolution problems.

The dispersion effect is very crucial for the proper description of induced anisotropy. In the dynamical problems in solids, the dispersive wave phenomena are generated the induced anisotropy of two different kinds. First, is generated by the residual stresses which result from very heterogeneous deformation process. Second, is caused by intrinsic microdamage mechanism, is observed experimentally and suggested by multiscale considerations. Both kinds of the induced anisotropy influence very much the development of fracture phenomena in solids.

Of course, the dispersion effects will also influence very much the initiation and development of localization phenomena. A thorough analysis of these consequences has been presented in Glema *et al.* [41, 42, 43].

Very recently, it has been widely recognized to consider an elastic-viscoplastic model of a material as a regularization method for solving mesh-dependent problems of plasticity. In these regularized initial-boundary value problems, wave propagation phenomena play a fundamental role. An elastic-viscoplastic model introduces dissipative as well as dispersive nature for the propagated waves. The dispersion property implies that in the elastic-viscoplastic medium any initial disturbance can break up into a system of group of oscillations or wavelets. On the other hand, the dissipation property causes the amplitude of a harmonic wavetrain to decay with time. In the evolution problem considered in such dissipative and dispersive medium, the stress deformation due to wave reflections and interactions are not uniformly distributed, and this kind of heterogeneity can lead to strain localization in the absence of geometrical or material imperfections.

Since the rate independent plastic response is obtained as the limit case when the relaxation time is equal to zero hence the theory of elasto-viscoplasticity offers the regularization procedure for the solution of the dynamical initial-boundary value problems. The viscoplastic regularization procedure assures the stable integration algorithm by using the finite difference or finite element methods.

Acknowledgment

The preparation of this paper has been supported by the friends from the Institute of Structural Engineering, Poznań University of Technology.

The material presented in this paper has been shown at Workshop 2012 on Dynamic Behavior of Materials and Safety of Structures, Poznan, 2–4 May, 2012.

References

1. Abraham R., Marsden J.E., *Foundations of Mechanics*, Second Edition, Addison-Wesley, Reading Mass., 1978.
2. Abraham R., Marsden, J.E., Ratiu T., *Manifolds, Tensor Analysis and Applications*, Springer, Berlin, 1988.
3. Barbee T.W., Seaman L., Crewdson R., Curran D., Dynamic fracture criteria for ductile and brittle metals, *J. Mater.*, **7**, 393–401, 1972.
4. Bernstein B., *Proof of Caratheodory's local theorem and its global application to thermostatics*, J. Math. Phys., **1**, 222–224, 1960.
5. Boehler J.P. (Ed.), *Yielding, Damage, and Failure of Anisotropic Solids*, Proc. IUTAM/ICM Symposium, Villard-de Lans, 24–28 August 1987, Mech. Eng. Public. Limited, London, 1990.
6. Born M., *Kritische Betrachtungen zur traditionellen Darstelllung der Thermodynamik*, Physik. Zeitschr., **22**, 218–224, 249–254, 282–286, 1921.
7. Boyling J.B., *Caratheodory's principle and the existence of global integrating*, Commun. Math. Phys., **10**, 52–68, 1968.
8. Boyling J.B., *An axiomatic approach to classical thermodynamics*, Proc. Royal Soc. London, A329, 35–70, 1972.
9. Bridgman P.W., The termodynamics of plastic deformation and generalized entropy, *Rev. Modern Phys.*, **22**, 56–63, 1950.
10. Buchdahl H.A., *A formal treatment of the consequences of the second law of thermodynamics in Caratheodory's formulation*, Zeitschrift Phys., **152**, 425–439, 1958.
11. Buchdahl H.A., *Entropy concept and ordering of states*, I, Zeitschrift Phys., **168**, 316–321, 1962.
12. Buchdahl H.A., Greve W., *Entropy concept and ordering of states*, II, Zeitschrift Phys., **168**, 386–391, 1962.
13. Campbell J.D., Ferguson W.G., The temperature and strain-rate dependence of the shear strength of mild steel, *Phil. Mag.*, **81**, 63–82, 1970.
14. Caratheodory C., (1909), *Untersuchungen über die Grundlagen der Thermodynamik*. Math. Annalen, **67**, 355–386.
15. Chakrabarti A.K., Spretnak J.W., (1975), "Instability of plastic flow in the direction of pure shear", Metallurgical Transactions, **6A**, 733–747.
16. Coleman B.D., *Thermodynamics of materials with memory*, Arch. Rat. Mech. Anal., **17**, 1–46, 1964.
17. Coleman B.D., Gurtin M.E., Thermodynamics with internal state variables, *J. Chem. Phys.*, **47**, 597–613, 1967.
18. Coleman B.D., Mizel V.J., *A general theory of dissipation in materials with memory*, Arch. Rat. Mech. Anal., **27**, 255–274, 1968.
19. Coleman B.D., Noll W., The thermodynamics of elastic materials with heat conduction and viscosity, *Arch. Rational Mech. Anal.*, **13**, 167–178, 1963.

20. Coleman B.D., Owen D.R., *On the thermodynamics of materials with memory*, Arch. Rat. Mech. Anal., **36**, 245–269, 1970.

21. Coleman B.D., Owen D.R., *A mathematical foundations for thermodynamics*, Arch. Rat. Mech. Anal., **54**, 1–104, 1974.

22. Cooper J.L.B., *The foundations of thermodynamics*, J. Math. Anal. Appls., **17**, 172–193, 1967.

23. Curran D.R., Seaman L., Shockey D.A., Dynamic failure in solids, *Physics Today*, January, 46–55, 1977.

24. Curran D.R., Seaman L., Shockey D.A., Linking dynamic fracture to microstructural processes, in: *Shock Waves and High-Strain Rate Phenomena in Metals: Concepts and Applications*, M.A. Meyers and L.E. Murr [Eds.], Plenum Press, New York, pp. 129–167 1981.

25. Curran D.R., Seaman L., Shockey D.A., Dynamic failure of solids, *Physics Reports*, **147**, 253–388, 1987.

26. Dafalias Y.F., Corotational rates for kinematic hardening at large plastic deformations, *J. Appl. Mech.*, **50**, 561–565, 1983.

27. Dornowski W., Perzyna P., Constitutive modelling of inelastic solids for plastic flow processes under cyclic dynamic loadings, *Transaction of the ASME, J. Eng. Materials and Technology*, **121**, 210–220, 1999.

28. Dornowski W., Perzyna P., Localization phenomena in thermo-viscoplastic flow processes under cyclic dynamic loadings, *Computer Assisted Mechanics and Engineering Sciences*, **7**, 117–160, 2000.

29. Dowling A.R., Harding J., Campbell D.J., The dynamic punching of metals, *J. Inst. of Metals*, **98**, 215–224, 1970.

30. Duszek M.K., Perzyna P., On combined isotropic and kinematic hardening effects in plastic flow processes, *Int. J. Plasticity*, **7**, 351–363, 1991.

31. Duszek M.K., Perzyna P., The localization of plastic deformation in thermoplastic solids, *Int. J. Solids Structures*, **27**, 1419–1443, 1991.

32. Duszek-Perzyna M.K., Perzyna P., Analysis of the influence of different effects on criteria for adiabatic shear band localization in inelastic solids, in: *Material Instabilities: Theory and Applications*, ASME Congress, Chicago, 9–11 November 1994, R.C. Batra and H.M. Zbib [Eds.], AMD-Vol. 183/MD-Vol.50, ASME, New York, pp. 59–85, 1994.

33. Duszek-Perzyna M.K., Perzyna P., Analysis of anisotropy and plastic spin effects on localization phenomena, *Arch. Appl. Mechanics*, **68**, 352–374, 1998.

34. Eckart C., *The thermodynamics of irreversible processes*, Phys. Review, **58**, 267–269. 369–275, 919–924, 1940; **73**, 373–382, 1948.

35. Engelking R., General Topology, Polish Scientific Publishers, Warsaw, 1977.

36. Falk G., Jung H., *Axiomatik der Thermodynamik*, Handbuch der Physik, III/2, Springer, pp. 119–175, 1959.

37. Feynman R.P., Leighton R.B., Sands M., *The Feynman Lectures on Physics*, I, II, III, Addison-Wesley, New York, 65, 1963.

38. Follansbee P.S., *Metallurgical Applications of Shock-Wave and High-Strain-Rate Phenomena*, (Murr LE, Staudhammer KP, Meyeres MA, eds.), pp.451–480, Marcel Dekker, New York, 1986.

39. Giles R., *Mathematical Foundations of Thermodynamics*, Pergamon Press, Oxford 1964.

40. Glema A., Łodygowski T., Nowak Z., Perzyna P., Voyiadjis G.Z., Thermo-elasto-viscoplastic model of a material with non-local and anisotropic intinsic microdamage, McMat 2005, Mechanics and Materials Conference, Baton Rouge, LA, USA, June 1–3, 2005.

41. Glema A., Łodygowski T., Perzyna P., Interacton of deformation waves and localization phenomena in inelastic solids, *Computer Methods in Applied Mechanics and Engineering*, **183**, 123–140, 2000.

42. Glema A., Łodygowski T., Perzyna P., The role of dispersion for the description of strain localization in materials under impact loading, European Conference on Computational Mechanics, June 26–29, Cracow, Poland, 2001.

43. Glema A., Łodygowski T., Perzyna P., Localization of plastic deformations as a result of wave interaction, *CAM&ES*, **3**, 81–91, 2003.

44. Glema A., Łodygowski T., Perzyna P., Numerical investigations of dynamic shear bands in inelastic solids as a problem of mesomechanics, *Comput. Mech.*, **41**, 219–229, 2008.

45. Grebe H.A., Pak H.R., Meyers M.A., Adiabatic shear band localization in titanium and Ti-6PctAl-4PctV alloy, *Met. Trans.*, **16A**, 761-775, 1985.

46. Jaumann G., *Geschlossenes System physikalischer und chemischer Differentialgesetze*, Sitzgsber. Akad. Wiss. Wien (IIa), **120**, 385–530, 1911.

47. Johnson J.N., Dynamic fracture and spallation in ductile solids, *J. Appl. Phys.*, **52**, 2812–2825, 1981.

48. Kelley J.L., *General topology*, Van Nostrand., New York, 1955.

49. Kosiński W., Perzyna P., The unique material structure, *Bull. Acad. Polon. Sci., Ser. Sci. Techn.*, **21**, 655–662, 1973.

50. Kosiński W., Wojno W., *Remarks on internal variable and history descriptions of material*, Arch. Mech., **25**, 709–713, 1973.

51. Kumar A., Kumble R.Gg., Viscous drag on dislocations at high strain rates in copper, *J. Appl. Physics*, **40**, 3475–3480, 1969.

52. Landsberg P.T., *Foundations of thermodynamics*, Rev. Modern Phys., **28**, 363–392, 1956.

53. Landsberg P.T., *Main ideas in the axiomatics of thermodynamics*, Pure and Applied Chemistry, **22**, 215–227, 1970.

54. Landsberg P.T., Time in statistical physics and special relativity, *Studium Generale*, **23**, 1108–1158, 1970.

55. Lederman L.M., Hill Ch.T., *Symmetry and the Beautiful Universe*, Prometheus Books, Amherst, 2004.

56. Leitman M.J., Mizel V.J., *On fading memory space and hereditary integral equations*, Arch. Rat. Mech. Anal., **55**, 18–51, 1974.

57. Loret B., On the effects of plastic rotation in the finite deformation of anisotropic elastoplastic materials, *Mech. Mater.*, **2**, 287–304, 1983.

58. Marsden J.E., Hughes T.J.R., *Mathematical Foundations of Elasticity*, Prentice-Hall, Englewood Cliffs, New York, 1983.

59. Meyers H.C., *Dynamic Behaviour of Materials*, John Wiley, New York, 1994.

60. Meyers M.A., Aimone C.T., Dynamic fracture (spalling) of metals, *Prog. Mater. Sci.*, **28**, 1–96, 1983.

61. Nagel E., *The Structure of Science*, Harcourt, Brace World, Inc., New York 1961.

62. Nemat-Nasser S., *Phenomenological theories of elastoplasticity and strain localization at high strain rates*, Appl. Mech. Rev., **45**, S19–S45, 1992.

63. Noether E., Invariante Variationsprobleme,*Goett. Nachr.*, **1918**, 235–257, 1918.

64. Noll W., *A new mathematical theory of simple materials*, Arch. Rat. Mech. Anal., **48**, 1–50, 1972.

65. Noll W., *Lectures on the foundations of continuum mechanics and thermodynamics*, Arch. Rat. Mech. Anal., **52**, 62–92, 1973.

66. Nowacki W.K., Nowak Z., Perzyna P., Pęcherski R.B., *Effect of strain rate on ductile fracture. A new methodology*, Jour. Theoretical and Applied Mechanics, **48**, 1003–1026, 2010.

67. Nowak Z., Perzyna P., Pęcherski R.B., Description of viscoplastic flow accounting for shear banding, *Arch. of Metallurgy and Materials*, **52**, 217–222, 2007.

68. Oldroyd J., On the formulation of rheological equations of state, *Proc. R. Soc. Lond.*, **A200**, 523–541, 1950.

69. Penrose R., *The Road to Reality, A Complete Guide to the Laws of the Universe*, A.A. Knopf, New York 2005.

70. Perzyna P., The constitutive equations for rate sensitive plastic materials, *Quart. Appl. Math.*, **20**, 321–332, 1963.

71. Perzyna P., Fundamental problems in viscoplasticity, *Advances in Applied Mechanics*, **9**, 343–377, 1966.

72. Perzyna P., Thermodynamic theory of viscoplasticity, *Advances in Applied Mechanics*, **11**, 313–354, 1971.

73. Perzyna P., *A gradient theory of rheological materials with internal structural changes*, Arch. Mech., **23**, 845–850, 1971.

74. Perzyna P., Internal variable description of plasticity, International Symposium on Foundation of Plasticity, Warsaw, Poland, August 30–September 2 1972 , in: *Problems of plasticity*, A. Sawczuk [Ed.], Nordhoof Publishing, Leyden, 1974, pp. 145–176, 1972.

75. Perzyna P., *Thermodynamics theory of rheological materials with internal changes*, Symposium franco-polonais, Problemes de la Rhéologie, Varsovie 1971, PWN, Varsovie, 1973, pp. 277–306.

76. Perzyna P., Physical theory of viscoplasticity, *Bull. Acad. Polon. Sci., Serie Sci. Tech.*, **21**, 123–139, 1973.

77. Perzyna P., Thermodynamics of a unique material structure, *Arch. Mechanics*, **27**, 791–806, 1975.

78. Perzyna P., *On material isomorphism in description of dynamics plasticity*, Arch. Mech., **27**, 473–484, 1975.

79. Perzyna P., Coupling of dissipative mechanisms of viscoplastic flow, *Arch. Mechanics*, **29**, 607–624, 1977.

80. Perzyna P., Modified theory of viscoplasticity. Application to advanced flow and instability phenomena, *Arch. Mechanics*, **32**, 403–420, 1980.

81. Perzyna P., *Thermodynamics of dissipative materials*, in Recent Developments in Thermodynamics of Solids, G. Lebon and P. Perzyna [Eds.], Springer-Verlag, Wien, New York, pp. 95–220, 1980.

82. Perzyna P., Constitutive modelling of dissipative solids for postcritical behaviour and fracture, *ASME J. Eng. Materials and Technology*, **106**, 410–419, 1984.

83. Perzyna P., Internal state variable description of dynamic fracture of ductile solids, *Int. J. Solids Structures*, **22**, 797–818, 1986.

84. Perzyna P., Constitutive modelling for brittle dynamic fracture in dissipative solids, *Arch. Mechanics*, **38**, 725–738, 1986.

85. Perzyna P., Temperature and rate dependent theory of plasticity of crystalline solids, *Revue Phys. Appl.*, **23**, 445–459, 1988.

86. Perzyna P., Instability phenomena and adiabatic shear band localization in thermoplastic flow processes, *Acta Mechanica*, **106**, 173–205, (1994).

87. Perzyna P., Interactions of elastic-viscoplastic waves and localization phenomena in solids, IUTAM Symposium on Nonlinear Waves in Solids, August 15–20, 1993, Victoria, Canada, J.L. Wegner and F.R. Norwood [Eds.], ASME, pp. 114–121, 1995.

88. Perzyna P., Constitutive modelling of dissipative solids for localization and fracture. In: *Localization and Fracture Phenomena in Inelastic Solids* P. Perzyna [Ed.], Springer, Wien, New York, pp. 99–242, 1998.

89. Perzyna P., Thermo-elasto-viscoplasticity and damage, In: *Handbook of Materials Behaviour Models*, J. Lemaitre [Ed.], Academic Press, New York, pp. 821–834, 2001.

90. Perzyna P., Thermodynamical theory of inelastic single crystals, *Engineering Transactions*, **50**, 107–164, (2002).

91. Perzyna P., The thermodynamical theory of elasto-viscoplasticity, *Engineering Transactions*, **53**, 235–316, (2005).

92. Perzyna P., The thermodynamical theory of elasto-viscoplasticity accounting for microshear banding and induced anisotropy effects, *Mechanics*, **27**, 25–42, (2008).

93. Perzyna P., The thermodynamical theory of elasto-viscoplasticity for description of nanocrystalline metals, *Engng. Trans.*, **58**, 15–74, (2010).

94. Perzyna P., Micromechanics of localized fracture phenomena in inelastic solids generated by impactg loaded adiabatic processes, *Engng. Trans.*, **59**, 299–348, (2011).

95. Perzyna P., Drabik A., Description of micro-damage process by porosity parameter for nonlinear viscoplasticity, *Arch. Mechanics*, **41**, 895–908, (1989).

96. Perzyna P., Kosiński W., (1973), A mathematical theory of materials, *Bull. Acad. Polon. Sci., Ser. Sci. Tech.*, **21**, 647–654.

97. Perzyna P., Voyiadjis G.Z., (2005), Thermodynamic theory of elasto-viscoplasticity for induced anisotropy effects, McMat 2005, Mechanics and Materials Conference, June 1–3, 2005, Baton Rouge, LA, USA.

98. Perzyna P., Wojno W., Thermodynamics of a rate sensitive plastic material, *Arch. Mech.*, **20**, 499–511, (1968).

99. Perzyna P., Wojno W., Unified constitutive equations for elastic-viscoplastic material, *Bull. Acad. Polon. Sci., Ser. Sci. Tech.*, **24**, 85–94, (1976).

100. Pęcherski R.B., Macroscopic effects of microshear banding in plasticity of metals, *Acta Mechanica*, **131**, 203–224, (1998).

101. Planck M., *Über das Prinzip der Vermehrung der Entropie*, Wied. Ann., **30**, 562–582; **31**, 189–203; **32**, 462–503, (1887).

102. Planck M., *Vorlesungen über Thermodynamic*, Elfte Auflage, Berlin 1964 (Erste Auflage 1897).

103. Planck M., Die Einheit des Physikalishen Weltbildes, Vortrag gehalten 9.12.1908 in Leiden, *Phys. Zeitschr.*, **10**, 62–75, (1909).

104. Popper K.R., *The Logic of Scientific Discovery*, Hutchinson Publishing Group Ltd., London. 1974.

105. Rastall P., *Classical thermodynamics simplified*, J. Math. Phys., **11**, 2955–2965, 1970.

106. Rosenfield A.R., Hahn G.T., (1966), Numerical decsription of the ambient low-temperature, and high-strain rate flow and fracture behaviour of plain carbon steel, *Trans. Am. Soc. Metals*, **59**, 962–980.

107. Seaman L., Curran D.R., Shockey D.A., Computational models for ductile and brittle fracture, *J. Appl. Phys.*, **47**, 4814–4826, 1976.

108. Seeger A., The temperature dependence of the critical shear stress and of work–hardening of metal crystals, *Phil. Mag.*, **745**, 771–773, 1954.

109. Seeger A., The generation of lattice defects by moving dislocations and its application to the temperature dependence of the flow-stress of f.c.c. crystals, *Phil. Mag.*, **46**, 1194–1217, 1955.

110. Seeger A., *Kristalplastizitat*, Handbuch der Physik VII/2, S. Flugge [Ed.], pp.1–208, Springer-Verlag, 1958.

111. Shockey D.A., Seaman L., Curran D.R., In: *Metallurgical Effects at High Strain Rates*, R.W. Rohde, B.M. Butcher, J.R. Holland, and C.H. Karnes [Eds.], Plenum Press, New York, p. 473, 1973.

112. Shockey D.A., Seaman L., Curran D.R., The microstatistical fracture mechanics approach to dynamic fracture problem, *Int. J. Fracture*, **27**, 145–157, 1985.

113. Teodosiu C., Sidoroff F., A theory of finite elastoplasticity of single crystals, *Int. J. Engng. Sci.*, **14**, 165–176, 1976.

114. Truesdell C., *Rational thermodynamics*, McGraw-Hill, New York, 1969.

115. Truesdell C., Noll W., The Non-Linear Field Theories of Mechanics, in: *Handbuch der Physik III/3*, S. Flűgge [Ed.], Springer-Verlag, Berlin 1965.

116. Valanis K.C., *Unified theory of thermodynamical behaviour of viscoplastic materials*, Symp. Mech. Behav. Mater. Dyn. Loads, San Anotnio 1967, Springer, pp. 343–364, New York, 1968.

117. Van der Giessen E., Micromechanical and thermodynamic aspects of the plastic spin, *Int. J. Plasticity*, **7**, 365–386, 1991.

118. Zaremba S., *Sur une forme perfectionnée de la théorie de la relaxation*, Bull. Int. Acad. Sci. Cracovie, 594–614, 1903.

119. Zaremba S., *Le principe des mouvements relatifs et les équations de la mécanique physique*, Bull. Int. Acad. Sci. Cracovie, 614–621, 1903.

Received January 11, 2011; revised version August 15, 2011.

DIRECTIONS FOR THE AUTHORS

The periodical *ENGINEERING TRANSACTIONS (ROZPRAWY INŻYNIERSKIE)* presents original papers which should not be published elsewhere.

As a rule, the volume of a paper should not exceed 40 000 typographic signs. The following directions are particularly important:

1. **The paper submitted for publication should be written in English.**
2. The title of the paper should be as short as possible. The text should be preceded by a brief introduction; it is also desirable that a list of notations used in the paper should be given.
3. Short papers should be divided into section and subsection, long papers into sections, subsections and points. Each section, subsection or point must bear a title.
4. The formula number consists of two figures: the first represents the section number and the other the formula number in that section. Thus the division into subsections does not influence the numbering of formulae. Only such formulae should be numbered to which the author refers throughout the paper. This also applies to the resulting formulae. The formula number should be written on the left-hand side of the formula; round brackets are necessary to avoid any misunderstanding. For instance, if the author refers to the third formula of the set (2.1), a subscript should be added to denote the formula, viz. $(2.1)_3$.
5. All the notations should be written very distinctly. Special care must be taken to distinguish between small and capital letters as precisely as possible. Semi-bold type must be underlined in black pencil. Explanations should be given on the margin of the manuscript in case of special type face.
6. Vectors are to be denoted by semi-bold type, transforms of the corresponding functions by tildes symbols. Trigonometric functions are denoted by sin, cos, tan and cot, inverse functions – by arc sin, arc cos, arc tan and arc cot; hyperbolic functions are denoted by sh, ch, th and cth, inverse functions – by Arsh, Arch, Arth and Arcth.
7. The figures in square brackets denote reference titles. Items appearing in the reference list should include the initials of the first name of the author and his surname, also the full of the paper (in the language of the original paper); moreover;
   a) In the case of books, the publisher's name, the place and year of publication should be given, e.g., 5. Ziemba S., *Vibration analysis*, PWN, Warszawa 1970;
   b) In the case of a periodical, the full title of the periodical, consecutive volume number, current issue number, pp. from ... to ..., year of publication should be mentioned; the annual volume number must be marked in semi-bold type as to distinguish it from the current issue number, e.g., 6. Sokołowski M., *A thermoelastic problem for a strip with discontinuous boundary conditions*, Arch. Mech., **13**, 3, 337–354, 1961.
8. The authors should enclose a summary of the paper. The volume of the summary is to be about 100 words, also key words are requested.
9. The preferable format for the source file is TeX or LaTeX while MS Word is also acceptable. Separate files for the figures should be provided in one of the following formats: EPS or PostScript (preferable), PDF, TIFF, JPEG, BMP, of at least 300 DPI resolution. The figures should be in principle in gray-scale and only if necessary the color will be accepted.

Upon receipt of the paper, the Editorial Office forwards it to the reviewer. His opinion is the basis for the Editorial Committee to determine whether the paper can be accepted for publication or not.

Once the paper is printed, the issue of Engineering Transactions free of charge is sent to the author. Also the PDF file of the paper is forwarded by the e-mail to the authors.

Editorial Committee

ENGINEERING TRANSACTIONS